Bettina Purgstaller, MSc

The Role of Amorphous Precursors on the Formation of Calcium Carbonate Minerals

Doctoral Thesis

to obtain the doctoral degree of natural sciences (Dr. rer. nat.) of

Graz University of Technology

Supervisors

Univ.-Prof. Dr. rer. nat. Martin Dietzel

Dr. rer. nat. Vasileios Mavromatis

Reviewers

Univ.-Prof. Dr. rer. nat. Martin Dietzel

Univ.-Prof. Dr. rer. nat. Adrian Immenhauser

Graz, March 2017

„Geologists have a saying: Rocks remember”

Neil Armstrong

STATUARY DECLARATION

I declare that I have authored this thesis independently, that I have not used other than the declared sources / resources, and that I have explicitly marked all material which has been quoted either literally or by content from the used sources

…… ……..

DATE **(SIGNATURE)**

THANKS TO…

…my supervisors Prof. Martin Dietzel and Dr. Vasileios Mavromatis

for your great support and guidance during the last years! I really appreciate our insightful discussions which helped me a lot to move ideas forward.

…Prof. Adrian Immenhauser

for your useful suggestions, remarks and corrections during writing manuscripts and for evaluating this doctoral thesis.

…Andre Baldermann and Florian Konrad

for your support concerning interpretation of the data and your helpful suggestions during writing manuscripts.

…CHARON

for great scientific meetings and discussions. I am thankful to be part of this wonderful network.

…DFG and NAWI Graz

for providing the financial support for this study.

…Judith Jerney, Andrea Wolf, Maria Hierz and Sylvia Perchthold

for analytical work and your support in the laboratory.

...Patrick Grunert and Gerald Auer

for your help conducting microscopic investigations

...Stephan Sacher (RCPE)

for providing access to in situ Raman spectroscopy.

... my colleagues Jessica Stammeier, Anja Füger, Cyrill Grenng, Isaac John Kell Duivestein, Dorothee Hippler, Ronny Boch, Dietmar Klammer, Albrecht Leis, Peter Schreiber, Daniela Sobian and Anna Pendl

for your support and the great working environment.

...my family and friends

for always being there with me. Thanks for making me laugh on my bad days!

My deepest gratitude goes to my wonderful parents who always supported me.

ABSTRACT

Our current understanding of the Earth`s climatic evolution in the geological past is mainly based on the isotopic and chemical composition of biogenic and inorganic carbonates. The biogenic deposition of carbonates is of great importance especially to the marine ecosystem; inorganic carbonates often occur in the form of speleothems, travertines, and alkaline lake deposits in terrestrial environments. The use of isotopic and chemical signatures of carbonates is based on the assumption that carbonates record the isotopic and chemical signature of their environment (e.g. sea water or dripping water in caves) at the time of their formation. However, recent studies documented that various carbonate minerals found in different natural environments are not only the product of "classical crystallization", but their formation are induced partial or in whole from an amorphous calcium carbonate (ACC) precursor. In this context, significant gaps of knowledge exist with respect to the mechanisms controlling the transformation of ACC into crystalline carbonates (e.g. to calcite or aragonite) as well as on the impact of such a precursor phase on the elemental and isotopic composition of the final crystalline phase.

In the course of this thesis, experiments were conducted under controlled physicochemical conditions in order to investigate the effects of initial aqueous Mg/Ca ratio, pH and temperature on the (trans)formation of Mg-rich amorphous calcium carbonate (Mg-ACC). The Mg-ACC transformation was monitored at a high temporal resolution (~30 sec) using in situ Raman spectroscopy, while the chemical and isotopic evolution of the solution and of the solid phase was followed by separate sample analysis. Overall, the obtained data revealed that a coupled dissolution and re-precipitation mechanism is taking place during Mg-ACC transformation. Accordingly, the chemical and isotopic composition of the precursor Mg-ACC is not preserved during its transformation into the final crystalline phase. Moreover, the results of this study showed that the transformation of Mg-ACC is significantly affected by the prevailing physicochemical conditions of the reactive fluid (Mg/Ca ratio of the fluid, etc.) and to a lesser extent by a potential proto-crystalline pre-structuring of the primary Mg-ACC. The mineralogical, isotopic and chemical results of this study improve our current understanding about the environmental controls and the formation mechanisms of carbonate minerals in natural systems. Furthermore, the results are of great relevance for the interpretation of isotopic and chemical signatures of carbonates, which are formed by amorphous precursor and are subsequently used as climate indicators.

KURZFASSUNG

Unser Verständnis über die klimatische Entwicklung der Erde in der geologischen Vergangenheit basiert in wesentlichen Aspekten auf der (isotopen)chemischen Zusammensetzung von biogen und anorganisch gebildeten Karbonaten. Die biogene Abscheidung von Karbonaten hat eine große Bedeutung insbesondere für das marine Ökosystem; anorganisch gebildete Karbonate treten häufig in Form von Speleothemen, Travertin und alkalischen Seeablagerungen in terrestrischen Umfeldern auf. Die Verwendung von (isotopen)chemischen Signaturen von Karbonaten basiert im Wesentlichen auf der Annahme, dass Karbonatminerale die (isotopen)chemische Signatur ihres Umfeldes (z.B. Meerwasser oder Tropfwasser in Höhlen) zum Zeitpunkt ihrer Entstehung aufzeichnen. Aktuelle Untersuchungen dokumentieren jedoch, dass zahlreiche Karbonatminerale in unterschiedlichsten natürlichen Umfeldern nicht nur das Produkt der „klassischen Kristallisation“ sind, sondern deren Bildung teilweise oder vollständig über eine amorphe Kalziumkarbonat (ACC) Vorläuferphase herbeigeführt wird. In diesem Zusammenhang gibt es noch signifikante Wissenslücken im Bereich der Mechanismen, welche die Umbildung von ACC zu kristallinen Karbonaten (z. B. zu Kalzit oder Aragonit) steuern, sowie auch über den Effekt einer solchen Vorläuferphase auf die (isotopen)chemische Zusammensetzung der kristallinen Endphase.

Im Rahmen dieser Arbeit wurden Experimente unter kontrollierten physikochemischen Bedingungen durchgeführt, um die Auswirkungen des initialen Mg/Ca Verhältnisses, des pH-Wertes und der Temperatur der Lösung auf die (Um)Bildung einer Mg-reichen, amorphen Kalziumkarbonat Vorläuferphase (Mg-ACC) aufzuklären. Der Umbildungsweg von Mg-ACC wurde mit hoher zeitlichen Auflösung (~ 30 Sek.) mittels in situ Raman Spektroskopie analysiert, während die (isotopen)chemische Entwicklung der Lösung und der festen Phase über separate Probenanalyse verfolgt wurde. Die erhaltenen Daten zeigen, dass ein gekoppelter Lösungs- und Wiederausfällungsmechanismus bei der Mg-ACC Umbildung statt findet. Demzufolge bleibt die (isotopen)chemische Zusammensetzung des Mg-ACC Vorläufers während der Umwandlung in die endgültige kristalline Phase nicht erhalten. Darüber hinaus zeigten die Ergebnisse dieser Studie, dass der Umbildungsweg von Mg-ACC erheblich von den physikochemischen Bedingungen der Umgebung (vorherrschendes Mg/Ca-Verhältnis der Lösung) beeinflusst wird und nicht durch eine potentielle proto-kristalline Vorstrukturierung des primären Mg-ACC gesteuert wird. Die mineralogischen und (isotopen)chemischen Ergebnisse dieser Studie werden

verwendet, um unser aktuelles Verständnis über die kontrollierenden Umweltfaktoren und die Entstehungsmechanismen von Karbonatmineralen in natürlichen Systemen zu verbessern. Darüber hinaus sind die Ergebnisse von großer Bedeutung für die Interpretation von (isotopen)chemischen Signaturen von Karbonaten, die über amorphe Vorläuferphasen gebildet wurden und als Klimasignale gedeutet werden.

TABLE OF CONTENTS

1. INTRODUCTION

1.1 Calcium carbonate formation in aqueous environments

The precipitation of calcium carbonate ($CaCO_3$) from aqueous solution is a widely occurring process in natural and man-made environments. Sedimentary rocks at the Earth´s surface comprise about 10-15 wt.% $CaCO_3$, mainly originated from biological activity (e.g. Dietzel, 2011). Numerous marine organisms (e.g. corals, bivalves and calcareous plankton) precipitate $CaCO_3$ for their skeletons, shells and spines. Environments where $CaCO_3$ precipitates abiotically include e.g. marine evaporites, alkaline lake deposits, travertines and speleothems (e.g. Morse and MacKenzie, 1990; Flügel, 2010). In the industry, $CaCO_3$ minerals with special morphologies are synthesized for their use as fillers in papers, paints, plastics and coatings (e.g. Park et al., 2004). On the other hand, precipitated $CaCO_3$ may cause clogging problems in drainage systems, heat exchangers and oil production wells (e.g. Zhang et al., 2001; Rinder et al., 2013).

Calcium carbonate occurs in six different forms: three anhydrous crystalline forms, calcite, aragonite and vaterite, two hydrous crystalline forms, monohydrocalcite and ikaite, and amorphous calcium carbonate (ACC). In biotic and abiotic precipitation environments, calcite and aragonite are the most frequent and widespread forms of $CaCO_3$ (e.g. Morse and Mackenzie, 1990). Vaterite is volumetrically much less important compared to calcite and aragonite in marine and meteoric depositional environments, but can be found e.g. in fish otoliths (Gauldie et al., 1997), ascidian spicules (Lowenstam et al., 1981) and calcareous sinter from cold saline springs (Ito et al., 1999). The calcium carbonate monohydrate mineral monohydrocalcite ($CaCO_3 \cdot H_2O$) is formed as a product of biomineralization by certain molluscs and flatworms (Lowenstam, 1981; Señorale-Pose et al., 2008) and has been found in recent abiotic precipitation environments including saline springs (Ito, 1993), marine polar systems (Dahl and Buchardt, 2006) and saline lakes (Solotchina et al., 2009). Ikaite is a hydrous crystalline calcium carbonate mineral ($CaCO_3 \cdot 6H_2O$) which is commonly found in modern abiotic precipitation environments characterized by temperatures < 9°C (Ito et al., 1993; Dahl and Buchardt, 2006; Oehlrich et al., 2013; Field et al., 2016). Amorphous calcium carbonate plays a significant role in $CaCO_3$ biomineralization processes of various organisms (Addadi et al., 2003). Moreover, ACC precipitation is of great importance for medical and industrial applications (e.g., Meiron et al., 2011; Matsunuma et al., 2014).

Despite the fact that calcite is the less soluble $CaCO_3$ phase under ambient conditions (**Fig. 1A**; Plummer and Busenberg 1982), it is not necessary the first phase formed from a supersaturated aqueous solution. The formation behavior of $CaCO_3$ is affected by physicochemical parameters including temperature (Fyfe and Bischoff, 1965; Weiss et al., 2014), pH (Han et al., 2006), organic molecules (Kitano, 1965; Niedermayr et al., 2012) and foreign ions like magnesium and phosphate (e.g. Lippmann, 1973; Reddy, 1977). For example, many studies have documented that high aqueous molar Mg/Ca ratios inhibit calcite nucleation and growth and lead to the precipitation of aragonite (Lippmann 1973; Berner, 1975; Fernández-Díaz et al., 1996; De Choudens-Sanchez and Gonzalez, 2009). In the crystal structure of calcite Ca^{2+} can be substituted by Mg^{2+} in varying amounts, whereas Mg^{2+} is not supposed to be incorporated into the crystal structure of aragonite. The dehydration of ions at the lattice growth sites is one of the most important rate-controlling processes during crystal formation (Nielsen, 1984). In this context, it has been shown that the exchange rate of Mg^{2+} with water is five orders of magnitude slower than that for Ca^{2+} (Bleuzen et al., 1997). The adsorption of Mg^{2+} ions on calcite growth sites inhibits the step advancement (Astilleros et al., 2010) and affects the growth rate of calcite (Reddy and Wang, 1980; Mavromatis et al., 2013).

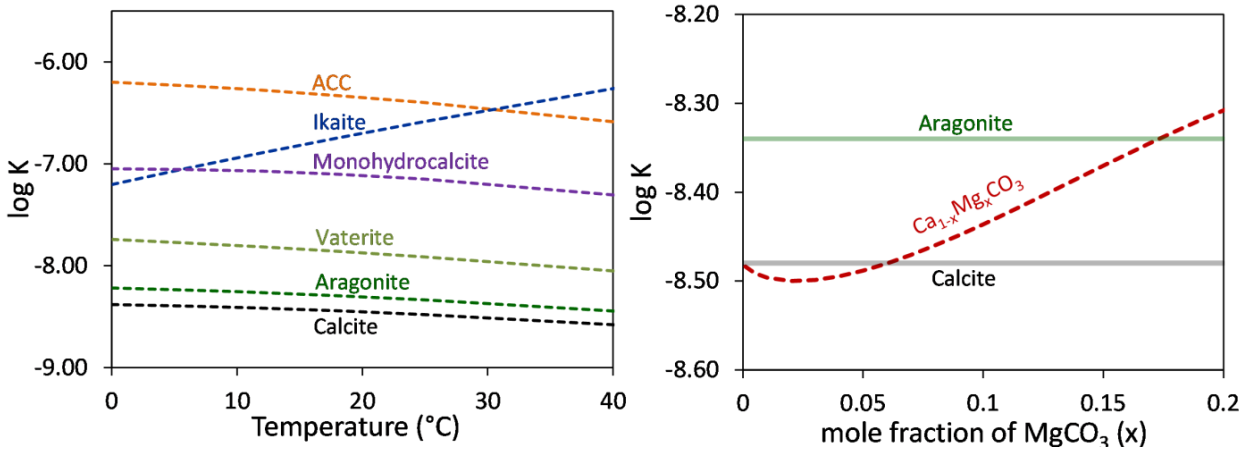

Fig. 1. (A) Temperature versus solubility product (K) for calcite, aragonite and vaterite (Plummer and Busenberg, 1982) as well as for monohydrocalcite (Kralj and Brecevic, 1995), ikaite (Bischoff et al., 1993) and amorphous calcium carbonate (ACC, Brevecic and Nielsen, 1989). **(B)** Solubility of Mg-calcite as a function of $MgCO_3$ mole fraction (Group I, Busenberg and Plummer, 1989).

Moreover, previous work documented that calcite becomes thermodynamically destabilized relative to aragonite by the uptake of Mg in its structure (**Fig. 1B**). Note here that calcites were divided into low (< 4 mol% Mg) and high Mg-calcites (> 4 mol% Mg) (Flügel, 2004; Long et al.,

2014). In the laboratory, the precipitation of thermodynamic metastable high Mg-calcites is an enigma under ambient conditions (Goldsmith et al., 1961). However, calcites with Mg-contents up to 44 mol% have been reported from biotic and abiotic precipitation environments (Schmidt et al., 2005; Bentov and Erez, 2005; Gayathri et al., 2007; Mavromatis et al., 2014b).

1.2 Elemental and isotopic fractionation during carbonate precipitation

Carbonate minerals record elemental and isotopic signals of the aqueous environments at the time of their formation and have potential to act as archives of Earth´s climate conditions over the geological past. In marine systems, the chemical and isotopic composition recorded in carbonates (e.g. exoskeletons of calcifying organism) is widely used by the geochemical community to reconstruct paleo-temperatures, chemical variations of the past seawater, oceanographic conditions and global changes in elemental cycles as well as in weathering regimes (e.g. Elderfield and Ganssen, 2000; Farkas et al., 2007; Gussone et al., 2004; Ripperdan, 2001; Pokrovsky et al., 2011). In terrestrial systems, inorganic calcium carbonate ($CaCO_3$) deposits in caves (speleothems) are increasingly used as archives of past climate variability (e.g. Riechelmann et al., 2011; Mosely et al., 2016).

In crystal lattice of $CaCO_3$ minerals Ca^{2+} can be substituted by other cations such as Mg^{2+}, Sr^{2+}, Co^{2+}, Ba^{2+}, Ni^{2+} and Zn^{2+} (Lorens, 1981; Mucci and Morse, 1983; Tesoriero and Pankow, 1996; Dietzel et al., 2004; Lakshtanov and Stipp, 2007; von Allmen et al., 2010). Geochemical proxies used in carbonate archive research include elemental ratios like Sr/Ca, Mg/Ca, Ba/Ca, and B/Ca (e.g. Lea and Boyle 1989; Beck et al., 1992; Gussone et al., 2004; Yan et al., 2013) and traditional stable isotopes ($\delta^{13}/^{12}C$, $\delta^{18}/^{16}O$ and $\delta^{34}/^{32}S$ (in Carbonated Associated Sulfate, CAS); e.g. Kapschulte and Strauss, 2004; Gussone et al., 2004; McDermott, 2004; Mosely et al., 2016). Based on recent improvements in analytical measurements (i.e. MC-ICP-MS), an increasing number of researchers is now applying new isotope systems (non-traditional isotopes), such as $\delta^{44}/^{40}Ca$, $\delta^{26}/^{24}Mg$, $\delta^{11}/^{10}B$ and $\delta^{88}/^{86}Sr$ (e.g. Hippler et al., 2006; Fantle and DePaolo 2006; Immenhauser et al., 2010; Prokrovsky et al., 2011; Foster et al., 2012) and clumped isotopes (Δ^{47}; e.g. Tripati et al., 2010; 2015; Tang et al., 2014) on carbonates to provide relevant information on past environmental conditions.

The interpretation of the chemical and isotopic signatures of natural samples however requires a detailed understanding of the distribution behavior of elements and isotopes during the formation of carbonate minerals. A number of experimental studies showed that the fractionation of

elements and isotopes during $CaCO_3$ formation depends on its structure (calcite, aragonite etc.) as well as on environmental factors such as temperature (Tang et al., 2008a, b; Dietzel et al., 2004, 2009; Marriott et al 2004), fluid chemistry (i.e. pH, ionic strength, foreign cations and organics: Tang et al., 2014; Lee et al., 2006; Mavromatis et al., 2015), the presence of crystal seeds (Lin and Singer, 2005) and growth rates (Lorens, 1981; Tang et al., 2008a, b; Dietzel et al., 2009; Immenhauser et al., 2010; Mavromatis et al., 2013). In this context, absence of knowledge exists with respect to the distribution of elements and isotopes during the formation of amorphous precursors and during their transformation into their crystalline counterparts.

Moreover, there is strong evidence that mineralogical and chemical properties of primary carbonates can be overprinted by diagenetic alteration. In sedimentary environments carbonates come into contact with various fluids, including e.g. sediment pore water and meteoritic water. The latest findings show that after achievement of chemical equilibrium between aqueous solution and solid an isotopic exchange between solid and co-existing fluid may still occur, owing to a dynamic dissolution/re-precipitation at the mineral surface layers (see Mavromatis et al., 2016b).

1.3 Formation and transformation of amorphous calcium carbonate

According to the classical step growth process, crystals grow by ion-by-ion attachment to the step edges of distinct mineral surfaces (terrace-ledge-king model; Burton et al., 1951; Chernov, 1984). Several studies, however, documented that this model cannot explain unusual carbonate textures and compositions that are found in modern natural settings (e.g. calcites with very high Mg contents; Bischoff et al., 1987). The formation of crystalline $CaCO_3$ (e.g. calcite and aragonite) via an amorphous calcium carbonate precursor (ACC, **Fig. 2**) represents an alternative pathway for calcium carbonate mineral formation in biotic and abiotic precipitation environments and might be the missing link in interpreting unusual carbonate compositions and structures. A large body of recent literature suggests that many groups of organism apply amorphous precursor strategies in biomineralization (e.g. Addadi et al., 2003; Politi et al., 2008, Immenhauser et al., 2010). In this context, it has been suggested that carbonate-secreting organisms accumulate ACC in vesicles, where additives (e.g. organic molecules and Mg ions) inhibit the deposition of crystalline $CaCO_3$ (Weiner and Dove, 2003; Weiner and Addadi, 2011). The amorphous precursor phase might be stored for extended time periods or is directly transported to the site of crystallization, where the transformation to calcite and/or aragonite takes place (Beniash et al.,

1999; Weiner and Addadi, 2011). The presence of ACC has been documented in a variety of organisms, such as bivalves (Jacob et al., 2011), sea urchins (Politi et al., 2008), brachiopods (Griesshaber et al., 2009), sponges (Sethmann et al., 2006), crustaceans (Tao et al., 2009), fresh water snails (Khairoun et al., 2002) and ascidians (Aizenberg et al., 2002). Moreover, amorphous carbonate phases were found in micro-domains of modern microbialites in lakes (Benzerara et al., 2006) and in biofilms formed in hot springs (Jones and Peng, 2012), where high local supersaturation degrees with respect to carbonate minerals are induced by e.g. microbial metabolism (Dupraz et al., 2009). In Lake Alchichica (Mexico) amorphous calcium-magnesium-strontium-barium carbonate is formed in intercellular inclusions of cyanobacteria, revealing an unexplored pathway for calcification (Couradeau et al., 2012). More recently, ACC formation and its transformation to calcite were, for instance, associated with speleothem formation in caves (Demény et al., 2016).

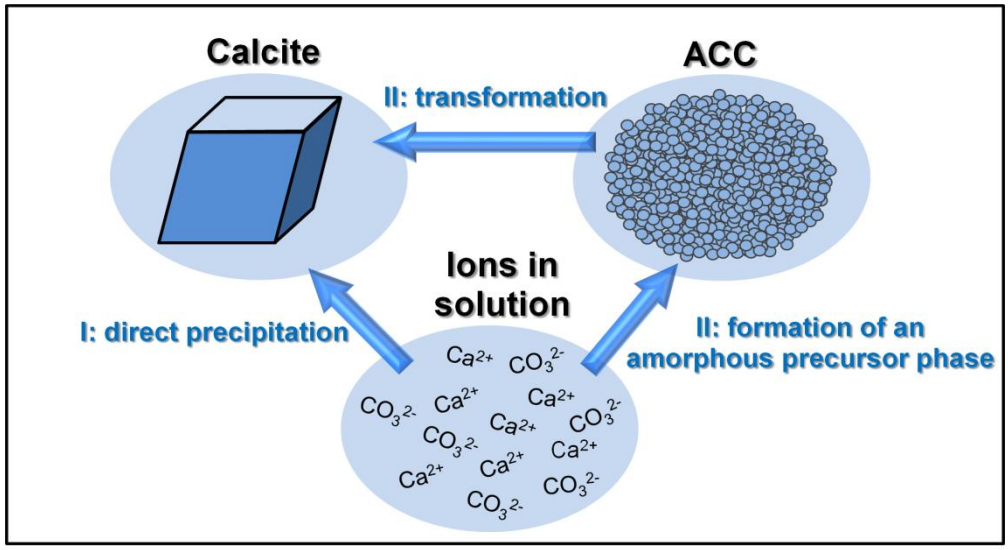

Fig. 2. Formation of crystalline calcium carbonate (e.g. calcite) directly from the fluid phase (I) or via the formation of an amorphous calcium carbonate (ACC) precursor (II)

The interpretation of elemental and isotopic signatures of biotic and abiotic carbonate archives is based on the generally accepted assumption that they record the chemical and isotopic signals of the aqueous environment prevailing at the time of carbonate mineral formation. In this sense, crystalline carbonates that have been formed via an amorphous precursor are prone to preserve a different chemical and isotopic composition, compared to crystalline carbonates that have been precipitated directly from a supersaturated solution. The question of how (isotope)chemical

signatures are affected during ACC formation and subsequent transformation is of key relevance for the accurate interpretation of paleo-climatic and environmental information recorded in biogenic and abiotic carbonates (e.g. skeletal hardparts and speleothems). Biogenic carbonate minerals (e.g. skeletons) formed from similar species often record elemental and isotopic compositions that do not reflect the environment in which the organisms lived and thus these signatures strongly deviate from those of abiotic carbonates (e.g. Weiner and Dove, 2003; Saenger and Wang, 2014). These also-called vital effects are believed to arise from physiological controls over biomineralisation, but they could also be attributed to different mineralization strategies (classical step growth process versus amorphous biomineralization strategy). Considering inorganic precipitation of $CaCO_3$ in caves (speleothems), fluid inclusions have the potential to provide direct measurements of the isotopic composition of paleo-meteoric water (Vanhof et al., 2006 and references therein). Recent work, however, indicates that the oxygen isotopic compositions of inclusion-hosted waters in speleothems do not necessarily correspond with those of the local drip water compositions (e.g. Vanhof et al., 2006; Demémy et al., 2016). In that sense, it has been speculated that the isotopic change in the fluid is caused by initial ACC formation that later recrystallized to calcite. Thus, the interpretation of isotopic and elemental proxy data of carbonates requires a detailed understanding about the transformation mechanisms of ACC, which are at present still under debate in the scientific community.

The composition and structure of ACC is often difficult to examine due to the high solubility of ACC under ambient conditions (**Fig. 1A**) and its rapid transformation (within seconds to minutes) into less soluble crystalline $CaCO_3$ (e.g. calcite and vaterite; Rodriguez-Blanco et al., 2012). For ACC, various H_2O contents were reported depending on the synthesis method and the treatment of the solid after ACC was isolated from the solution (Rhada et al., 2010; Ihli et al., 2013). Recently, the composition of synthetic ACC, after removal of adsorbed water, was described by the chemical formula $CaCO_3 \cdot 0.4H_2O$ (Schmidt et al., 2014; Konrad et al., 2016). Additives like magnesium ions and organic molecules play a significant role in temporarily stabilizing both synthetic and biogenic ACC (Loste et al., 2003; Lam et al., 2007; Politi et al., 2010; Han et al., 2013). Along these lines, it has been documented that ACC can accommodate up to 42 mol% Mg (Loste et al., 2003; Long et al., 2011; Han et al., 2013; Lin et al., 2015). Several studies suggested the formation of ACCs with different short-range structures (protostructures), depending on the physicochemical parameters involved during their synthesis (Lam et al., 2007; Gebauer et al., 2008; 2010). For instance, Gebauer et al. (2008) documented the formation of ACC with a

vaterite or a calcite-like structure depending on the pH of the mixing solution. This short-range structure is suggested to control the crystallization of ACC to a distinct $CaCO_3$ phase (e.g. calcite or vaterite). In contrast, based on distribution function analysis and nuclear magnetic resonance spectroscopy, Michel et al. (2008) concluded that the short-range structure of synthetic ACC shows no distinct match to any known crystalline calcium carbonate phase. Thus, different ACC crystallization mechanisms were suggested: ACC transforms to crystalline $CaCO_3$ via a (i) solid state mechanism, involving dehydration and structural reordering of ACC (Lam et al., 2007; Politi et al., 2008; Rhada et al., 2010; Gong et al. 2012), (ii) nucleation controlled dissolution and re-precipitation reaction (Ogino et al., 1987; Han et al., 2013; Rodriguez-Navarro et al., 2015; Giuffre et al., 2015) or a (iii) combination between a solid state and dissolution-re-precipitation process (Ihli et al., 2014; Nielsen et al., 2014). Questioning which of these processes is predominant has high significance for the interpretation of elemental and isotopic signatures recorded in carbonates. In contrast to a solid-state transformation, the chemical and isotopic signals of the ACC precursor are not expected to be preserved in the final crystalline phase that is formed via dissolution and re-precipitation of ACC (Giuffre et al., 2015).

A number of studies suggested different crystallization pathways of ACC depending on the physicochemical conditions of the mixing solutions (Ogino et al., 1987; Rodriguez-Blanco et al., 2012; 2014). For example, the synthesis of ACC from a low pH solution (~ 7) results in its crystallization into calcite, whereas ACC synthesized from a high pH solution (≥ 9.5) transforms into calcite (25°C) and aragonite (>60°C) via intermediate vaterite (Ogino et al., 1987; Rodriguez-Blanco et al., 2012; Bots et al., 2012). In contrast, in the presence of aqueous Mg, Mg-rich ACC (Mg-ACC) transforms into Mg-calcite, monohydrocalcite and/or hydromagnesite (Loste et al., 2003; Han et al., 2013; Rodriguez-Blanco et al., 2010; 2014). In most of these studies, ACC was synthesized by batch methods with $NaHCO_3$/$NaCO_3$ and $(Ca,Mg)Cl_2$ solutions, where the pH may significantly change during the formation of ACC and its transformation into the crystalline phase (from ~11 to ~8; Rodriguez-Blanco et al., 2008; Bots et al. 2012). Due to different synthesis routines and mostly non-revealed evolution of the solution composition during synthesis (e.g. Loste et al., 2003), the physicochemical conditions (e.g. solution chemistry, temperature) that control the transformation pathways of amorphous precursor phases are still not clear.

2. OUTLINE OF THE DOCTORAL THESIS

Considering that the (trans-)formation of amorphous carbonate phases is of humongous relevance in many natural surroundings, rigorous experimental work is now needed in order to (i) investigate the distribution of elements and isotopes during the formation of ACC and its subsequent transformation into crystalline $CaCO_3$, (ii) elucidate the effect of the chemical composition on the stability/reactivity of such amorphous phases and (iii) decipher the physicochemical conditions controlling the formation of distinct crystalline carbonate minerals (e.g. (Mg-)calcite or aragonite) via an amorphous precursor.

In the context of this thesis, precipitation experiments were carried out under controlled physicochemical conditions (const. T and pH). Specifically, the (trans)formation of Mg-rich ACC (Mg-ACC) was investigated as a function of initial aqueous Mg/Ca ratio (1/3 to 1/8), pH (7.8 to 8.8) and temperature (6°C to 25°C). The transformation of the amorphous to the crystalline phase was monitored in situ by Raman spectroscopy with high temporal resolution of ~30 sec. Homogeneous sub-samples of the solid and liquid phase were sampled over time in order to follow the chemical composition of the fluid, as well as changes in the mineralogy of the solid phase and its bulk Mg-isotope composition. The obtained results are presented and discussed in CHAPTER 3 to 6.

CHAPTER 3 deals with the formation of high Mg-calcite that occurs either via the transformation of an amorphous precursor phase or via direct nucleation from solution. This chapter highlights the importance of fluid alkalinity and aqueous Mg/Ca ratio on the enrichment of Mg in calcite (up to 20 mol% of Mg) throughout and subsequent to ACC transformation. Chapter 3 has been published in *Geochimica et Cosmochimica Acta 174 (2016) 180-195* (B. Purgstaller, V. Mavromatis, A. Immenhauser and M. Dietzel). The development of the experimental setup, the experimental runs and the chemical analyses required for this chapter were conducted by me. My co-authors supported me with data interpretation and when compiling the manuscript.

CHAPTER 4 provides new insights on Mg-isotope signatures of Mg-calcites formed in the presence or absence of an amorphous precursor phase. The experimental results are of relevance for the interpretation of isotopic signatures recorded in biominerals. Chapter 4 was accepted in

Earth and Planetary Science Letters 464 (2017) 227-236 (V. Mavromatis, B. Purgstaller, M. Dietzel, D. Buhl, A. Immenhauser and J. Schott). The text in this chapter was written by V. Mavromatis. I contributed the experimental work and the sample analysis to this chapter. Moreover, I repeatedly and critically reviewed and commented on the paper.

CHAPTER 5 contributes to a refined understanding of the mechanisms involved during the formation of Mg-calcite or monohydrocalcite via an amorphous precursor phase. Essentially, the effect of aqueous Mg^{2+} to Ca^{2+} activity ratios on Mg-ACC metastability and Mg-ACC transformation pathways is discussed. Chapter 5 has been published in *Crystal Growth & Design 17 (2017) 1069-1078* (B. Purgstaller, F. Konrad, M. Dietzel, A. Immenhauser and V. Mavromatis). For this chapter, I conducted all the experimental work and the sample analyses. Moreover, I evaluated the data and I worte the manuscript. My co-authors supported me with data interpretation and manuscript preparation.

CHAPTER 6 covers the effect of temperature on the (trans)formation of Mg-ACC. At low temperatures (< 12°C), the formation of ikaite rather than that of Mg-ACC occurs. This chapter discusses the temperature limits of ikaite formation in natural environments and the control of physicochemical conditions on the transformation of ikaite into anhydrous $CaCO_3$ polymorphs. Chapter 6 was submitted to *Geochimica et Cosmochimica Acta* (B. Purgstaller, M. Dietzel, A. Baldermann and V. Mavromatis). The experimental work and the chemical analyses required for this chapter were conducted by me. Furthermore, I evaluated the data and I wrote the manuscript. My co-authors provided useful suggestions and corrections during the preparation of the manuscript.

3. Transformation of Mg-bearing Amorphous Calcium Carbonate to Mg-calcite – In Situ Monitoring

Bettina Purgstaller[1], Vasileios Mavromatis[1,2], Adrian Immenhauser[3], Martin Dietzel[1]

[1]*Institute of Applied Geosciences, Graz University of Technology, Rechbauerstrasse 12, 8010 Graz, Austria*
[2] *Géosciences Environnement Toulouse (GET), CNRS, UMR 5563, Observatoire Midi-Pyrénées, 14 Av. E. Belin, 31400 Toulouse, France*
[3]*Institute of Geology, Mineralogy and Geophysics, Bochum, Universitätsstraße 150, 44801 Bochum, Germany*

Published in Geochimica et Cosmochimica Acta 174 (2016) 180–195

ABSTRACT

The formation of Mg-bearing calcite via an amorphous precursor is a poorly understood process that is of relevance for biogenic and abiogenic carbonate precipitation. In order to gain an improved insight on the controls of Mg incorporation in calcite formed via an Mg-rich amorphous calcium carbonate (Mg-ACC) precursor, the precipitation of Mg-ACC and its transformation to Mg-calcite was monitored by in situ Raman spectroscopy. The experiments were performed at 25.0 ±0.03°C and pH 8.3 ±0.1 and revealed two distinct pathways of Mg-calcite formation: (i) At initial aqueous Mg/Ca molar ratios ≤ 1:6, Mg-calcite formation occurs via direct precipitation from solution. (ii) Conversely, at higher initial Mg/Ca molar ratios, Mg-calcite forms via an intermediate Mg-rich ACC phase. In the latter case, the final product is a calcite with up to 20 mol % Mg. This Mg content is significant higher than that of the Mg-rich ACC precursor phase and that of the Mg-rich calcite formed without an ACC precursor. Thus, a strong net uptake of Mg ions from the solution into the crystalline precipitate throughout and also subsequent to ACC transformation is postulated. Moreover, the temporal evolution of the geochemical composition of the reactive solution and the Mg-ACC has no significant effect on the obtained "solubility product" of Mg-ACC. The enrichment of Mg in calcite throughout and subsequent to Mg-ACC transformation is likely affected by the high aqueous Mg/Ca ratio and carbonate alkalinity concentrations in the reactive solution. The experimental results have a bearing on the formation mechanism of Mg-rich calcites in marine early diagenetic environments, where high carbonate alkalinity concentrations are the rule rather than the exception, and on the insufficiently investigated inorganic component of biomineralisation pathways in many calcite secreting organisms.

3.1. INTRODUCTION

The nucleation and precipitation of biogenic and abiotic calcium carbonate minerals in natural settings has been the topic of numerous studies (e.g., Lowenstam, 1981; Reeder, 1990; Morse and Mackenzie, 1990; Weiner and Dove, 2003; Morse et al., 2007; Dietzel, 2011). The two most common calcium carbonate ($CaCO_3$) polymorphs in marine and meteoric depositional environments are calcite and aragonite. Moreover, the thermodynamically metastable polymorphs vaterite, monohydrocalcite, and ikaite have been documented in a wide range of precipitation environments, where they are volumetrically less important (Lowenstamm, 1981; Ito, 1993; Burchardt et al., 2001; Lu et al., 2012).

Former studies document that an important control of these different polymorphs is the Mg/Ca ratio of the parent fluid (Richelmann et al., 2014). In the calcite crystal lattice Ca^{2+} can be substituted by Mg^{2+} in significant amounts (e.g., Reeder, 1990; Böttcher and Dietzel, 2010). The quantity of Mg incorporation into calcite is related to the physicochemical conditions prevailing during its formation (e.g., Morse and Mackenzie, 1990), with the rate of crystal growth to likely be the most important mechanism (Mavromatis et al., 2013). At elevated fluid Mg/Ca ratios, inhibition of calcite precipitation from homogenous solutions results mostly in the formation of aragonite (e.g., Lippmann, 1973; Berner, 1975; Dietzel and Usdowski, 1996; De Choudens-Sanchez and Gonzalez, 2009; Wassenburg et al., 2012; Niedermayr et al., 2013). The most prominent kinetic barrier to calcite nucleation and growth is likely the dehydration of aqueous Mg prior to its incorporation into calcite lattice (Lippmann, 1973). Moreover, under increasing Mg contents, calcites become thermodynamically less stable at ambient conditions (Bischoff et al., 1987; Busenberg and Plummer, 1989; Böttcher et al., 1997; Bischoff, 1998). The formation of Mg-rich calcites with up to 44 mol% Mg, however, has been known to occur in abiotic and biotic precipitation environments. Under the present-day seawater Mg/Ca ratios (molar Mg/Ca ~ 5.2), early marine calcite cements with Mg contents of 12-20 mol% are precipitated in shallow tropical carbonate factories (Mackenzie et al., 1983), or where marine sediments are affected by anaerobic methane oxidation (Hensen et al., 2004; Peckmann et al., 2001; Schmidt et al., 2005; Mavromatis et al., 2014b). In biominerals, calcite with 20-44 mol% Mg has been reported from foraminifera (Bentov and Erez, 2005) and echinoderms such as starfish (Gayathri et al., 2007) or sea urchins teeth (Ma et al., 2009).

The interest in the formation pathways of crystalline $CaCO_3$ via an amorphous calcium carbonate (ACC) precursor phase has been established in the late 19th century (Krukenberg, 1882; Minchin, 1898). Over the years, numerous studies have focused on amorphous calcium carbonates with different short order ranges both in the biomineralization domain and with reference to inorganic carbonate precipitation environments (Aizenberg et al., 1996; Beniash et al., 1997; Griesshaber et al., 2009; Wehrmeister et al., 2012; Radha et al., 2012; Cartwright et al., 2012). Moreover, it has been documented that the presence of impurities such as Mg, plays an important role in stabilizing both natural and synthetic ACC (Raz et al., 2000; Raz et al., 2003; Rodriguez-Blanco et al., 2012). Along these lines, recent experimental studies report the synthesis of calcite with up to 50 mol% Mg via the transformation of Mg enriched ACC (Long et al., 2011; Wang et al., 2012a; Xu et al., 2014). Therefore, this formation pathway is of particular interest as it could explain some of the anomalous high Mg contents of calcites that are observed in biotic and abiotic precipitation environments. Finally, spatially disordered carbonate phases are also of great importance for medical and industrial applications (e.g., Meiron et al., 2011; Matsunuma et al., 2014).

These considerations form a strong motivation for the present study. Particularly, the formation of Mg-calcite from Mg-ACC is an aspect that is most likely significant but poorly understood. In order to shed light on the physicochemical parameters controlling the formation of Mg-calcite, we investigated the precipitation of Mg-ACC and its subsequent transformation to ordered crystalline carbonate minerals under controlled physicochemical conditions. Note that previous studies report the synthesis of Mg enriched calcite from ACC at high pH conditions (>9.5) by batch methods with $NaHCO_3/Na_2CO_3$ solutions (Long et al., 2011; Rodriguez-Blanco et al., 2012; Han et al., 2013) or by the ammonium carbonate diffusion technique (Wang et al., 2012a).

The present study aims at (1) establishing an experimental setup for Mg-ACC (trans)formation under conditions of quasi-constant temperature (25.00 ± 0.03°C) and pH (8.3 ±0.1); (2) monitoring of the mineralogical and chemical composition of resulting precipitates as a function of reaction time; (3) investigating the Mg uptake during Mg-rich ACC formation and its subsequent transformation to calcite and (4) assessing the role of Mg on Mg-ACC transformation kinetics and mechanisms. Note that earlier studies set a boundary of 12 mol% Mg between intermediate (4-12 mol%) and high Mg-calcite (>12 mol%) (Bischoff et al., 1987; Busenberg and Plummer, 1989; Böttcher et al., 1997; Bischoff, 1998). Calcite precipitated in the context of this

study qualifies as intermediate to high-Mg calcite. Here we use the catch-it-all term "Mg-calcite" to describe these precipitates.

3.2. METHODS

3.2.1. Experimental setup

Mg-ACC formation and transformation experiments were carried out at pH 8.3 and 25°C. The experimental setup used is illustrated in **Fig. 1A** and consists of two titrating units coupled with a temperature controlling Easy Max^{TM} 102 system (Mettler Toledo) equipped with a 150 ml borosilicate glass reactor (25.00 ±0.03°C). Initially 50 ml of a 1 M $NaHCO_3$ solution were placed in the reactor, which was stirred at 200 rpm. During the first 25 min of each experiment, 50 ml of a 0.6 M $(Ca,Mg)Cl_2$ solution was titrated into the reactor at a rate of 2 ml per min by a 702 SM Titrino titrator (Methrom), inducing precipitation of $Ca_{1-x}Mg_xCO_3$. The second titrating unit (Schott; TitroLine alpha plus) kept the pH of the reactive solution constant at pH 8.3 ±0.1 by automatic titration of a 1 M NaOH solution at addition steps of 0.1 ml at minimum (**Fig. 1B**). The pH was controlled in this way for the first 60 min of the reaction. Afterwards the reactive solution was transferred into a 150 ml glass bottle and was placed air-tight on a compact shaker (Edmund Bühler GmbH; KS-15) operating at 150 rpm in a temperature controlled room at 25 ±1°C. In order to gain precipitates for solid analyses and to monitor the solution chemistry during the experiment 5 ml of the reactive solution were sampled after 5, 12.5, 25, 60, 180 min and after 1, 3, and 14 days of reaction time. In addition after 1, 9, and 18 min of reaction time, 1 ml aliquots of the experimental solution were sampled and filtered only for solution analyses. The solids were separated by a 0.2 µm cellulose acetate filter using a suction filtration unit and were dried in a desiccator by using silica gel at room temperature.

All solutions were prepared by analytical grade chemicals ($CaCl_2{\cdot}2H_2O$, $MgCl_2{\cdot}6H_2O$ and $NaHCO_3$ from Roth) dissolved in ultrapure water (Millipore Integral 3: 18.2 $M\Omega cm^{-1}$). Prior to each experiment the pH of the $(Ca,Mg)Cl_2$ and $NaHCO_3$ solutions was adjusted to 8.3 ±0.1 using a diluted NaOH solution. The pH was measured with a Schott Blueline 28 combined electrode, which was calibrated against NIST buffer standard solutions at pH 4.01, 7.00 and 10.00. In total, 4 experiments were carried out in the presence of Mg. The Mg/Ca ratios used in the 0.6 M $(Ca,Mg)Cl_2$ solutions were 1:4, 1:5, 1:6, and 1:8, thus, the experiments are labeled as MgCa4, MgCa5, MgCa6 and MgCa8, where the number represents the multiple of the concentration of

Ca with respect to Mg (**Table 1**). A replicate of experiment MgCa4, hereafter mentioned as MgCa4_2, has been used to establish the reproducibility of the method. In addition, one experiment was carried out without Mg (MgCa0).

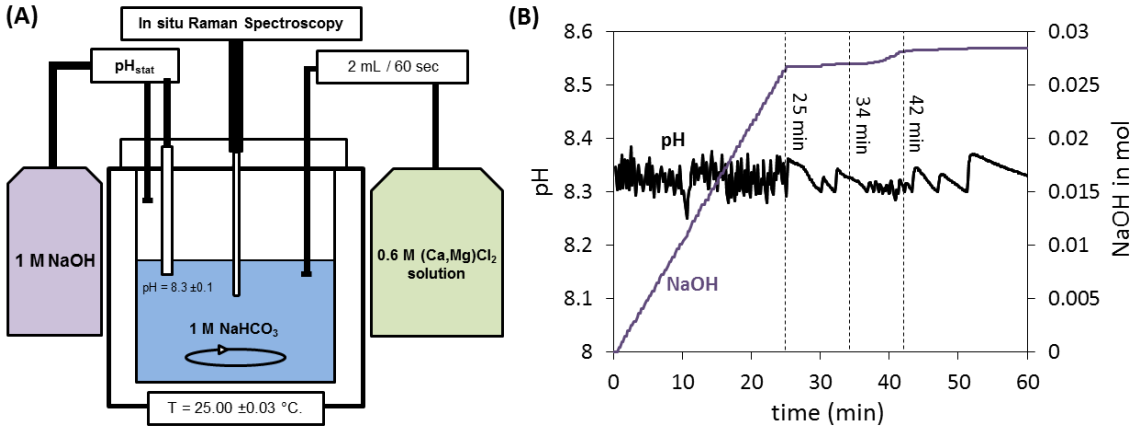

Fig. 1. (A) The experimental setup used for the precipitation of calcium carbonate during the experimental runs of this study. **(B)** Temporal evolution of the pH of the reactive solution and of the mole NaOH added to the experimental solution due to titration to keep the pH constant versus the time of experiment MgCa4. The titration of the $(Ca,Mg)Cl_2$ solution into the $NaHCO_3$ solution was stopped after a reaction time of 25 min. The transformation of Mg-ACC to Mg-calcite was indicated by Raman spectroscopy to occur between 34 and 42 min of experimental run time.

3.2.2. Analytical procedures

Aqueous cation concentrations were measured using ion chromatography (IC) unit (Dionex IC S 3000, IonPac® AS19 and CS16 column), with an analytical precision of ±3 %. The total alkalinity of the solutions was determined by a Schott TitroLine alpha plus titrator using a 0.02 M HCl solution, with an analytical precision of ±2 %. In situ Raman Spectroscopy of the reactive solution was carried out at a high temporal resolution using a RAMAN RXN2™ analyzer from Kaiser Optical Systems with a Kaiser MR Probe head equipped with a quarter-inch immersion optic. The Raman spectra were collected in the 100-1890 cm^{-1} region with a resolution of 1 cm^{-1} using a laser beam with an excitation wavelength of 785 nm. The in situ Raman spectra of the solution were acquired every 35 sec for 60 min after the onset of the experiment. At 180 min and 1, 3 and 14 days of reaction time Raman spectra were collected for 5 min. The baseline of the individual Raman spectra was corrected by the Pearson´s method using the iC Raman™ 4.1 software (Mettler Toledo).

Immediately after filtration the mineralogy of the collected solids was determined using an Attenuated Total Reflectance - Fourier Transform Infrared Spectroscope (ATR-FTIR; Perkin

Elmer Spektrum 100) in the range 450 to 4000 cm^{-1}. X-ray powder diffraction (XRD) patterns of the dried precipitates were recorded by PANalytical X´Pert PRO diffractometer using Co-Kα-radiation (40mA, 40kV) at a 2θ range from 4° to 85° and a scan speed of 0.03° s^{-1}. The mineral phases were quantified by Rietveld refinement using the PANalytical X'Pert HighScore Plus software with the PDF-2 database. Amorphous phases were not considered for quantification, as the dried samples that were analyzed had been completely transformed to crystalline products.
Selected precipitates were gold-coated and imaged using a ZEISS DSM 982 Gemini scanning electron microscope (SEM) operating at 5 kV accelerating voltage. The Mg content of the solids (in mol%) sampled at a given reaction time was calculated according to the equation:

$$[Mg]_{solid} = \frac{n_{Mg_{add}} - [Mg]_{aq}}{n_{Mg_{add}} - [Mg]_{aq} + n_{Ca_{add}} - [Ca]_{aq}} \times 100 \quad (1)$$

where $n_{Mg_{add}}$ and $n_{Ca_{add}}$ are the amount of titrated moles of Mg and Ca per liter in the reactive solution, after correction for volume changes and $[Mg]_{aq}$ and $[Ca]_{aq}$ are the measured molar concentrations of Mg and Ca in the reactive solutions. The error of this method was estimated to be ±5 %. The calculated $[Mg]_{solid}$ values obtained from Eq. 1 are in very good agreement with the Mg contents of solid measured after digestion of selected solid samples in 6% HNO3 (**Appendix A1a**). The analytical precision of the latter measurement is ±3%.

3.2.3. Hydrochemical modelling

The aqueous speciation of the reactive solutions, ion activities and saturation degrees were calculated using the PHREEQC software in combination with its minteq.v4 database. The formation reaction for Mg-calcite and Mg-ACC is defined according to the equation:

$$(1\text{-}x)\ Ca^{2+} + x\ Mg^{2+} + CO_3^{2-} \rightleftarrows Ca_{1-x}Mg_xCO_3 \quad (2)$$

Earlier studies have argued that 1 to 2 molecules of H_2O may be present per mole unit in amorphous calcium carbonate (Radha et al., 2012). In Eq. 2, however, H_2O is not present as we assume its activity to be 1 in our experimental solutions. For the estimation of the saturation state (Ω) of Mg-calcite we used the solubility products (K_{sp}) of Mg-calcite reported by Busenberg and Plummer (1989). The ion activity product for $Ca_{1-x}Mg_xCO_3$, such as Mg-calcite and Mg-ACC, was determined as:

$$IAP = (a_{Ca^{2+}})^{1-x} (a_{Mg^{2+}})^{x} (a_{CO_3^{2-}}) \quad (3)$$

where *a* denotes the activity of the i^{th} species in solution and *x* is the mole fraction of $MgCO_3$ in the precipitated solid phase ($Mg_{[solid]}$ in **Table 1**; see Eq. 2). The Ω with respect to ACC is expressed by

$$\Omega_{ACC} = \frac{(a_{Ca^{2+}}) - (a_{CO_3^{2-}})}{K_{sp}} \quad (4)$$

where $K_{sp} = 10^{-6.39}$ at 25°C (Brečević and Nielsen, 1989). Note here that the latter value refers to ACC that does not contain Mg.

3.3. RESULTS

3.3.1. Chemical evolution of the reactive solutions

The aqueous compositions of the reactive solutions are reported in **Table 1**. In experiments MgCa4, MgCa5, and MgCa6 the pH decreased from 8.35 ±0.05 to 8.16 ±0.01 between 180 min and 1 day of reaction time. In contrast, the pH of the reactive solution remained near-stable at 8.38 ± 0.07 in experiment MgCa8 and increased from 8.39 to 8.51 in experiment MgCa0. The titration of the $(Ca,Mg)Cl_2$ solution in the reactor caused the nucleation/precipitation of magnesium-rich calcium carbonate. Accordingly, the carbonate alkalinity decreased from 1 M down to an overall value of ~0.1 M after 25 min of reaction time. The temporal decrease of carbonate alkalinity is similar in all experimental runs (**Table 1**). Chemical steady state condition with respect to carbonate alkalinity was attained after about 60 min of reaction time.

The $[Ca]_{aq}$ of the reactive solutions did not exceed 0.006 M due to instant nucleation/precipitation of $CaCO_3$. After the titration of the $(Ca,Mg)Cl_2$ solution was stopped, about 98 % of the $n_{Ca_{add}}$ was removed from the reactive solution. The $[Mg]_{aq}$ of the reactive solution significantly increased over time during the addition of the $(Ca,Mg)Cl_2$ solution (**Fig. 2A**). After 25 min of reaction time about 45 % of the $n_{Mg_{add}}$ was incorporated into $CaCO_3$ in experiments MgCa4, MgCa5 and MgCa6. The $[Mg]_{aq}$ in the latter experiments, however, decreased significantly after 25 min of reaction time (**Fig. 2A**), and the overall removal of $n_{Mg_{add}}$ increased to about 85 % after

1 day. In contrast in experiment MgCa8 the $[Mg]_{aq}$ remained constant at about 0.009 M between 25 min and 14 days, which accounts for a consumption of about 65 % of the n_{Mgadd}.

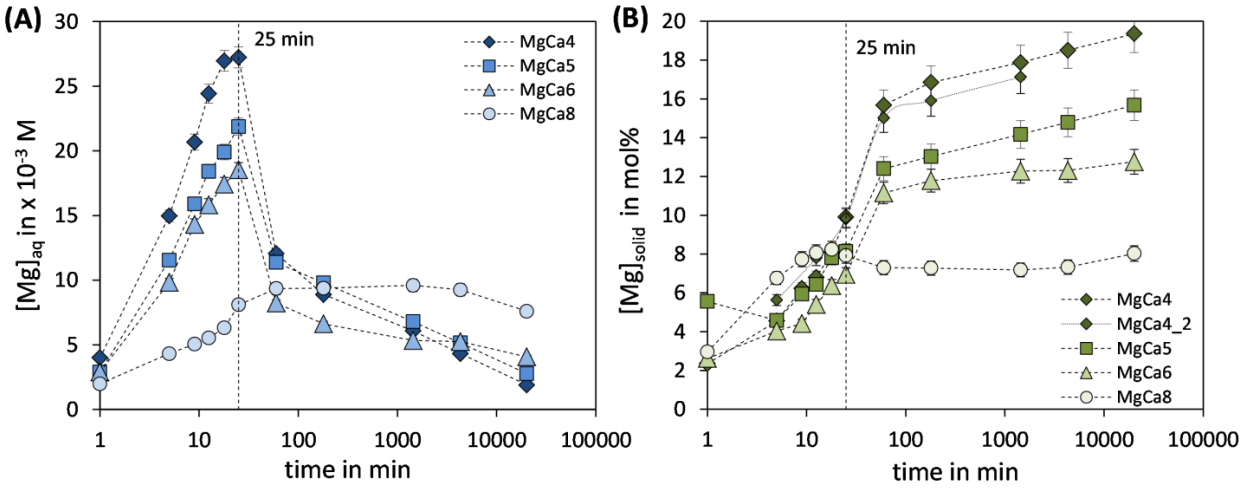

Fig. 2. (A) Concentration of dissolved Mg ions of the reactive solution and **(B)** Mg content of the precipitated solid, $[Mg]_{solid}$, calculated according to Eq. 1, versus the experimental run time. The titration of the $(Ca,Mg)Cl_2$ solution into the $NaHCO_3$ solution was stopped after 25 min of experimental run time. Analytical uncertainty is included in symbol size.

3.3.2. Temporal evolution of the solid Mg composition

The temporal evolution of the $[Mg]_{solid}$ in all experiments is shown in **Fig. 2B** and reported in **Table 1**. The progressive increase of the $[Mg]_{aq}$ within 25 min of reaction time (**Fig. 2A**) is accompanied with an increase of the $[Mg]_{solid}$. The highest $[Mg]_{solid}$ values are obtained at experiment MgCa4. As illustrated in **Fig. 2B**, $[Mg]_{solid}$ in experiments MgCa4, MgCa5, and MgCa6 continues to increase considerably after 25 min of reaction time. This is despite the fact that the injection of the $(Ca,Mg)Cl_2$ solution was stopped and a decrease of the carbonate alkalinity was not detected (**Table 1**). The increase of the $[Mg]_{solid}$ is similar in experiment MgCa4 and in the replicate experiment MgCa4_2 (**Fig. 2B**). The overall variability of the $[Mg]_{solid}$ values between these replicate experiments is below ±1 mol% of Mg in $CaCO_3$.

A slight decrease of carbonate alkalinity due to subsequent mineral precipitation was monitored for experiment MgCa4 between 34 and 42 min by the consumption of NaOH keeping the pH constant (see NaOH content due to titration in **Fig. 1B**). In experiment MgCa8, the $[Mg]_{solid}$ remained constant at about 8 mol% between 5 min and 14 days of reaction time (**Fig. 2B**).

3.3.2. In situ determination of aqueous carbonate species

The in situ Raman spectroscopy allows a qualitative monitoring of aqueous carbonate species during the experimental runs. In all experiments performed in the context of this study, aqueous HCO_3^- exhibits vibrations at 1017 cm^{-1} (C-OH stretch), 1363 cm^{-1} (symmetric stretch), 634 cm^{-1}, and 675 cm^{-1} (HO-CO-bend), whereas aqueous CO_3^{2-} has a single vibration band at 1067 cm^{-1}. These vibration bands are similar to those reported in the literature (Oliver and Davis 1972; Souchon et al., 2011; Geisler et al., 2012). The initial intensity of the vibration band of dissolved HCO_3^- is significantly higher than the intensity of the dissolved CO_3^{2-} (**Fig. 3**), owing to the predominance of HCO_3^- aqueous species at the working pH 8.3. During the experimental runs however, the intensity of the characteristic HCO_3^- vibration band at 1017 cm^{-1} decreased rapidly due to subsequent precipitation of Mg-ACC (see v_1 in **Fig. 3**). Note here that although carbonate alkalinity concentrations are above 0.1 M after 25 min (**Table 1**), the characteristic HCO_3^- peak is barely visible (**Fig. 3**) owing to detection limitations of in situ Raman spectroscopy.

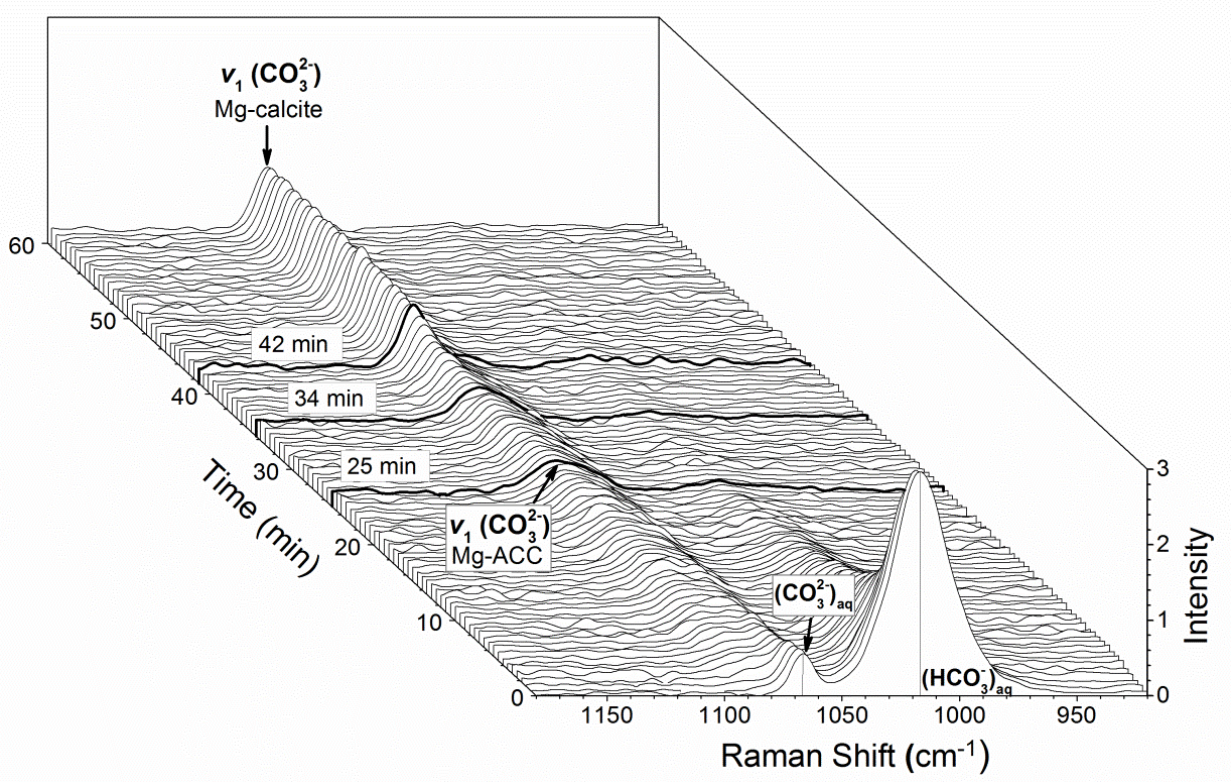

Fig. 3. Waterfall plot of Raman spectra showing the vibration band of aqueous HCO_3^- ($(HCO_3^-)_{aq}$) aqueous CO_3^{2-} ($(CO_3^{2-})_{aq}$) and of v_1 band of CO_3^{2-} related to Mg-ACC/Mg-calcite collected by *in situ* Raman spectroscopy within 60 min of reaction time of experiment MgCa4.

3.3.3. Solid phase characterization

Raman spectroscopic analysis

The Raman spectra of amorphous calcium carbonate are characterized by the presence of a broad carbonate symmetric stretching band (ν_1) at 1080-1088 cm^{-1} and the absence of lattice modes (libration and translation mode) at lower frequencies (Wang et al., 2012b; Addadi et al., 2003). The Raman peak positions and maximum intensities (I_{max}) of the ν_1 vibration band and of the libration mode detected after certain experimental times are given in **Table A1** in the **Appendix**.

The collected in situ Raman spectra in the experiment MgCa4 showed that Mg-ACC was present during the addition of the $(Ca,Mg)Cl_2$ solution, as it is indicated by the increase of the intensity of the ν_1 vibration band of solid CO_3^{2-} at 1085 ±1 cm^{-1} (**Fig. 3**). After the titration of the $(Ca,Mg)Cl_2$ solution stopped, the maximum intensity (I_{max}) of the ν_1 vibration band of Mg-ACC remained constant between 25 and 34 min of reaction time (**Figs. 3 and 4**). Upon this time point the I_{max} of the ν_1 vibration band increased rapidly (**Fig. 3 and 4**) indicating the transformation of Mg-ACC to a crystalline phase (Addadi et al., 2003; Rodriguez-Blanco et al., 2008). The formation of Mg-calcite was confirmed by the contemporaneous rise of the libration mode at 286 ±1 cm^{-1} (Bischoff et al., 1985). In the context of Mg-ACC to Mg-calcite transformation the frequency of the ν_1 vibration band moved from 1085 ±1 cm^{-1} to 1089 ±1 cm^{-1} (**Fig. 3, Table A1** in **Appendix**). In the experiments MgCa5 and MgCa6 the transformation of Mg-ACC to Mg-calcite was observed earlier, after 26 and 15 min of reaction time, respectively, as it was indicated by the rapid increase of the I_{max} of ν_1 band (**Fig. 4**) and the rise of the intensity of the libration mode of Mg-calcite at 284 ±1 cm^{-1} (**Table A1, Appendix**). In the experiment MgCa8 the intensity of the ν_1 band (**Fig. 4**) and of the libration mode of Mg-calcite increased immediately after the onset of the experimental run. The frequency of the ν_1 band remained constant at 1087 ±1 cm^{-1}. After 1 day of reaction time the presence of aragonite was indicated in addition to Mg-calcite by a weak Raman band at 205 cm^{-1} (Edwards et al., 2005). In the experiment MgCa0 the in situ Raman spectra showed a rise of the intensity of the vibration bands at 1074 ±1 cm^{-1}, 1086 ±1 cm^{-1} and of the libration mode of calcite at 281 ±1 cm^{-1} during the addition of the $CaCl_2$ solution. The presence of a double ν_1 vibration band at 1074 cm^{-1} and 1089-1090 cm^{-1} in the experiment MgCa0 (**Table A1, Appendix**) is characteristic of vaterite (Kontoyannis and Vagenas, 2000; Gabrielli et al., 2000). As it can be seen in **Fig. 4** the I_{max} of the ν_1 vibration band at 1086 ±1 cm^{-1} continues to increase after 25 min of reaction time. After the duration of one experimental day,

the intensity of the v_1 band at 1086 ±1 cm^{-1} has risen significantly, while the v_1 band at 1074 ±1 cm^{-1} was no longer visible (**Table A1, Appendix**). The occurrence of the libration mode at 281 cm^{-1} indicates the presence of calcite.

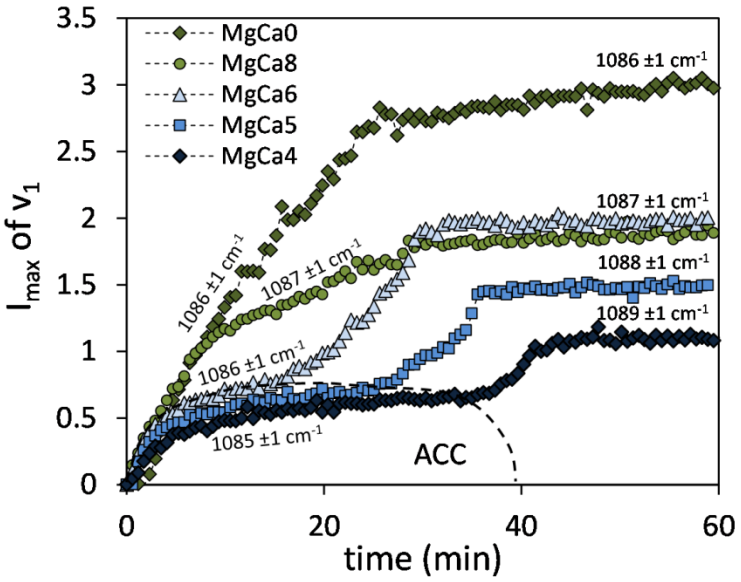

Fig. 4. Evolution of the maximal intensity (I_{max}) of the v_1 vibration band of solid CO_3^{2-} during 60 minutes of reaction time for all experiments, where individual wave numbers at I_{max} are given. The transformation of Mg-ACC to Mg-calcite is indicated by the rapid increase of I_{max} (dotted line) in experiments with Mg/Ca ratios ≥ 1:6.

ATR-FTIR spectra analysis

The observed infrared frequencies of characteristic carbonate v_1, v_2, and v_4 vibration bands of all analyzed solid samples are given in **Table A1** in the **Appendix**. The lack of the v_4 absorption band at ~713 cm^{-1} and the presence of broad v_1 and v_2 bands at 1073-1075 cm^{-1} and 860-861 cm^{-1}, respectively, in the ATR-FTIR analyses are indicative of the presence of an amorphous carbonate phase in the sampled precipitates. The presence of these bands are in agreement with published FTIR data at 1065-1075 cm^{-1} (v_1) and at 860-873 cm^{-1} (v_2) (Addadi et al., 2003; Loste et al., 2003) for ACC. In experiments MgCa4 and MgCa5, Mg-ACC was found in precipitates sampled after 13 and 25 min of reaction time, respectively (experiment MgCa4 in **Fig. 5a**). The analyzed ACC spectra from our experiments are in good agreement with ACC reference material that was synthesized following the approach described in Rodriguez-Blanco et al. (2012) (**Fig. 5a**). The transformation of Mg-ACC to Mg-calcite is indicated by the rise of the v_4 band at 711-713 cm^{-1} and the shift of the v_2 and v_1 bands from 860-861 to 871-872 cm^{-1} and from 1073-1074 to 1082-1085 cm^{-1}, respectively (**Fig. 5a**). These vibration bands are characteristic of Mg-calcite

(White, 1974; Böttcher et al., 1997; Loste et al., 2003; Mavromatis et al., 2012). The occurrence of the v_1 band at 1082-1085 cm^{-1}, which is not infrared active in well-ordered calcite, is caused by incorporation of Mg in the calcite structure (White, 1974; Böttcher et al., 1997). The v_2 band of Mg-calcite is sharper than that of ACC (**Fig. 5a**) a feature that is consistent with data shown in Addadi et al. (2003). In experiments MgCa6 and MgCa8, all of the analyzed ATR-FTIR spectra show characteristics of Mg-calcite, whereas in situ Raman spectra of experiment MgCa6 are indicative of the presence of ACC during 15 min of reaction time. Note that a weak v_4 band at 700 cm^{-1} of aragonite was present after 25 min of reaction time in experiment MgCa8 (**Table A1**, **Appendix**). In experiment MgCa0, the ATR-FTIR spectra of the precipitates that were sampled during 180 min of reaction time showed strong vibration bands at 744 cm^{-1} and 1088 cm^{-1} corresponding to the v_4 and v_1 band of vaterite (Dupont et al., 1997) and a weak band of calcite at 712 cm^{-1} (**Table A1**, **Appendix)**. In the solids collected after 1 day, the characteristic bands of vaterite were absent. This is in good agreement with the results obtained by in situ Raman spectroscopy.

X-ray diffraction

Quantitative XRD results show that the dried precipitates of experiments MgCa4, MgCa5 and MgCa6 mainly consist of Mg-calcite (≥ 96 wt.%) and traces of aragonite (up to 4 wt.%) as reported in **Table 2**. In experiment MgCa8, minor amounts of aragonite (1-17 wt.%) and vaterite (up to 13 wt.%) were detected besides Mg-calcite (≥ 83 wt.%). The precipitates of experiment MgCa0 (5 to 180 min of reaction time) consist of vaterite (0 - 90 wt.%) and calcite (10 - 27 wt.%). Vaterite was absent from the collected solids after 180 min and 1 day of reaction time, respectively in experiments MgCa8 and MgCa0 **(Table 2)**. The XRD patterns of the precipitates sampled after 24h of reaction time show that the $d_{(104)}$ calcite characteristic peak exhibits an increase from 2.99 to 3.01 Å (**Fig. 5b**), which is in agreement with the decrease of the $[Mg]_{solid}$ in experiments MgCa4, MgCa5, MgCa6, and MgCa8 (**Fig. 2b**). The Mg content was calculated from the d_{104} according to the approach shown in Goldsmith et al. (1961), $[Mg]_{solid(XRD)}$, ranges from 15 to 7 mol% in experiment MgCa4, MgCa5, MgCa6, and MgCa8, respectively. Note that, the uncertainty in this calculation is about ±1 mol% of Mg. The calculated $[Mg]_{solid(XRD)}$ values are in good agreement with the Mg contents calculated from solid digestion (**Fig. A1b**, **Appendix**).

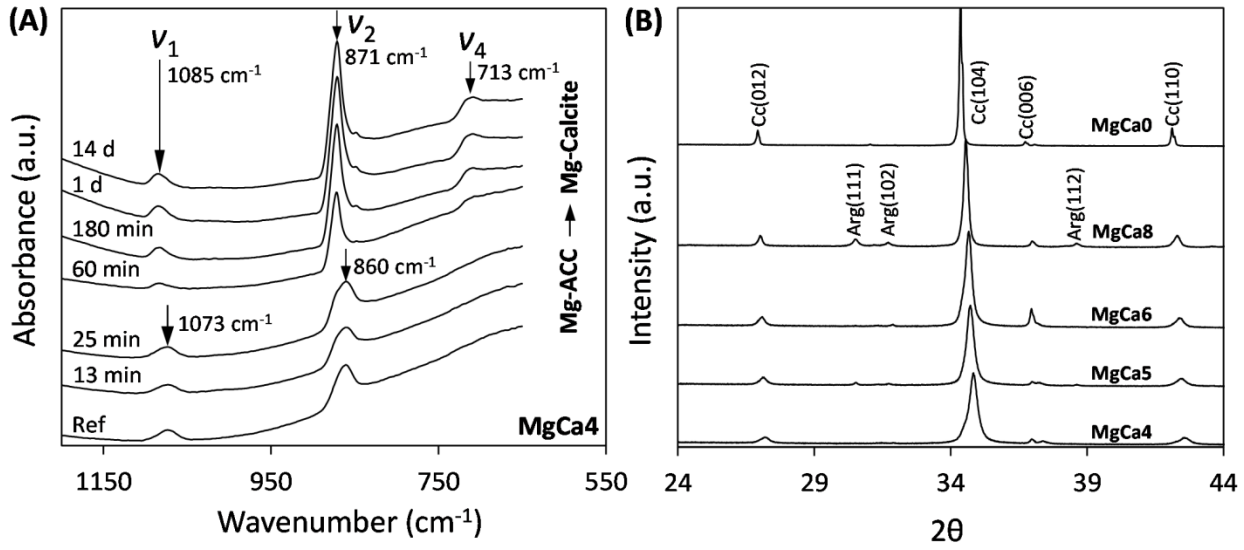

Fig. 5. (A) ATR-FTIR spectra of sampled precipitates at certain reaction times of the experiment MgCa4 and of an ACC reference (Ref) synthesized according to Rodriguez-Blanco et al., 2012 (*experiment 3*). **(B)** XRD pattern of solids obtained after 1 day of reaction time from all experiments.

Scanning electron microscopy observations

Mg-ACC sampled in experiments MgCa4, MgCa5, and MgCa6 were completely transformed to Mg-calcite within about 30 min after sample filtration. Thus, SEM images of synthesized Mg-ACC could not be realized. The SEM images of the precipitates of experiments MgCa4, MgCa5, and MgCa6, sampled after 60 min of reaction time, indicate Mg-calcite aggregates consisting of sub- to anhedral nanocrystals (experiment MgCa4, **Fig. 6A and B**). Note that SEM images are not shown for experiments MgCa5 and MgCa6 as the precipitated solids show morphologies that are similar to from experiment MgCa4. During the experimental runs of experiments MgCa4, MgCa5, and MgCa6, no significant changes in shape and size of the Mg-calcite crystals and aggregates were observed. In experiment MgCa8, the sampled Mg-calcite display aggregates of aligned rhombohedral crystals (**Fig. 6C**). These crystals are larger in size than those resulting from experiments MgCa4 (**Fig 6A**), MgCa5 and MgCa6. Furthermore needle-like aragonite, about 4 µm in size, was recognized in experiment MgCa8 (**Fig 6D**). The vaterite precipitates observed after the onset of experiment MgCa0 consists of large spherical aggregates (**Fig. 6E**) composed of nanoparticles < 100 nm in size. Calcite end products are euhedral and subhedral in morphology (**Fig. 6F**).

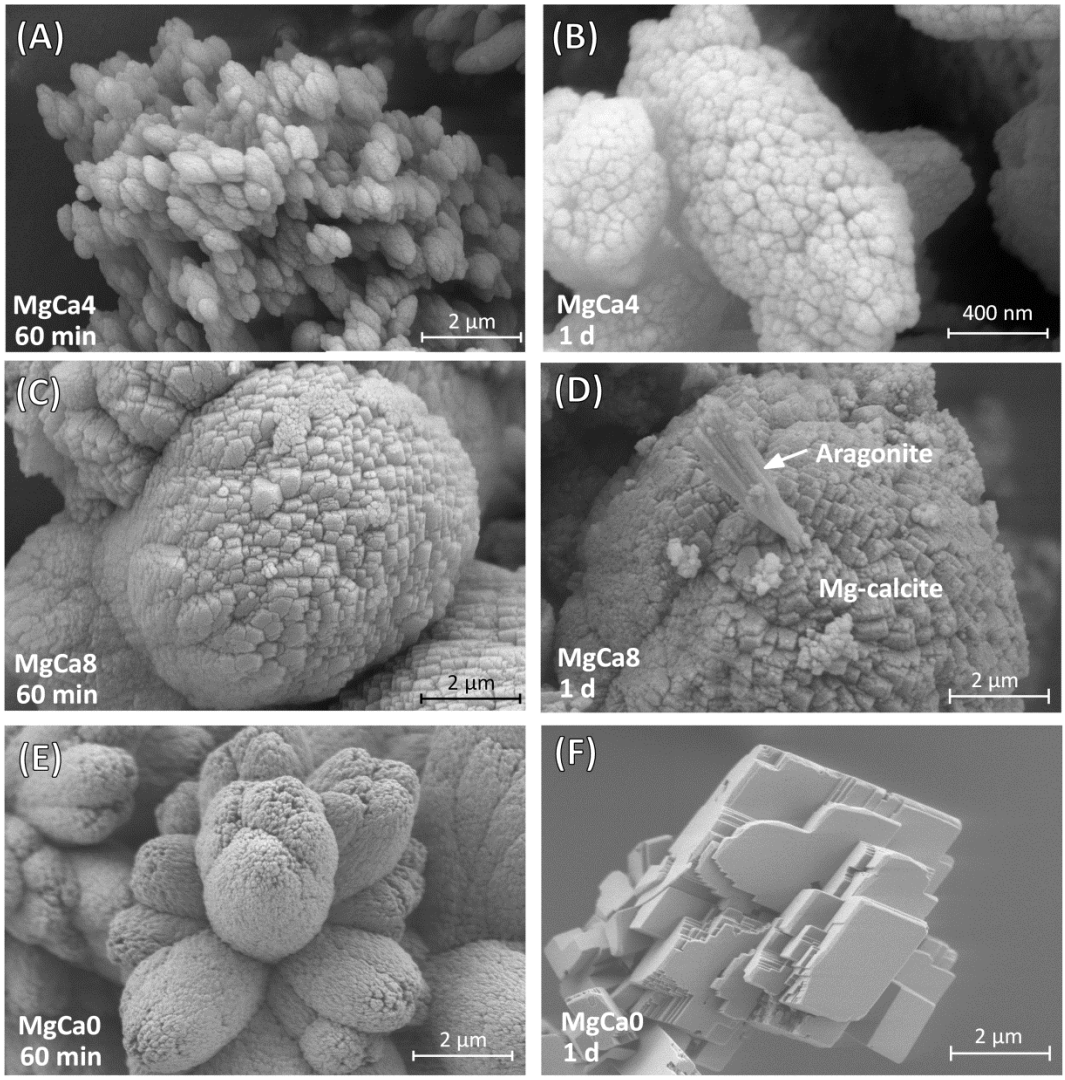

Fig. 6. SEM images of sampled precipitates from experiment MgCa4 after 60 min **(A)** and 1 day **(B)** of reaction time, from experiment MgCa8 after 60 min **(C)** and 1 day **(D)** of reaction time and from experiment MgCa0 after 60 min **(E)** and 1 day **(F)** of reaction time.

Table 1

Chemical composition of experimental solutions, Mg/Ca: Mg to Ca ratio of the 0.6 M $(Ca,Mg)Cl_2$ solution; time: reaction time during the experimental run; pH: pH of the reactive solution; $[Ca]_{aq}$, $[Mg]_{aq}$: Ca and Mg concentration of the reactive solution; $n_{Ca_{add}}$, $n_{Mg_{add}}$: amount of moles of Ca and Mg added in the reactive solution; Alkalinity: carbonate alkalinity of the reactive solution; $[Mg]_{solid}$: Mg content of the solid calculated according to Eq. 1.

Experiment	Mg/Ca	time	pH	$[Ca]_{aq}$	$[Mg]_{aq}$	$n_{Ca_{add}}$	$n_{Mg_{add}}$	Alkalinity	$[Mg]_{solid}$
		min/d		x 10^{-3} M	x 10^{-3} M	x 10^{-3} M	x 10^{-3} M	x 10^{-3} M	mol%
		0 min	8.37	-	-	-	-	1020	-
		1 min	8.31	2.78	4.00	17.41	4.35	977	2.34
		5 min	8.31	3.69	14.97	73.12	18.28	707	4.54
		9 min	8.30	3.66	20.68	111.30	27.82	491	6.22
		13 min	8.35	3.84	24.42	136.29	34.07	380	6.79
MgCa4	1:4	18 min	8.36	4.15	26.96	164.20	41.05	226	8.09
		25 min	8.36	6.18	27.23	190.80	47.70	119	9.98
		60 min	8.33	0.39	12.06	186.92	46.73	94	15.67
		180 min	8.30	0.20	8.89	186.92	46.73	89	16.85
		1 d	8.16	0.14	6.08	186.92	46.73	81	17.87
		3 d	8.07	0.13	4.32	186.92	46.73	82	18.50
		14 d	8.13	0.16	1.89	186.92	46.73	72	19.36
		0 min	8.32	-	-	-	-	1016	-
		1 min	8.31	0.36	2.89	20.30	4.06	971	5.69
		5 min	8.29	0.43	11.55	75.80	15.16	705	4.58
		9 min	8.33	0.39	15.90	115.91	23.18	500	5.93
		13 min	8.31	0.52	18.42	140.09	28.02	399	6.44
MgCa5	1:5	18 min	8.32	0.61	19.91	172.46	34.49	237	7.82
		25 min	8.37	0.67	21.87	195.78	39.16	130	8.14
		60 min	8.37	0.39	11.38	193.90	38.78	114	12.40
		180 min	8.40	0.39	9.79	193.90	38.78	111	13.03
		1 d	8.17	0.14	6.79	193.90	38.78	108	14.17
		3 d	8.12	0.18	5.15	193.90	38.78	102	14.79
		14 d	8.18	0.18	2.77	193.90	38.78	96	15.67
		0 min	8.33	-	-	-	-	1015	-
		1 min	8.30	1.62	2.90	20.40	3.40	968	2.62
		5 min	8.30	0.15	9.83	78.82	13.14	684	4.03
		9 min	8.31	0.53	14.31	118.62	19.77	479	4.42
		13 min	8.31	0.11	15.83	144.38	24.06	378	5.40
MgCa6	1:6	18 min	8.25	0.35	17.43	176.46	29.41	217	6.37
		25 min	8.31	0.19	18.53	201.42	33.57	113	6.95
		60 min	8.31	0.33	8.23	199.34	33.23	96	11.19
		180 min	8.30	0.23	6.62	199.34	33.23	92	11.81
		1 d	8.17	0.06	5.34	199.34	33.23	90	12.30
		3 d	8.12	0.08	5.25	199.34	33.23	86	12.33
		14 d	8.12	0.12	4.07	199.34	33.23	87	12.78
		0 min	8.32	-	-	-	-	1015	-
		1 min	8.30	0.92	1.99	20.76	2.59	986	2.96
		5 min	8.30	0.12	4.32	82.12	2.59	674	6.76
		9 min	8.34	0.14	5.05	122.48	10.27	450	7.73
		13 min	8.31	0.14	5.54	148.63	15.31	360	8.07
MgCa8	1:8	18 min	8.34	0.33	6.32	178.93	18.58	186	8.25
		25 min	8.27	0.64	8.10	206.52	22.37	88	7.92
		60 min	8.31	0.45	9.35	201.40	25.81	55	7.30
		180 min	8.35	0.28	9.38	201.40	25.17	48	7.28
		1 d	8.32	0.14	9.60	201.40	25.17	57	7.18

		3 d	8.41	0.14	9.25	201.40	25.17	61	7.33
		14 d	8.45	0.15	7.59	201.40	25.17	55	8.03
		0 min	8.34	-	-	-	-	1025	-
		1 min	8.33	2.82	-	25.77	-	945	-
		5 min	8.33	0.15	-	91.80	-	670	-
		9 min	8.34	0.14	-	133.02	-	479	-
		13 min	8.31	0.11	-	166.25	-	344	-
MgCa0	0:1	18 min	8.29	0.19	-	200.32	-	169	-
		25 min	8.29	0.36	-	230.28	-	81	-
		60 min	8.42	0.19	-	230.28	-	87	-
		180 min	8.39	0.07	-	230.28	-	89	-
		1 d	8.56	0.03	-	230.28	-	92	-
		3 d	8.54	0.01	-	230.28	-	93	-
		14 d	8.56	0.05	-	230.28	-	104	-

Table 2
Mineralogical composition of precipitates sampled after 180 min and 1 day of reaction time. The quantification was realized by Rietveld refinement. Values are given in wt.%. The weighted profile R-factor ranges between 9 and 14. Small amounts of halite (3 ±1 wt.%) occur in the precipitates due to drying, except in experiment CaMg8.

Experiment	time min/d	(Mg-) Calcite	Aragonite	Vaterite
	25 min	100	-	-
MgCa4	180 min	100	-	-
	1d	100	-	-
	25 min	100	-	-
MgCa5	180 min	96	4	-
	1d	96	4	-
	25 min	100	-	-
MgCa6	180 min	100	-	-
	1d	100	-	-
	5 min	87	-	13
	13 min	91	1	8
	25 min	86	9	5
MgCa8	180 min	85	15	-
	1d	83	17	-
	5 min	27	-	73
	13 min	18	-	82
	25 min	10	-	90
MgCa0	180 min	20	-	80
	1d	100	-	-

3.4. DISCUSSION

3.4.1 In situ monitoring of $Ca_{1-x}Mg_xCO_3$ formation

Mg-ACC formation and its subsequent transformation to Mg-calcite

The collected Raman spectra reveal that the formation of Mg-calcite in the experimental runs took place by two distinctive reaction mechanisms, either through an Mg-ACC precursor or directly from the fluid phase.

In experiments MgCa4, MgCa5, and MgCa6, the initially formed Mg-ACC acts as a precursor of the Mg-calcite. The Raman v_1 band of ACC is significantly broadened compared to that of crystalline phases owing to its poorly ordered structure (Addadi et al., 2003; Rodriguez-Blanco et al., 2008). The obtained results demonstrate that the increase of the maximum intensity of (I_{max}) of the v_1 Raman vibration band can be used to follow the Mg-ACC to Mg-calcite transformation (**Fig. 4**). The formation of Mg-calcite from Mg-ACC was further confirmed by the contemporaneous rise of the lattice vibration; amorphous phases do not exhibit lattice vibration. In experiments MgCa4, MgCa5, and MgCa6, the transformation of Mg-ACC to Mg-calcite occurs rapidly, i.e. within 12 ±4 min of reaction time (**Fig. 4**). It is likely that the bulk of the Mg-ACC is transformed to Mg-calcite as soon as the I_{max} of the v_1 vibration band exhibits constant values over time (**Fig. 4**). Given that the v_1 band of Mg-ACC cannot be distinguished from that of Mg-calcite, the presence of minor amounts of Mg-ACC for prolonged periods of time cannot be excluded at this stage.

In the context of Mg-ACC to Mg-calcite transformation, the Raman v_1 band shifted to higher frequencies in experiments MgCa4, MgCa5, and MgCa6 (**Fig. 4** and **Table A1** in **Appendix**). This likely occurs due to the substitution of Ca^{2+} by Mg^{2+} ions in ACC and calcite that causes a decrease in the average length of the metal-oxygen bond due to the shorter Mg-O bonds compared to Ca-O bonds in the solid phase (Bischoff et al., 1985; Wang et al., 2012b). Indeed, the evolution of the $[Mg]_{solid}$ suggests that the incorporation of Mg in the Mg-calcite lattice continues throughout Mg-ACC transformation in experiments MgCa4, MgCa5, and MgCa6 (Fig. 2b).

As illustrated in **Fig. 4**, the relative intensities of the v_1 vibration band differ among the various experiments. Raman spectroscopic studies showed that the peak broadening of the Raman v_1 band is correlated with the increased Mg content in calcite and ACC (Bischoff et al., 1985; Falini

et al., 1998; Wang et al., 2012b). This feature is probably linked to the Mg-induced positional disorder of the CO_3^{2-} group (Bischoff et al., 1985). In our study, the relative intensities of the ν_1 band reveal that the Mg content in ACC in experiment MgCa4 is slightly higher than of that in experiments MgCa5 and MgCa6 (**Fig. 4**). Michel et al. (2008) suggested that OH^- groups may possibly play a role within the ACC structure. However, during Mg-ACC formation in experiments MgCa4, MgCa5, and MgCa6 less than 0.01 % of the total $[Mg]_{aq}$ and $[Ca]_{aq}$ is bounded in $MgOH^+$ and $CaOH^+$ aquo-complexes, owing to the moderate alkaline pH of 8.3. Moreover, Raman and ATR-FTIR spectra do not indicate the presence of distinct OH^- vibrations for Mg-OH and Ca-OH units within the precipitates. Thus rigid OH^- groups are not suggested to play a significant role in the Mg-ACC structure of the present experiments. Nuclear magnetic resonance spectroscopy studies on Mg-ACC recently showed that the coordination shell of Mg in Mg-ACC contains at least one water molecule (Lin et al., 2015). The longer lasting occurrence of Mg-ACC in experiment MgCa4 (~34 min) compared to experiment MgCa6 (~15 min) can be likely attributed to the structural water bound to Mg ions that retards the process of dehydration (Lin et al., 2015). In experiments with lower Mg contents, sampled Mg-ACC transformed to Mg-calcite in a short time after the filtration. As such, a discrepancy between the in situ Raman and ATR-FTIR results is observed in experiment MgCa6 (**Table 2**). This pattern clearly highlights the importance of time-resolved in situ analyses in order to capture the near-instantaneous transformation of Mg-ACC to Mg-calcite in this highly dynamic system.

In contrast to experiments MgCa4, MgCa5, and MgCa6, experiment MgCa8 displays Mg-calcite precipitation from solution immediately after the onset of the experimental run in the Raman spectra (**Table A1**, **Appendix**). The absence of Mg-ACC in experiment MgCa8, however, cannot be established beyond doubt owing to the overlapping of ν_1 characteristic Mg-ACC band with that of Mg-calcite. The direct formation of Mg-calcite in experiment MgCa8 is, however, supported by the observation of aligned rhombohedral crystals in SEM images (**Fig. 6C**). These rhombohedral crystals are significantly larger in size than the nanocrystals in experiments MgCa4, MgCa5, and MgCa6, where Mg-ACC was clearly detected after the onset of the experimental run (experiment MgCa4, **Fig. 6B**).

Vaterite formation and its subsequent transformation to calcite

Similar to experiment MgCa8, no formation of ACC was observed in the Mg-free experiment MgCa0. The in situ Raman spectra of this experiment point towards formation of calcite via a

vaterite precursor, a common reaction path for calcite formation via dissolution/ reprecipitation (Ogino et al., 1987; Rodriguez-Blanco et al., 2011; 2012; Bots et al., 2012). Note that the v_1 band of vaterite is overlapping with that of calcite at 1086 cm^{-1}. During vaterite to calcite transformation, the intensity of the v_1 band at 1086 cm^{-1} increased significantly, while the second v_1 band of vaterite at 1075 cm^{-1} decreased between 25 min and 1 day of reaction time (**Table A1**, **Appendix**). These changes in intensity likely occur due to the poor crystallinity observed in vaterite compared to that of calcite (Wehrmeister et al., 2010). Thus, the Raman v_1 band at 1086 cm^{-1} became sharper during the formation of calcite (Fig. 4). The formation of calcite was further confirmed by the contemporaneous rise of its libration mode at 218 cm^{-1} (**Table A1**, **Appendix**).

3.4.2. Control of Mg on Mg-ACC transformation mechanisms

Experiments MgCa4, MgCa5, and MgCa6 demonstrate that the Mg content of the precipitated calcite increased throughout Mg-ACC transformation (**Fig. 2B**; **Table 1**). Thus, the Mg content of all Mg-ACC precipitates is lower than that of Mg-calcite that subsequently forms from these precursor phases (**Fig. 7**). Recent studies document that ACC undergoes a continuous transition from more hydrated to less hydrated states in solution at ambient temperature prior to its transformation to a crystalline phase (Ihli et al., 2014; Rodriguez-Navarro et al., 2015). The rate of ACC dehydration is most likely controlled by the presence of Mg in its structure, with slower dehydration rates to be expected at higher Mg contents. This occurs due to the presence of larger amounts of structural water at high Mg contents (Lin et al., 2015) and it is likely the case for experiments MgCa4, MgCa5, and MgCa6 (**Fig. 4**). Ihli et al. (2014) suggested that the complete dehydration of ACC is associated with a high activation energy of ~245 kJ mol^{-1}, thus transformation of ACC to calcite via a solid-state mechanism is unlikely to occur at low temperatures (Rodriguez-Navarro et al., 2015). Hence, based on the evolution of the solution chemistry during the experimental runs of this study, it is likely that the formation of Mg-calcite took place via a dissolution and re-precipitation process of the already partly dehydrated Mg-ACC. ACC transformation to Mg-calcite via dissolution/re-precipitation has been also recently verified by isotope trace experiments (Giuffre et al., 2015). During Mg-calcite formation Ca^{2+}, Mg^{2+}, and CO_3^{2-} ions are removed from the reactive solution (**Table 1**) owing to higher oversaturation of Mg-calcite in the reactive solution compared to that of ACC (cf. exp. MgCa4, **Fig. 8a**). The continuous precipitation of Mg calcite during the experimental runs, results in a reactive solution undersaturated with respect to ACC. The inhibiting effect of aqueous Mg on the

nucleation of calcite (Lippmann, 1973) might be overcome by the precipitation of Mg-calcite on the surface of the remaining, not fully transformed, ACC precursor phase. The obtained Raman results show that the complete transformation of Mg-ACC to Mg-calcite occurs in rather short periods of time (i.e., 12 ±4 min), thus a rather slow solid state ion diffusion mechanism (Putnis, 2014) can be refuted to take place for this transformation process.

After the complete Mg-ACC transformation to Mg-calcite, the reactive solutions in experiments MgCa4, MgCa5, and MgCa6 are still supersaturated with respect to Mg-calcite ($\log(\Omega_{\text{Mg-calcite}}) = 1.13 \pm 0.09$ after 60 min). At this stage the $[Mg]_{aq}/[Ca]_{aq}$ ratio is about 30 in experiments MgCa4, MgCa5, and MgCa6 (**Table 1**). Note here that increased Mg concentrations in the aqueous phase have been shown to significantly retard the growth rate of calcite (Berner 1975; Falini et al., 1994; De Choudens-Sanchez and Gonzalez, 2009; Astilleros et al., 2010). The ongoing Mg enrichment in calcite after Mg-ACC transformation may be explained by the partial dehydration of aqueous Mg ions by Mg-carbonate aquocomplex formation as a result of elevated carbonate alkalinity concentrations (~0.1 M) prevailing in the reactive solutions. Indeed, in the reactive solutions of experiments MgCa4, MgCa5, and MgCa6, the overall molar fraction of $[MgHCO_3^-]_{aq}$ and $[MgCO_3^o]_{aq}$ complexes sums up to 35 % of the total $[Mg]_{aq}$, after the transformation of Mg-ACC took place. The detailed mechanisms that control and affect the uptake of these Mg-carbonate aqueous complexes in calcite, however, are not clear and require further experimental work.

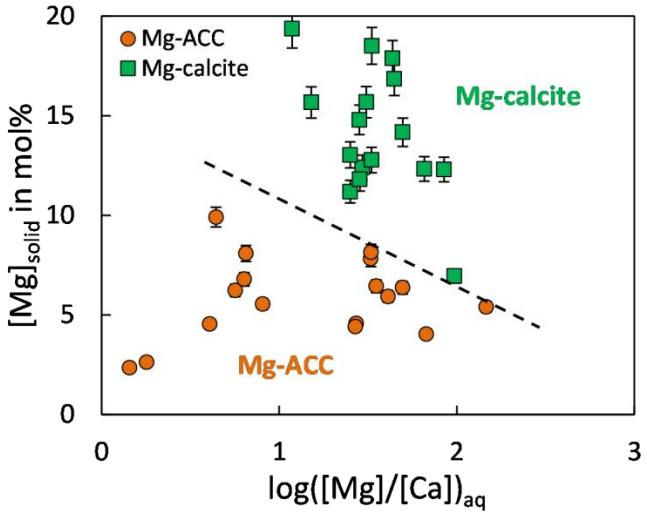

Fig. 7. Mg content of precipitates, calculated according to **Eq. 1**, as a function of the molar Mg/Ca ratio of the aqueous solutions for experiments MgCa4, MgCa5, and MgCa6. Dashed line denotes the boundary between the Mg-ACC and Mg-calcite for the present experiments. Analytical uncertainty is included in symbol size.

In the present study, Mg-calcites that formed via the transformation of an initial amorphous phase exhibit significantly higher Mg contents compared to those formed directly from solution. Along these lines, Mucci and Morse (1984) documented the formation of Mg-calcite with ≤ 11 mol% Mg in experiments conducted in synthetic sea water solutions with Mg/Ca ratios ranging from 1 to 20 and carbonate alkalinity concentrations of about 0.001 M. Our data show that even though the initial Mg/Ca ratio was as low as 0.25 in experiment MgCa4, Mg-calcite with up to 20 mol% Mg was formed in solutions at carbonate alkalinities of 0.1 M. An important implication of this data set is that calcite precipitated inorganically from high supersaturated solutions is not in equilibrium with the Mg/Ca ratio of its parent fluid. Specifically, the reaction pathway of calcite nucleation and precipitation via precursor phases and Rayleigh type distillation processes may impose non-equilibrium processes that may as well affect the isotope distribution of Mg in the solid phase (cf. Mavromatis et al., 2013). The first order empirical relations extracted from these experiments are: (i) ACC precursors with a high Mg content result in calcites with an equally high Mg content, and (ii) the Mg content of ACC is positively correlated to Mg/Ca ratios of titrated solution.

In the present experiments, the Mg content of ACC ranges between 2 and 10 mol%. Radha et al. (2012) suggested that this range of Mg concentration should correspond to the formation of a "homogeneous amorphous single phase". Accordingly, the activities of Ca and Mg ions in solution and the solid stoichiometry were used to calculate individual IAP values according to Eq. 3 as a function of reaction time (**Fig. 8B**). Constant IAPs of -6.14 ±0.04 and -7.01 ±0.06 were obtained during experiments MgCa4 and MgCa5, respectively. These are obviously adjusted by ongoing Mg-ACC formation at the given experimental conditions. These IAP values for Mg ACC lay within the range of ACC solubility products without Mg ($K_{sp} = 10^{-6.39}$: Brečević and Nielsen (1989); $K_{sp} = 10^{-7.51}$ for ACC 1: Gebauer (2008)). The near-constant IAPs during an individual run typify a highly dynamic system. In such a system, the temporal evolution of composition of reactive solution and Mg-ACC has no significant effect on the obtained "solubility product" for Mg-ACC. The physicochemical characteristics of the experiment are suggested to play a decisive role in determining composition, structure, hydration state of Mg-ACC and that this in turn is responsible for the different calculated "solubility products" for experiments MgCa4 and MgCa5. As variations in the chemical composition of Mg-ACC do not change "solubility products" in the experiments MgCa4 and MgCa5 (**Fig. 8B**), the individual

structure of Mg-ACC may be the main factor in determining ACC solubility. Note, however, that that the low aqueous Ca concentrations (**Table 1**) may be introducing large errors in the estimation of IAP values in these experimental runs. Further experimental data are required to verify the complex interplay between composition, structure, and hydration state of Mg ACC throughout its formation and in particular as a function Mg content.

3.4.3. Implications for Mg-calcite formation in natural environments

It is well established that high Mg-calcite formation is less favorable compared to low Mg-calcite or aragonite formation in seawater (Berner, 1975; Busenberg and Plummer, 1989). However, high Mg-calcites are often found in marine sediment settings where formation mechanisms remain unclear (Swart, 2015). In order to test the relative stability of the precipitated phase for the presented study, we compare the saturation state of the reactive solution with respect to the precipitated Mg-calcite as well as with that of calcite and aragonite. Essentially, the reactive solutions exhibit a higher saturation state with respect to Mg-calcite compared to all other $CaCO_3$ phases (experiment MgCa4 in **Fig. 8A**). This is due to the high activities of aqueous Mg^{2+} and aqueous CO_3^{2-} ions, which result in high IAP values (see Eq. 3) and thus elevated Ω values with respect to Mg-calcite. Thus, the thermodynamic stability sequence with respect to various Mg-calcite and aragonite, determined by solubility data at a given temperature, depends strongly on the Mg:Ca stoichiometry of the solution. We observed similar trends in the $\Omega_{Mg\text{-}calcite}$ temporal evolution during all the experimental runs; refer to **Fig. 8C** for calculated $\Omega_{Mg\text{-}calcite}$ and $\Omega_{calcite}$ values. In any case an upper limit of $\log(\Omega_{Mg\text{-}calcite}) = 1.4$ for the formation of Mg-calcite from Mg-ACC is observed. Above this threshold value, metastable Mg-ACC precipitates.

With respect to microbially induced carbonates precipitated in natural aquatic environments, the presence of an amorphous phase has been associated with high Mg-calcites and/or disordered dolomite (Schmidt et al., 2005; Bontognali et al., 2010). Given its rapid transformation to a crystalline phase, however, quantitative experimental work in natural settings remains notoriously difficult. Independent of these problems, our findings clearly document that the uptake of Mg ions in calcite continues after transformation of Mg-ACC. The mechanisms related to this formation require further experimental work, whilst the physicochemical conditions in the context of this study, i.e. circumneutral pH, high alkalinity concentration, and high fluid Mg/Ca ratio, are rather typical for natural early diagenetic environments. For example, marine sediments affected by anaerobic oxidation of methane (AOM) provide alkalinity concentrations of >50 mM

(Hensen et al., 2004; Peckmann et al., 2001; Schmidt et al., 2005; Mavromatis et al., 2014b). In these settings the Mg/Ca ratio is significantly higher compared to that of bulk seawater, as precipitation of $CaCO_3$ minerals occurs readily owing to their lower solubility.

The presence of ACC with variable Mg contents has also been documented for a variety of biomineralization environments (Aizenberg et al., 1996; Beniash et al., 1997; Raz et al., 2003; Politi et al., 2010). Advantages of shell formation via an amorphous precursor phase include the possibility to temporarily store divalent cations and organic macromolecules and to exploit them as building blocks at a later stage (see Immenhauser et al., 2015 for discussion). In order to prevent spontaneous transformation of ACC, its formation must take place in a delineated space that is sealed off from its aquatic environment. In many cases, biogenic ACC is precipitated from a highly supersaturated body fluid and is then stored in vesicles where organic additives and high Mg/Ca ratios inhibit deposition of crystalline phases (Weiner & Dove, 2003; Weiner et al., 2005). During the transformation of ACC to the crystalline phase, the additives that inhibited spontaneous mineralization are either occluded in the crystal or excluded from the crystallization front (Weiner & Addadi, 2011). Our results indicate that - besides control by associated organic molecules - the aqueous Mg/Ca ratio and carbonate concentration in a biomineralization space might play a significant role in the further enrichment of Mg in calcite throughout the transformation of Mg-ACC. Although, in the case of the experimental work shown here, the effects of Mg on ACC (trans)formation take place in a strictly inorganic setting, this aspect is of relevance for an in-depth understanding of biomineralization strategies using ACC precursors, e.g. in the aspects of active pumping of Mg^{2+} away or to the calcification sites.

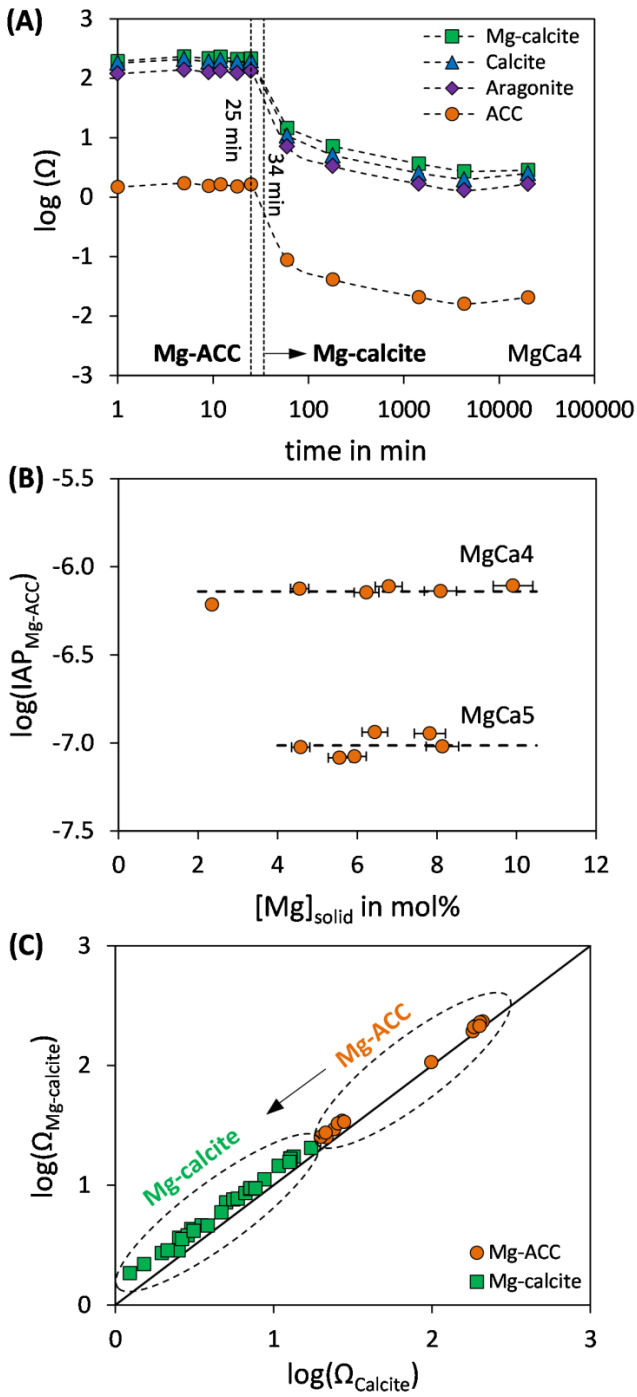

Fig. 8. (A) Evolution of the saturation state (Ω) with respect to ACC, calcite, aragonite and Mg calcite over the experimental time of the reactive solution of experiment MgCa4. The transformation of Mg-ACC to Mg-calcite started after 34 min of reaction time. (B) Calculated ion activity product for Mg-ACC according to Eq. 3 as a function of the Mg content of the solids, calculated according to Eq. 1. Results for experiments MgCa4 and MgCa5 with a high stability of Mg-ACC are plotted. A mean log($IAP_{Mg\text{-}ACC}$) value of -6.14 ±0.04 and -7.01 ±0.06 is obtained for MgCa4 and MgCa5 with a Mg/Ca ratio used in the $(Ca,Mg)Cl_2$ solution of 1:4 and 1:5, respectively. (C) Saturation state with respect to calcite ($\Omega_{calcite}$) versus the saturation state with respect to the forming Mg-calcite ($\Omega_{Mg\text{-}calcite}$) at certain reaction times of all experiments.

3.5. SUMMARY AND CONCLUSIONS

The formation of Mg-ACC and Mg-calcite at high fluid carbonate alkalinity has been investigated experimentally under controlled physicochemical conditions (pH = 8.3 ±0.1, T = 25.00 ±0.03°C). In situ Raman spectroscopy was successfully applied to monitor the formation of amorphous calcium carbonate and its near-instantaneous transformation to a crystalline phase at a temporal resolution of about 30 seconds. Results were verified by analyzing the chemical composition of the solution as well as the composition and structure of the precipitates in parallel. Formation of Mg-calcite was documented by Raman, ATR-FTIR and XRD pattern as well as SEM imaging.

Data obtained reveal two distinctive mechanisms of Mg-calcite formation: (i) in experiments with high initial Mg/Ca ratios (1:4, 1:5 and 1:6), Mg-ACC acts as a precursor for Mg-calcite formation with calcites containing up 20 mol% Mg. In this sense Mg-ACC represents an energetically favorable pathway for high Mg-calcite formation. (ii) Conversely, under increasing fluid Mg/Ca ratios, the stability of Mg-ACC is extended due to reduced kinetics of Mg^{2+} dehydration. At lower initial Mg/Ca ratios or in the absence of aqueous Mg, crystalline $CaCO_3$ precipitated directly from the solution. The initial Mg/Ca of 1:8 resulted in the precipitation of an Mg-calcite with about 8 mol%, while in the Mg free experiment calcite was formed via a vaterite precursor.

The calculated "solubility products" of the Mg-ACC phases precipitated in the experiments with elevated initial Mg/Ca ratios are independent of the ongoing change of ion stoichiometry of solid and solution. An upper limit of $\log(\Omega_{\text{Mg-calcite}}) = 1.4$ for the transformation of Mg-ACC to Mg-calcite was obtained. The Raman spectra document that in our experiments the transformation of Mg-ACC to Mg-calcite took place within a reaction time of about 11 min. Considering an ACC transformation step, the Mg content in ACC is low, but high net uptake of Mg ions in the precipitate throughout and subsequent its transformation, results in calcite with an unexpected high Mg concentration of 20 mol%, whereas the more likely formation of aragonite is prohibited. Hence, based on the Raman results and on the evolution of the solution chemistry during the experimental runs of this study, it is suggested that the transformation of Mg-ACC takes place via a dissolution and reprecipitation process. The experimental data clearly document the importance of fluid alkalinity and aqueous Mg/Ca ratio on the formation of calcite with high Mg content from Mg-ACC precursor. Essentially, our findings suggest that the Mg content of both abiotic

and biogenic calcite precipitates depends on reaction pathway of formation and does not directly trace the chemical composition of the precipitating solution.

3.6. APPENDIX

Table A1

Frequencies (cm^{-1}) of observed characteristic carbonate vibration bands from in situ Raman and ATR-FTIR spectra at certain reaction times. Maximum intensities (I_{max}) are given for the Raman v_1 bands and libration modes.

Experiment		**Raman**		ATR-FTIR		
	time min/d	$\boldsymbol{v_1}$ cm^{-1} (I_{max})	libration mode cm^{-1} (I_{max})	v_1 cm^{-1}	v_2 cm^{-1}	v_4 cm^{-1}
	13 min	1085 (0.58)	-	1073	860	-
	25 min	1085 (0.60)	-	1073	860	-
	60 min	1089 (1.11)	285 (0.11)	1084	872	713
MgCa4	180 min	1089 (1.18)	286 (0.10)	1084	871	713
	1 d	1089 (1.19)	286 (0.11)	1085	871	713
	3 d	1089 (1.16)	287 (0.09)	1085	871	713
	14 d	1090 (1.19)	287 (0.10)	1085	871	713
	13 min	1086 (0.59)	-	1074	861	-
	25 min	1086 (0.71)	-	1075	871	-
	60 min	1088 (1.48)	284 (0.15)	1083	872	712
MgCa5	180 min	1088 (1.33)	285 (0.11)	1082	871	712
	1 d	1088 (1.39)	285 (0.12)	1083	871	712
	3 d	1088 (1.32)	285 (0.11)	1083	872	713
	14 d	1089 (1.38)	285 (0.14)	1084	872	713
	13 min	1086 (0.72)	-	1083	871	711
	25 min	1088 (1.34)	283 (0.07)	1084	871	712
	60 min	1088 (2.00)	283 (0.20)	1084	871	713
MgCa6	180 min	1088 (1.41)	283 (0.11)	1085	871	713
	1 d	1088 (1.39)	283 (0.16)	1085	872	713
	3 d	1088 (1.32)	283 (0.14)	1085	871	713
	14 d	1088 (1.38)	283 (0.11)	1085	871	713
	13 min	1087 (1.24)	282 (0.08)	1082	870	712
	25 min	1087 (1.61)	282 (0.14)	1082	870	712/700
	60 min	1087 (1.87)	282 (0.16)	1082	870	712/700
MgCa8	180 min	1087 (2.32)	282 (0.14)	1082	870/856	712/699
	1 d	1087 (2.12)	205 (0.04)/282 (0.15)	1083	870/856	712/699
	3 d	1087 (2.33)	205 (0.06)/282 (0.15)	1083	870/856	711/699
	14 d	1087 (1.97)	205 (0.07)/282 (0.13)	1083	871/856	711/700
	13 min	1074 (0.55)/1086 (1.60)	281 (0.15)	1088	871	744/712
	25 min	1074 (0.62)/1086 (2.68)	281 (0.32)	1088	872	744/712
	60 min	1075 (0.66)/1086 (3.01)	281 (0.40)	1088	872	744/712
Mg0Ca	180 min	1075 (0.59)/1086 (2.86)	281 (0.37)	1088	871	744/712
	1 d	1086 (5.86)	281 (1.15)	-	871	712
	3 d	1086 (5.96)	281 (1.08)	-	871	712
	14 d	1085 (5.66)	281 (1.05)	-	871	712

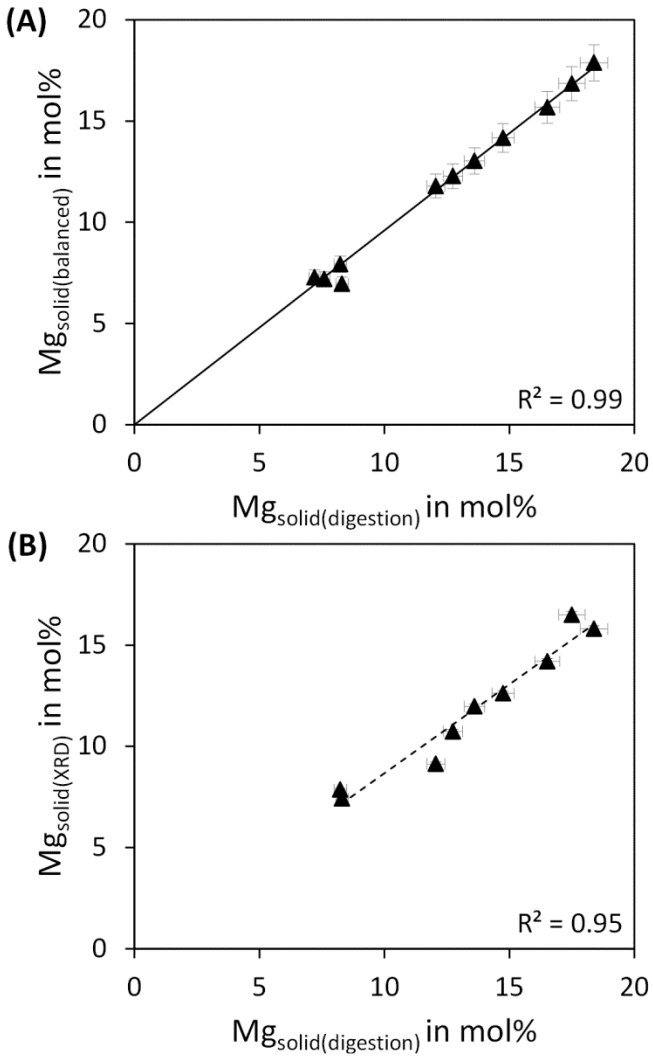

Fig. A1 Mg content of the solid calculated from digestion ($[Mg]_{solid(digestion)}$) versus (A) the Mg content of the solid calculated according to Eq. 1 and (B) the Mg content of the solid calculated from the $d_{(104)}$ obtained from XRD ($[Mg]_{solid(XRD)}$) according to Goldsmith et al. (1961). The analytical uncertainty of this calculation is included in symbol size. Solid line (A) is obtained by the linear regression $[Mg]_{solid(balanced)} = 1.0414[Mg]_{solid(digestion)}$.

4. Impact of Amorphous Precursor Phases on Magnesium Isotope Signatures of Mg-Calcite

Vasileios Mavromatis[1,2], Bettina Purgstaller[1], Martin Dietzel[1] ,Dieter Buhl[3], Adrian Immenhauser[3], Jacques Schott[2]

[1]*Institute of Applied Geosciences, Graz University of Technology, Rechbauerstrasse 12, 8010 Graz, Austria*
[2] *Géosciences Environnement Toulouse (GET), CNRS, UMR 5563, Observatoire Midi-Pyrénées, 14 Av. E. Belin, 31400 Toulouse, France*
[3]*Institute of Geology, Mineralogy and Geophysics, Bochum, Universitätsstraße 150, 44801 Bochum, Germany*

Published in Earth and Planetary Science Letters 464 (2017) 227-236

ABSTRACT

Various marine calcifiers form exoskeletons via an amorphous calcium carbonate (ACC) precursor phase and magnesium plays an important role in the temporary stabilization of this metastable phase. Thus, the use of Mg isotope ratios of marine biogenic carbonates as a proxy to reconstruct past seawater chemistry calls for a detailed understanding of the mechanisms controlling Mg isotope signatures during the formation and transformation of ACC to the final crystalline carbonate mineral. For this purpose we have investigated the Mg isotope fractionation between $(Ca,Mg)CO_3$ solids and aqueous fluids at 25°C and pH = 8.3 during (i) the direct precipitation of crystalline Mg-calcite and (ii) the formation of Mg-rich ACC (Mg-ACC) and its transformation to Mg-calcite. The outcome documents that the small Mg isotope fractionation between Mg-ACC and reactive fluid ($\Delta^{26}Mg_{ACC\text{-}fluid}$ = -1.0 ± 0.1‰) is not preserved during the transformation of the ACCs into Mg-calcite. Following a pronounced isotopic shift accompanying the transformation of Mg-ACC into Mg-calcite, $\Delta^{26}Mg_{calcite\text{-}fluid}$ progressively decreases with reaction progress from ~ -3.0‰ to -3.6‰, reflecting both the approach of isotopic equilibrium and the increase of calcite Mg content (to near 20 mol % Mg). In contrast the crystalline Mg-calcite precipitated directly from the reacting fluid, i.e. lacking a discernable formation of an amorphous precursor, exhibits only small temporal variations in $\Delta^{26}Mg_{calcite\text{-}fluid}$ which overall is affected by the precipitation kinetics. The values found in this study at the onset of Mg-ACC precipitation for Mg isotope fractionation between Mg-ACC and the fluid ($\Delta^{26}Mg_{ACC\text{-}fluid}$ = -1.0‰) and between Mg-ACC and Mg^{2+}(aq) ($\Delta^{26}Mg_{ACC\text{-}Mg^{2+}(aq)}$ = + 2.0‰) are consistent with the formation of a hydrated Ca nanoporous solid accommodating Mg

bicarbonate/carbonate species in combination with hydrated magnesium. This material crossed by percolating channels filled with the reacting fluid easily converts to Mg-rich calcite via exchange and/or dissolution/precipitation reactions. The results of this study provide new insights on the acquisition of the Mg chemical and isotopic signatures by the skeletal marine carbonates precipitated in confined media from strongly supersaturated fluids. They also offer new guides for the interpretation of the isotopic signature of these organisms for paleo-environmental reconstructions.

4.1. INTRODUCTION

Magnesium is a major component of seawater and in a large number of continental water bodies. It plays a key role in the precipitation of carbonate minerals in the ocean as well as during diagenetic reactions (Swart, 2015). As a result, much attention has been devoted in the last years to the Mg isotope composition of marine carbonates and their potential for the reconstruction of past seawater chemistry (Higgins and Schrag, 2010) and for providing new insights into the global Mg cycle and the temporal evolution of continental weathering (Higgins and Schrag 2010; Riechelmann et al., 2012; Pogge von Stradmann et al., 2014; Beinlich et al., 2014; Mavromatis et al., 2014a; 2016a).

In order to reconstruct past seawater Mg isotope signatures from carbonate archives, the Mg isotope fractionation between carbonate minerals and fluids and specifically between calcite and seawater must be known. As a result a number of recent studies have been carried out to calibrate the Mg isotope fractionation during calcite precipitation (Immenhauser et al., 2010; Li et al., 2012; Mavromatis et al., 2013). These studies have focused on the inorganic calcite crystal growth and the quantification of the impact of growth kinetics on Mg partitioning and isotope fractionation between calcite and the fluid. This raises the question, however, whether these inorganic experiments could provide a robust description of the fractionation of Mg isotopes in biogenic carbonates (Hippler et al., 2009). The answer to this question is important because (i) the biomineralization pathways differ between different groups of organisms (Immenhauser et al., 2016) and (ii) marine limestones, whether neritic or pelagic in origin, consist of a complex admixture of biogenic and abiogenic Mg-bearing carbonates (Morse and Mackenzie, 1990).

Indeed, Mg concentrations in inorganic $CaCO_3$ precipitated in seawater-type fluids do not exceed 1-3 mol % (Politi et al., 2010), whereas Mg content of biogenic marine carbonates can reach up to 30 mol % (Chave, 1954). Furthermore, a large body of recent literature suggests that many groups of organisms apply amorphous precursor strategies in biomineralization (Politi et al., 2004; 2008; Immenhauser et al., 2016 and references therein) and that the confined peculiar fluid chemical environment (including high alkalinity and Mg(aq)/Ca(aq) ratio) controlling the formation and transformation of this precursor seems to be a prerequisite for the formation of Mg-rich calcite (X_{Mg} > 10 mol %; Raz et al., 2000; Politi et al., 2010; Purgstaller et al., 2016). In this regard, the formation of a nanoporous calcium-rich framework, accommodating hydrated Ca and Mg with reduced coordination and supporting interconnected/percolating channels containing

water and carbonate molecules, likely plays a key role in the transient stabilization of the amorphous structure and its crystallization into a Mg-rich calcite (Addadi et al., 2003; Goodwin et al., 2010; Lin et al., 2015).

The elementary mechanisms that control the formation of Mg-calcites from a metastable ACC are clearly different from the classical ion-by-ion attachment of solutes to advancing steps involved in the inorganic crystal growth of Mg–calcite in slightly supersaturated forming solutions. The ways of acquisition and preservation of Ca and Mg isotopic signatures in calcites formed from an ACC precursor are also expected to be distinctly different from those operating during calcite inorganic crystal growth. To our knowledge, no study until now has monitored the evolution of the Mg isotope composition of the forming fluid and the precipitated solid phases during the formation of Mg-bearing ACCs (Mg-ACC) and their transformation to crystalline Mg-calcite. This is remarkable, as without this information, any attempt to reconstruct past seawater composition from marine biogenic carbonates must remain poorly constrained.

In an effort to characterize Mg isotope fractionation between aqueous solutions and Mg-calcites formed from ACC precursors, as well as during and after the transformation of these amorphous phases to Mg-calcites, we have measured the Mg isotope signatures of Mg-ACC, Mg-calcite, and experimental fluids performed under controlled pH conditions as reported earlier by Purgstaller et al. (2016). The intention of this study is not to simulate biomineralization in its complex and individual behavior, but to decouple the distinct effects of ACC (trans)formation on Mg isotope fractionation between aqueous Mg and Mg-calcite at well-defined physicochemical experimental conditions.

4.2. METHODS

4.2.1 Experimental setup and analytical procedures

The experimental setup and the analytical methods have been described in detail in Purgstaller et al. (2016). Briefly, the experiment was hosted in a temperature controlled (25.00 ±0.03°C) Easy MaxTM 102 system (Mettler Toledo) within a 150 ml borosilicate glass reactor. Mg-ACC formation was induced by titration of 50 ml of a 0.6 M (Ca,Mg)Cl_2 solution via an automatic titrator (702 SM Titrino; Methrom) at a rate of 2 mL/min into 50 ml of a 1 M $NaHCO_3$ solution (stirred at 200 rpm). The pH of the reactive fluid was kept constant at 8.3 ±0.1 by automatic injection of a 1 M NaOH solution (Schott; TitroLine alpha plus). The temporal evolution of

mineral precipitation was monitored by in situ Raman spectroscopy (Raman RXN2^{TM} analyzer, Kaiser Optical Systems). After 60 min of reaction time the reactive solution was transferred into a 150 ml glass bottle and was placed air-tight on a compact shaker (Edmund Bühler GmbH; KS-15) operating at 150 rpm in a temperature controlled room at 25 ±1°C. The evolution of the chemical and Mg-isotope composition of the reactive fluids and the precipitated solids were followed via homogenous sampling of 5 ml that were subtracted from the reactor at 5, 12.5, 25, 60, 180 min and after 1, 3 and 14 days of reaction time. In addition after 1, 9 and 18 min of reaction time, 1 ml aliquots of the experimental solution were sampled and filtered only for solution analyses. The solids were separated by a 0.2 µm cellulose acetate filter using a suction filtration unit and were immediately analyzed using Attenuated Total Reflectance - Fourier Transform Infrared Spectroscope (ATR-FTIR; Perkin Elmer Spektrum 100). Afterwards the solids were dried in a desiccator containing silica gel at room temperature. The mineralogy of the dried precipitates was determined using X-ray diffraction (PANalytical X´Pert PRO). Aqueous Mg and Ca concentrations were measured using an ion chromatography unit (Dionex IC S 3000) and the total alkalinity of the solutions was determined by a Schott TitroLine alpha plus titrator. The Mg contents of the solids (in mol%), calculated based on mass balance calculations (see Purgstaller et al., 2016, for further details) are in excellent agreement with the Mg contents of solid measured by digestion of selected solid samples in 6% HNO_3.

In total, 4 experiments were carried out in the presence of Mg. The Mg/Ca ratios used in the 0.6 M (Ca,Mg)Cl_2 solutions were 1:4, 1:5, 1:6 and 1:8, thus, the experiments are labeled as MgCa4, MgCa5, MgCa6 and MgCa8, similar to Purgstaller et al. (2016). Note here that this ratio does not reflect the composition of reactive fluids and solids after the onset of the runs.

The apparent growth rate (mol/s) of the precipitating solid phase over time for these experimental runs can be estimated by mass balance of Ca and Mg introduced in the reactor by the titration of the inlet (Ca,Mg)Cl_2 solution and the actual aqueous Ca and Mg concentrations according to the equation:

$$Rate_{app} = \frac{Ca_{add} - Ca_{meas} + Mg_{add} - Mg_{meas}}{t} \quad (1)$$

where the subscripts *add* and *meas* denote the moles of Ca and Mg added and measured respectively in the reactor and *t* is the elapsed reaction time in seconds from the onset of the experimental run. The temporal evolution of the apparent growth rate is illustrated in **Fig. 1**.

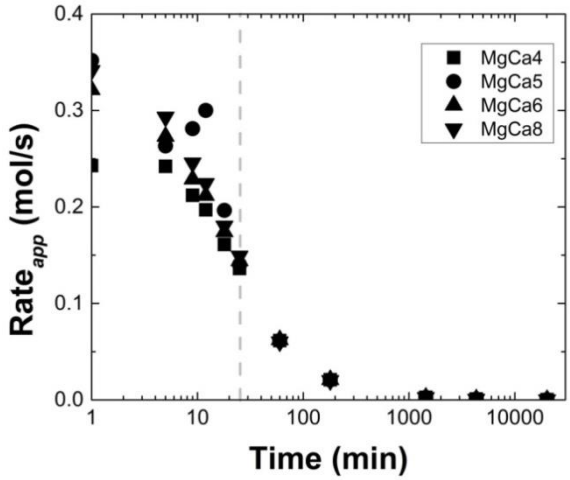

Fig. 1. Temporal evolution of the apparent growth rate ($Rate_{app}$), calculated according to **Eq. 1**, for all experimental runs.

4.2.2 Magnesium isotope analyses

Magnesium isotope analyses of reacting solutions and precipitated solids followed the protocol described earlier by Immenhauser et al. (2010) and detailed in Geske et al. (2015). Solid and fluid samples were eluted with 1.25M HNO_3 through the BioRad ion exchange resin AG50W-X12 (200-400 mesh) for chemical separation of matrix elements (i.e. Na, Ca). The ratios of Mg isotopes in the samples were determined with a Thermo Fisher Scientific Neptune MC-ICP-MS in a 500 ppb Mg 3.5% HNO_3 solution at the facilities of the Ruhr-University-Bochum (Germany). The Mg concentration of the analyzed sample was kept within ±15% of the standard, which proved to minimize potential isobaric interferences from matrices. A positive effect on signal stability and reduction of matrix interferences was achieved by combining two desolvating systems (ApexIR (ESI), Aridus (Cetac)) and the medium-resolution slit of the Thermo Fisher Scientific Neptune. The instrumental mass fractionation effects were corrected by sample-standard bracketing, and all results are presented in delta notation relative to the DSM3 reference material as: $\delta^{x}Mg = (({}^{x}Mg/{}^{24}Mg)_{sample}/({}^{x}Mg/{}^{24}Mg)_{DSM3} -1)\times 1000)$, where x is the mass of interest. Each measurement value comprises a sequence of five repetitions of sample measurements. The reproducibility of Mg isotope measurements was assessed using samples of (i) the internal carbonate standard RUB (Solnhofen Plattenkalk), (ii) the mono elemental solution Cambridge1, (iii) IAPSO seawater and (iv) a dolomite sample (HDK7). Each standard sample was processed identically, except different ion exchange columns were used. Please refer to Riechelmann et al. (2016) for details on the reproducibility of the analyses.

4.2.3 Calculation of aqueous speciation and isotopic composition of magnesium aqueous species

Aqueous speciation in reactive solutions was calculated using the computer code PHREEQC and its llnl.dat data base, which is derived from the slop98.dat data base of the SUPCRT92 software (Johnson et al., 1992). The B-dot activity model (Helgeson, 1969) was used to compute the activity coefficients of aqueous species. The database was modified to include the recent determinations of carbonic acid dissociation constants (Millero et al., 2007; Stefánsson et al., 2013) and the equilibrium constant for the first Mg^{2+} hydrolysis (Palmer and Wesolowski, 1997) and the formation of Mg bicarbonate and carbonate ion pairs (Stefánsson et al., 2014).

The isotope composition of the main Mg aqueous species present in the reactive solutions was derived from PHREEQC speciation calculations using the values reported by Schott et al. (2016) of the $^{26/24}$Mg reduced partition function ratios for Mg^{2+}(aq) and Mg bound to a number of inorganic and organic ligands.

4.3. RESULTS

4.3.1 Chemical and isotopic evolution of the reactive fluid

The concentrations of Ca, Mg and alkalinity over the course of the experiments have been reported in detail by Purgstaller et al. (2016) and are tabulated in **Supplementary Data** (**Table S1**). Owing to the high supersaturation with respect to all $CaCO_3$ polymorphs in the reactive fluid, instant nucleation of Mg-ACC was observed after the onset of the titration of the $(Ca,Mg)Cl_2$ inlet solution in the reactor in experiments MgCa4, MgCa5, and MgCa6. In contrast, the initial formation of ACC could not be detected in experiment MgCa8 for which Mg concentration of the inlet fluid was the lowest. The carbonate alkalinity decreased from the initial concentration of 1 M down to an overall value of ~0.1 M after 25 min of reaction time whereas Ca aqueous concentration never exceeded 0.006 M (Purgstaller et al., 2016). The concentrations of aqueous Ca remained quasi-constant after 60 min of reaction in all experimental runs, denoting chemical steady state conditions with respect to this parameter. Carbonate alkalinity in contrast, exhibits a small reduction over time. Aqueous Mg concentration exhibits a strong increase during the 25 min of titration followed by a continuous decrease over the remaining time of the experimental runs (**Fig. 2A**). An exception is found in the case of experiment MgCa8 where aqueous Mg concentration remained nearly constant after 25 min reaction time.

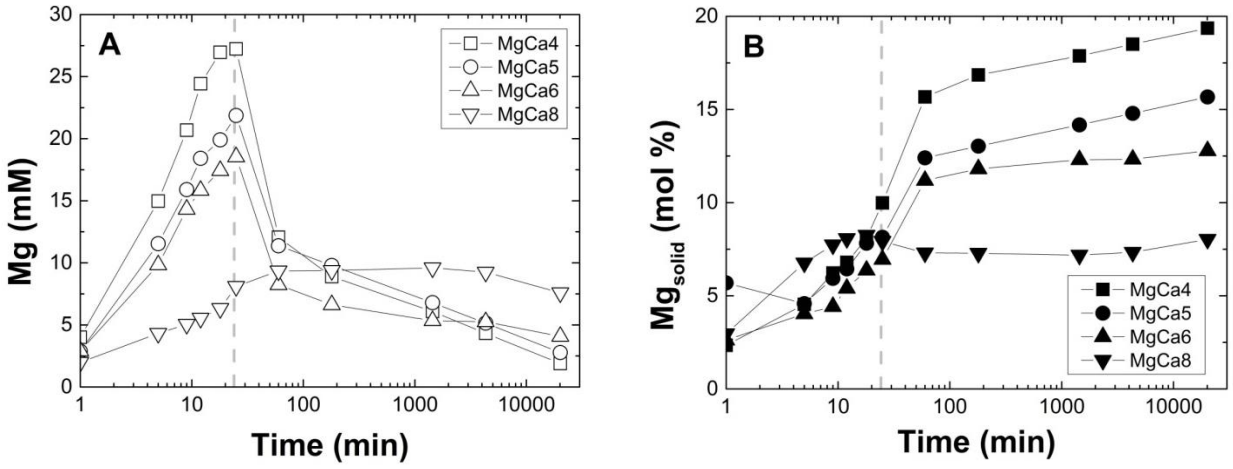

Fig. 2. Temporal evolution of Mg concentration in **(A)** the fluid phase and **(B)** in the precipitating solid. The grey dashed line denotes the termination of the titration of the $(Ca,Mg)Cl_2$ inlet solution after 25 min of reaction time. Analytical uncertainties are included in the symbol size.

The Mg isotope composition of the reactive fluid ($\delta^{26}Mg_{fluid}$) exhibited an overall increase, which is more pronounced as the [Mg]/[Ca] ratio in the inlet fluid is higher (see **Table 1** and **Fig. 2A**). It increases from the initial value of 0.35 ‰ in the inlet fluids to a value of 3.84 ‰ at the end of experiment MgCa4 ([Mg]/[Ca] = 0.25), whereas the $\delta^{26}Mg_{fluid}$ composition at the end of experiments MgCa5 ([Mg]/[Ca] = 0.20) and MgCa6 (Mg]/[Ca] = 0.17) are ~3.5 ‰ (**Fig. 3**). In experiment MgCa8 (Mg]/[Ca] = 0.125) the isotopic composition of the reactive fluid at the end of the experimental run is significantly lower with a $\delta^{26}Mg_{fluid}$ value of 2.0 ‰. The isotopic composition of the reactive fluid exhibits a significant increase of about 1.5‰ after the transformation of Mg-ACC to Mg-calcite in experiment MgCa4, for which the most detailed analyses are available (**Fig. 3**).

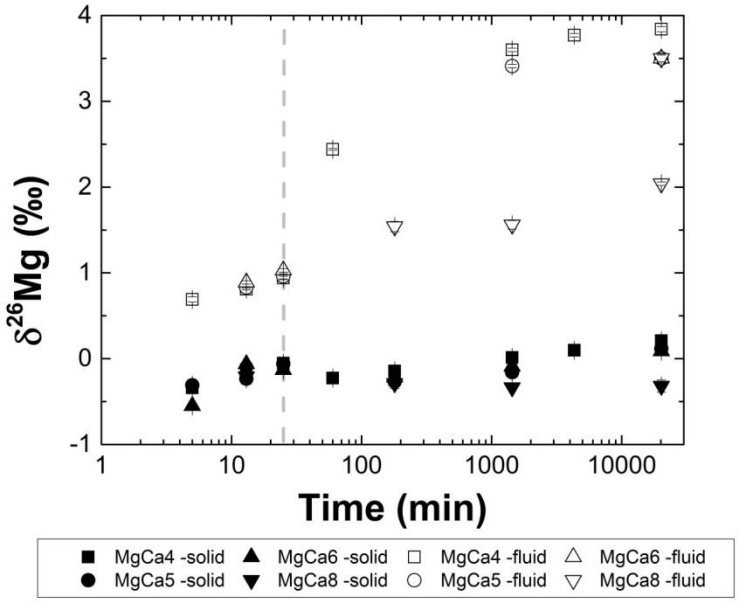

Fig. 3. Temporal evolution of Mg isotope composition in the reactive fluid (open symbols) and in the precipitating solid (closed symbols). The grey dashed line denotes the termination of the titration of the $(Ca,Mg)Cl_2$ inlet solution after 25 min of reaction time.

4.3.2 Chemical and isotopic evolution of the solid phase

Mg-ACC instantaneously forms in experiments MgCa4, MgCa5, and MgCa6 and its presence last up to 34, 25, and 15 min of reaction time, respectively, before its transformation into Mg-rich calcite took place (Purgstaller et al., 2016). In contrast, Mg-calcite precipitation occurs immediately after the onset of experiment MgCa8. An illustrative example of the transition from Mg-ACC to Mg-calcite can be seen in the Raman spectra waterfall plot in **Fig. 4**. Scanning Electron Microphotographs of Mg-calcite formed via an Mg-ACC precursor and via direct precipitation are shown in **Fig. 5**.

The temporal evolution of the Mg concentration, $[Mg]_{solid}$, in the forming solid phase can be seen in **Fig. 2B**. During the 25 min of injection of the $(Ca\text{-}Mg)Cl_2$ solution in the reactor, the $[Mg]_{solid}$ follows the increase of the aqueous Mg concentration (**Fig. 2A**). As illustrated in **Fig. 2B**, in experiments MgCa4, MgCa5, and MgCa6, $[Mg]_{solid}$ continues to increase considerably after 25 min of reaction time although the titration of the inlet fluid was stopped. This is attributed to the continuous interaction of Mg-ACC and Mg-calcite with the reactive fluid. Note also that the enrichment of the solid phases in Mg after Mg-ACC transformation occurs at near thermodynamic equilibrium conditions as illustrated by the low and constant Ca concentration in

the fluid, which are referring to quasi zero growth rates (**Table S1**; **Fig. 1**) and is further supported by the low and stable saturation state with respect to the forming Mg-calcite phase (i.e. Ω = 1.5 for run MgCa4 assuming the precipitated solid-solutions are ideal; **Table S1**; assuming formation of regular solid-solutions will yield ever lower Ω values) as it has been earlier documented by Purgstaller et al. (2016; **Fig. 8A**)

The Mg isotope composition of the precipitated solid ($\delta^{26}Mg_{solid}$) exhibits an overall variation that does not exceed 0.6‰ in all the measured samples (**Fig. 3**, **Table 1**). The Mg-bearing ACC samples precipitated in experiments MgCa4, MgCa5 and MgCa6 exhibit an increase of about 0.3 ‰ in their isotopic composition over the period of time where these phases are present. After the transformation of Mg-ACC to Mg-calcite the isotopic composition of the crystalline phase is somewhat lighter compared to the Mg-ACC precursor from which it was formed (**Fig. 3**). The $\delta^{26}Mg_{solid}$ of Mg-calcite exhibited an overall increase over the duration of the experimental runs from -0.2‰ to 0.2‰ with exception of experiment MgCa8 where $\delta^{26}Mg_{solid}$ remained constant over the whole duration of the experimental run (**Fig. 3**). This run was the only one where crystalline Mg-calcite nucleated directly from the reactive fluid and the final Mg-calcite had a much lower Mg content than those formed in the other runs. The small temporal evolution of $\delta^{26}Mg_{solid}$ compared to that of $\delta^{26}Mg_{fluid}$ (it increases from 0.7 to almost 4‰ in MgCa4) results from the fact that most of the Mg resides in the solids for all experiments (**Table 1**).

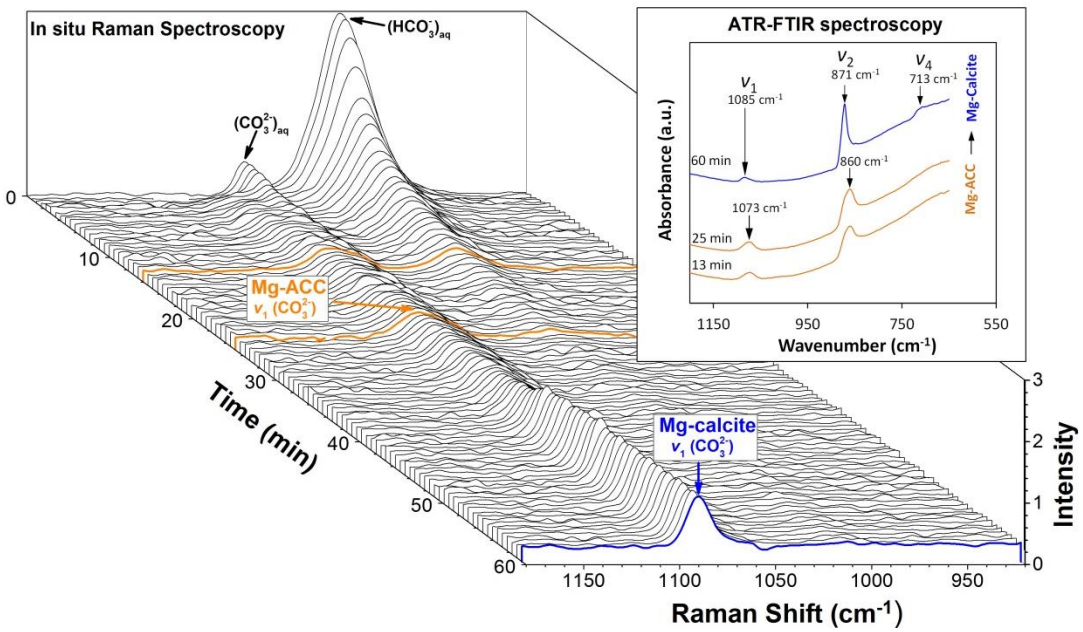

Fig. 4. Waterfall plot of Raman spectra illustrating the transition of Mg-ACC to Mg-calcite and associated ATR-FTIR spectra of Mg-ACC and Mg-calcite subsamples.

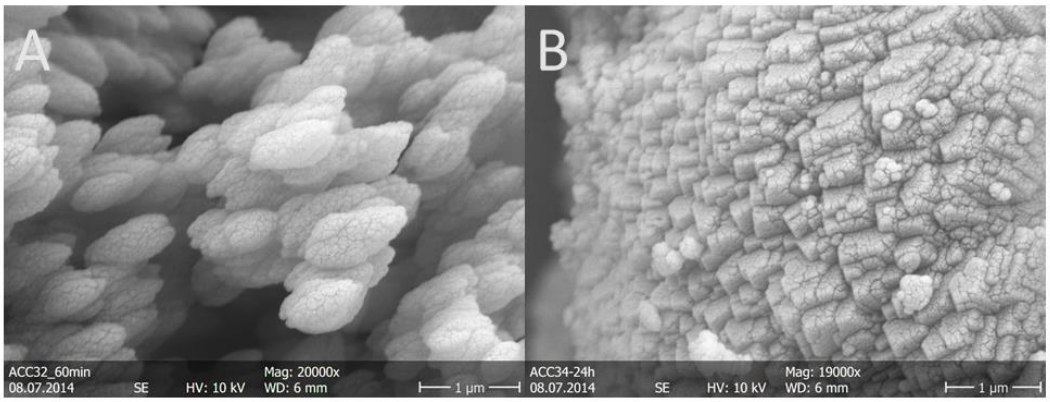

Figure 5. Scanning Electron Microphotographs of Mg-calcite formed via: (**A)** an Mg-ACC precursor in experiment MgCa4 and (**B)** via direct precipitation in experiment MgCa8.

4.3.3 Measured Mg isotope fractionation between solid and fluid

Mg isotope fractionation between the solid and reactive fluid, $\Delta^{26}_{meas}Mg_{solid-fluid} \approx 1000 \ln(\alpha^{26}_{meas}Mg_{solid-fluid})$, has been estimated as:

$$\Delta^{26}_{meas}Mg_{solid-fluid} = \delta^{26}Mg_{solid} - \delta^{26}Mg_{fluid} \quad (2)$$

The results are reported as a function of time in **Fig. 6A**. It can be seen that the extent of Mg isotopes fractionation increases considerably after 25 minutes of reaction after the transformation of Mg-ACC into Mg-calcites, from -1‰ to about -3.5‰.

During the first 20-25 minutes of the experiments MgCa4, MgCa5 and MgCa6 when Mg-ACCs are the only solid phases present, the measured fractionation factor between Mg-ACC and the reactive fluid is constant and equal to -1.0 ±0.1‰ for the three experimental runs (**Fig. 6A**). It should be reminded that using **Eq. 2** to calculate the isotope fractionation requires a homogeneous composition of the solid phase. During the first 25 min of the experimental runs of this study, however, the continuous addition of Mg results in variations of chemical and isotopic compositions of the fluid and solid phase (**Fig. 2A**, **2B**). Thus a more rigorous estimate of the temporal isotope evolution of the fluid phase and precipitated solids could be made based on isotopic mass balance in the fluid assuming constant Mg isotope fractionation between the fluid and the solids, based on a mass balance equation.

$$\delta^{26}Mg_{fluid} = \delta^{26}Mg_{inlet\ fluid} - \Delta^{26}_{meas}Mg_{solid-fluid} \times f_{Mg_{aqueous}} \quad (3)$$

where $\delta^{26}Mg_{inlet,fluid}$ is the Mg isotope composition of the inlet fluid and $\delta^{26}Mg_{fluid}$ and $f_{Mg_{aqueous}}$ stand for the isotope composition of the reactive fluid and the fraction of inlet Mg precipitated at a given time. As a first approximation, the value derived from **Eq. 2** ($\Delta^{26}_{meas}Mg_{solid-fluid}$ = -1.0 ±0.1‰) was used for this calculation. Mg isotope composition of the solid phase is deduced from the calculated $\delta^{26}Mg_{fluid}$ using **Eq. 2.** It can be seen on **Fig. 7A** that the calculated isotope composition of precipitated Mg-ACC is significantly higher than the measured one at the onset of precipitation reaction (1.2 vs 0.7‰ after 5 minutes, run MgCa4), whereas after 25 minutes of reaction time, there is a good agreement between calculated and measured values for both fluids and solids (runs MgCa4, MgCa5 and MgCa6). In order to reproduce the observed fluid isotope composition after five minutes of reaction a $\Delta^{26}_{meas}Mg_{solid-fluid}$ value of -0.4‰ is required (see **Fig. 7A**). This smaller solid-fluid isotope fractionation at the onset of Mg-ACC precipitation compared to the end of the titration likely reflects the incorporation of a significant amount of hydrated Mg in the ACC due to the very fast precipitation rate (**Fig. 1**), as hydrated Mg has a similar isotope composition to that of the aqueous Mg^{2+}. The shift between the measured and calculated $\delta^{26}Mg_{solid}$ reflects the isotopic heterogeneity of the Mg-ACCs precipitated under strongly decreasing precipitation rates during the first 25 minutes of reaction (**Fig.1**).

After 25 minutes, the titration of the inlet $(Ca,Mg)Cl_2$ solution is stopped and the reaction proceeds in a closed system with the rapid transformation of Mg-ACC into Mg-calcite. As shown by **Fig. 3**, this is accompanied by a sharp increase of the fluid $\delta^{26}Mg$ from 1‰ (25 min) to 3.9‰ (60 min., run MgCa4). Using the Mg chemical and isotopic compositions measured in the fluid at 25 min and assuming again constant Mg isotope fractionation between the fluid and the solids, the temporal isotope evolution the fluid phase and the newly formed Mg-calcites can be derived from **Eq. 3** in which $\delta^{26}Mg_{inlet\ fluid}$ is replaced by $\delta^{26}Mg_{fluid\text{-}25}$, which is the $\delta^{26}Mg_{fluid}$ after 25 min, at the end of titration. The average value of the Mg isotope composition of reactive fluid in experiments MgCa4, MgCa5 and MgCa6 (i.e. 0.98 ‰, **Table 1**) was selected for $\delta^{26}Mg_{fluid\text{-}25}$. The evolution of the isotope compositions of the reactive fluid and precipitated solid as a function of the fraction of Mg precipitated in the experiments MgCa4, MgCa5 and MgCa6 is shown in **Fig. 7B**. The good fit of experimental data, obtained with a value of $\Delta^{26}_{meas}Mg_{solid-fluid}$ equal to -3.1±0.25‰, confirms that Mg isotope fractionation occurred at (or near) equilibrium as it has been suggested by Schott et al (2016). However, in runs MgCa4 and MgCa5 and for the highest

$f_{Mg_{aqueous}}$ values (≥0.8), the solids tend to exhibit lower $\delta^{26}Mg$ values (corresponding to $\Delta^{26}_{meas}Mg_{solid-fluid}$ = -3.6‰) than predicted by the model. This likely reflects the increase of Mg isotope fractionation with the increase of calcite content and/or the formation of a thermodynamically more stable solution as discussed in detail in § 4.3.

4.3.4 Calculated Mg isotope fractionation between the solids and aqueous Mg^{2+}

Magnesium speciation in the reactive fluid considerably evolves during the course of the experimental runs (**Table S2**). At the onset of the experiments when Mg-ACC precipitation starts, Mg^{2+}(aq) accounts for only ~ 25% of dissolved magnesium (with about 51% $MgHCO_3^+$ and 26% $MgCO_3$°) due to the very high alkalinity of the reactive fluid. Mg^{2+}(aq) mole fraction progressively increases with the reaction progress and the subsequent alkalinity decrease, and accounts for about 70-75% of total dissolved magnesium ($\Sigma Mg_{(aq)}$) at the end of the runs. Because Mg^{2+}(aq) isotope composition is significantly lighter than those of the Mg bicarbonate and carbonate complexes (at 25°C $\delta^{26}Mg^{2+}$(aq) is about 4.0‰ and 5.2‰ more negative than $\delta^{26}MgHCO_3^+$ and $\delta^{26}MgCO_3$°, respectively, Schott et al., 2016), it is also lighter compared to $\Sigma Mg_{(aq)}$ in aqueous carbonate solutions. This results in isotopically lighter Mg in Mg-calcite, assuming that Mg is incorporated as Mg^{2+} in the growing carbonate. The isotopic composition of $Mg^{2+}_{(aq)}$ in the reacting fluid has been determined using the $^{26}Mg/^{24}Mg$ reduced partition function ratios (β) of Mg aqueous species derived from density-functional electronic structure calculations reported by Schott et al. (2016). An example of the temporal evolution of Mg aqueous speciation and the isotopic composition of Mg^{2+} and $MgHCO_3^+$ aqueous species for experiment MgCa4 can be seen in **Fig. S1**. Calculated $\delta^{26}Mg^{2+}_{(aq)}$ and $\Delta^{26}_{calc}Mg_{solid-Mg^{2+}(aq)}$ are reported in **Table S2** together with Mg speciation in the reacting fluids during the experimental runs (see the caption of this table for more information on these calculations).

The evolution of $\Delta^{26}_{calc}Mg_{solid-Mg^{2+}(aq)}$ as a function of time is plotted in **Fig. 6B**. $\Delta^{26}_{calc}Mg_{solid-Mg^{2+}(aq)}$ for experiments MgCa4, MgCa5 and MgCa6 evolves from positive values of ~2.0‰ at the onset of Mg-ACC precipitation to negative values of about -2.5 to -3.0‰ at the end of Mg-calcite growth. During experiment MgCa8, where Mg-calcite directly precipitated, calcite Mg concentration and $\Delta^{26}_{calc}Mg_{solid-Mg^{2+}(aq)}$ (≈ -1.7‰) kept roughly constant.

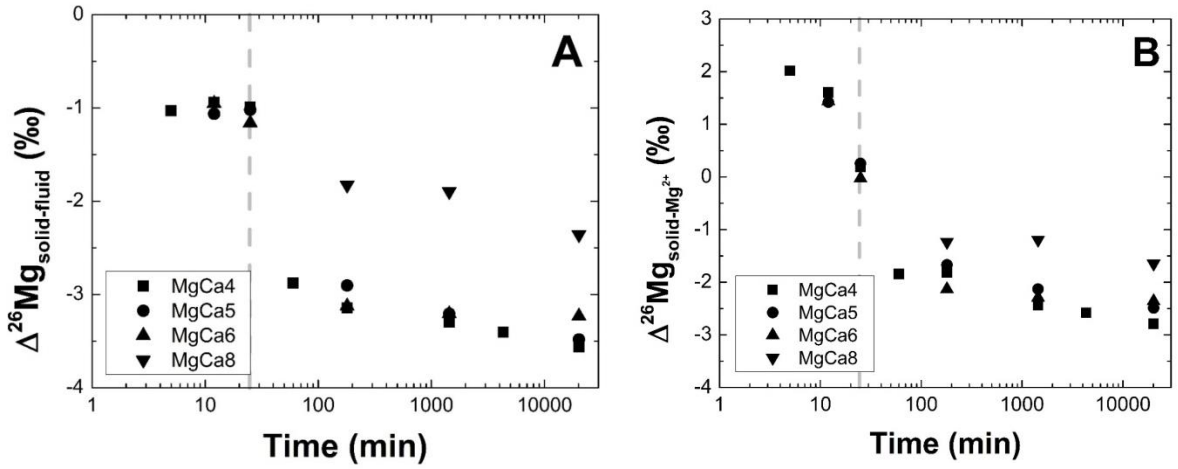

Fig. 6. Temporal evolution of **A)** measured Mg isotope fractionation between the solid and the reactive fluid and **B)** calculated Mg isotope fractionation between the solid and Mg^{2+}(aq) speciation for all experimental runs. Note that the isotopic composition of the fluid, in the case this parameter has not been measured, has been deduced from mass balance calculations using **Eq. 3**.

Table 1
Temporal evolution of Mg content, Mg isotope composition of the solid and the fluid phase and measured and calculated Mg isotope fractionation factors of samples measured in this study.

		Solid					Solution						
Experiment	Elapsed time (min)	Mg (mol %)	δ^{25}Mg (‰)	± 2σ	δ^{26}Mg (‰)	± 2σ	Mg (mM)	δ^{25}Mg (‰)	± 2σ	δ^{26}Mg (‰)	± 2σ	$\Delta^{26}Mg_{solid\text{-}fluid}$ (measured)	$\Delta^{26}Mg_{solid\text{-}Mg2+}$ (calculated)
MgCa4	5	4.54	-0.16	0.04	-0.34	0.02	15.0	0.36	0.01	0.69	0.03	-1.03	2.02
MgCa4	13	6.79	-0.06	0.03	-0.13	0.05	24.4	0.42	0.03	0.81	0.01	-0.94	1.6
MgCa4	25	9.98	-0.03	0.01	-0.05	0.04	27.2	0.48	0.03	0.94	0.02	-0.99	0.19
MgCa4	60	15.67	-0.11	0.01	-0.23	0.03	12.1	1.26	0.01	2.44	0.01	-2.67	-1.84
MgCa4	180	16.85	-0.07	0.03	-0.15	0.02	8.9						
MgCa4	1440	17.87	0.01	0.02	0.01	0.05	6.1	1.86	0.02	3.60	0.02	-3.59	-2.44
MgCa4	4320	18.50	0.05	0.02	0.10	0.03	4.3	1.94	0.01	3.77	0.02	-3.67	-2.58
MgCa4	20160	19.36	0.12	0.01	0.21	0.04	1.9	1.99	0.03	3.84	0.03	-3.63	-2.79
MgCa5	5	4.58	-0.16	0.02	-0.31	0.03	11.6						
MgCa5	13	6.44	-0.12	0.01	-0.23	0.02	18.4	0.44	0.01	0.83	0.01	-1.06	1.42
MgCa5	25	8.14	-0.03	0.01	-0.06	0.03	21.9	0.50	0.01	0.96	0.03	-1.02	0.26
MgCa5	180	13.03	-0.14	0.01	-0.27	0.02	9.8						
MgCa5	1440	14.17	-0.08	0.04	-0.16	0.05	6.8	1.75	0.02	3.41	0.02	-3.57	-2.13
MgCa5	20160	15.67	0.07	0.03	0.12	0.04	2.8	1.80	0.04	3.50	0.04	-3.38	-2.499
MgCa6	5	4.03	-0.28	0.01	-0.55	0.02	9.8						
MgCa6	13	5.40	-0.03	0.02	-0.06	0.02	15.8	0.46	0.01	0.89	0.02	-0.95	1.44
MgCa6	25	6.95	-0.06	0.01	-0.13	0.01	18.5	0.54	0.02	1.03	0.02	-1.16	-0.02
MgCa6	180	11.81	-0.10	0.03	-0.22	0.05	6.6						
MgCa6	1440	12.30	-0.05	0.03	-0.09	0.06	5.3						
MgCa6	20160	12.78	0.05	0.02	0.09	0.03	4.1	1.80	0.04	3.50	0.04	-3.41	-2.36
MgCa8	13	8.07	-0.10	0.02	-0.21	0.04	5.5						
MgCa8	180	7.28	-0.15	0.04	-0.29	0.06	9.4	0.79	0.03	1.54	0.06	-1.83	-1.24
MgCa8	1440	7.18	-0.17	0.03	-0.34	0.03	9.6	0.80	0.02	1.56	0.05	-1.90	-1.20
MgCa8	20160	8.03	-0.15	0.03	-0.32	0.07	7.6	1.06	0.01	2.04	0.02	-2.36	-1.65
MgCa4 (initial fluid)								0.17	0.01	0.34	0.03		
MgCa6 (initial fluid)								0.20	0.04	0.37	0.06		

4.4. DISCUSSION

4.4.1 Magnesium isotope fractionation at equilibrium

The determination of an equilibrium value for the isotope fractionation factor between a solid and the fluid from which it forms is the most important prerequisite in order to describe kinetic deviation phenomena during mineral growth. In the case of Mg isotope fractionation between Mg-calcite and fluids, the value of isotope fractionation at equilibrium conditions is to date under debate. So far two experimental studies have reported on this value. Using batch reactors Li et al. (2012) suggested that at isotopic equilibrium the Mg isotope fractionation factor between Mg-calcite and fluid is -2.6‰. Afterwards Mavromatis et al. (2013), based on the deviation from the theoretical equilibrium value in a three-isotope-plot suggested that equilibrium in the same mineral-fluid system is significantly larger at -3.5‰ for a calcite containing ≤ 0.3 Mg mol%. Recently, two studies provided new insights on other parameters that control Mg isotope fractionation at equilibrium and may explain the observed discrepancy. Based on ab-initio calculations Pinilla et al. (2015) suggested that the increase of the Mg content in calcite, which induces longer Mg-O bond length, controls Mg isotope fractionation at equilibrium, with larger Mg isotope fractionation factors to be attributed to calcites with higher Mg content. More recently Schott et al. (2016) showed that a large isotope fractionation occurs between Mg^{2+}(aq) and aqueous Mg (bi)carbonate complexes. Thus in carbonate-rich fluids with a significant proportion of aqueous Mg-bicarbonate/carbonate complexes, Mg^{2+}(aq) isotope composition can be significantly different from that of the bulk fluid. That for corrections are required for estimating the actual $\delta^{26}Mg^{2+}$(aq) value. For example after correction for the presence of $MgHCO_3^+$(aq) the Mg isotope fractionation between Mg-calcite and the Mg^{2+} (aq) reported by Mavromatis et al. (2013), is decreased to -3.1 ‰, whereas no significant changes occur in that reported by Li et al. (2012) owing to the low proportion of $MgHCO_3^+$ and $MgCO_3^\circ$ in their experimental solutions (Schott et al., 2016).

4.4.2 Magnesium isotope fractionation during Mg-ACC formation

In all the runs where Mg-ACCs are formed, a significant impact of kinetics on Mg isotopes fractionation has been detected at the onset of titrations owing to the fast precipitation rates (see **Figs. 1** and **7A**). However, Mg aqueous speciation could imprint as well Mg isotopes fractionation during Mg-ACCs formation as discussed in section 4.1. Indeed, assuming that

Mg^{2+}(aq) is the only Mg species incorporated in ACC during its formation, the calculated Mg isotope fractionation between the solids and Mg^{2+}(aq), $\Delta^{26}_{calc}Mg_{ACC-Mg^{2+}(aq)}$, varies between +2.0 and 0.0‰ as a function of time (**Fig. 6B**). This fractionation pattern is significantly different from the value of the isotope fractionation between the Mg-ACC and total dissolved magnesium ($\Delta^{26}_{meas}Mg_{ACC-Mg(aq,tot)}$ = - 1.0 ±0.1‰; **Fig. 6A**).

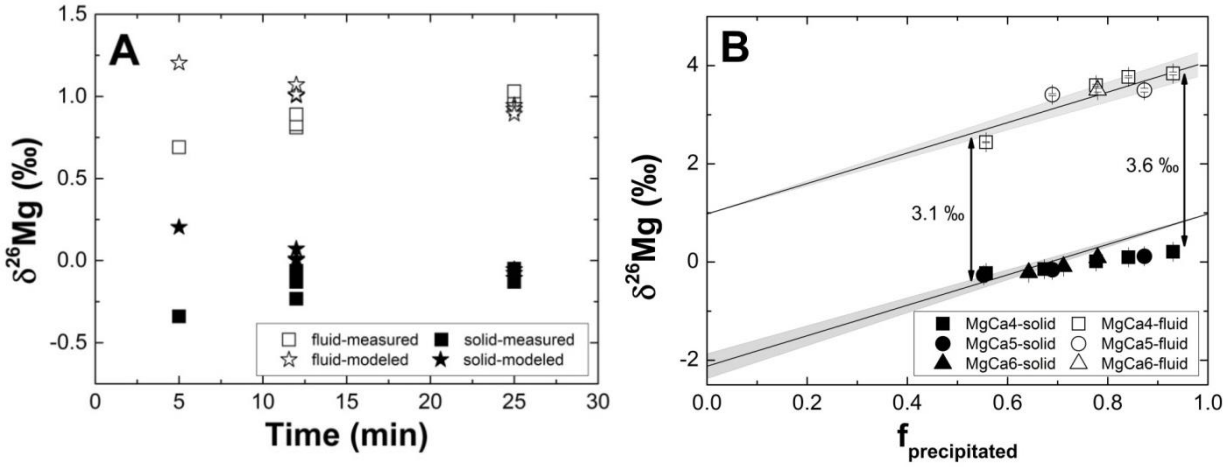

Fig. 7. A) Measured Mg isotope composition of precipitated MgACC (closed rectangle) and fluids (open rectangle) and modeled results (open and closed stars) as a function of time during the 25 minutes titration of the inlet solution in all experimental runs. The modeled values were acquired using Eq. 2 with a fractionation factor between the MgACCs and the fluid $\Delta^{26}_{meas}Mg_{solid-fluid}$ = -1‰. It can be seen that the observed compositions at 5 min reaction time can only be reproduced using a fractionation factor of -0.4‰. **B)** Mg isotope composition of Mg-calcites (closed symbols) and fluids (open symbols) plotted as a function of the fraction of aqueous Mg incorporated in the solid phase during the reaction progress in closed system after the 25 minutes titration.; the solid lines represent the modeled isotope compositions using Eq. 3 with a fractionation factor between Mg-calcites and the fluid $\Delta^{26}_{meas}Mg_{solid-fluid}$ = -3.1‰. It can be seen that for the runs MgCa4 and MgCa5 $\Delta^{26}_{meas}Mg_{solid-fluid}$ decreases to -3.6‰ at the end of the runs.

At first sight, the positive values derived for $\Delta^{26}_{calc}Mg_{ACC-Mg^{2+}(aq)}$ is counter-intuitive because ^{24}Mg is generally found to be preferentially incorporated into crystalline carbonates (i.e. magnesite, Pearce et al;, 2012; dolomite, Li et al., 2015; calcite, Immenhauser et al., 2010, Li et al., 2012, Mavromatis et al., 2013). The preferential incorporation of ^{24}Mg is consistent with the longer average Mg-O bond lengths in these crystalline carbonates than in the Mg^{2+} aquo ion (Li

et al., 2014; Schott et al., 2016) and the general rule that ^{26}Mg isotopes are relatively more stable having shorter, stronger bonds given the same coordination (e.g. Criss, 1999; Schauble, 2004). In Mg-ACC, however, the average Mg-O bond length is significantly shorter than in the Mg aquo ion. Politi et al. (2010), using Mg *K*-edge X-ray absorption spectroscopy (XAS), reported a Mg-O bond length in Mg-ACC of ~2.04 Å compared to 2.08/2.09 Å in the Mg aquo ion (Pavlov et al., 1998; Pinilla et al., 2015; Schott et al., 2016). This could induce a preferential enrichment in ^{26}Mg of precipitating Mg-ACC as observed during the crystallization of the hydrous Mg-carbonates hydromagnesite and nesquehonite whose crystals exhibit mean Mg-O bond lengths of 2.069/2.076 Å (see Mavromatis et al., 2012a; Shirokova et al., 2013; Schott et al., 2016). Within the framework of this scenario, the temporal reduction of $\Delta^{26}_{calc}Mg_{ACC-Mg^{2+}(aq)}$ during the continuous titration of the inlet (Ca,Mg)Cl_2 solution in the reactor (**Fig. 6B**) may reflect an increase over time of Mg-ACC average Mg-O bond length. This follows the continuous re-equilibration between the Mg-ACC and the fluid phase and the subsequent enrichment of solids in Mg together with a progressive dehydration of Mg in ACC (**Fig. 2B**). This feature is consistent with the recent results of Lin et al. (2015) who demonstrated, based on the systematic variation in the ^{25}Mg solid-state NMR chemical shifts, that the Mg-O bond lengths of Mg-ACC increase as their Mg content increase.

Alternatively, these positive $\Delta^{26}_{calc}Mg_{ACC-Mg^{2+}(aq)}$ values may not reflect the actual isotope fractionation between Mg-ACC and Mg^{2+}(aq) if Mg^{2+} is not the only magnesium species incorporated in the precipitated solids. The precipitated Mg-ACC consist of a nanometer-scale porous Ca-rich framework that supports interconnected channels containing water and carbonate molecules but also Mg bicarbonate and carbonate complexes (Goodwin et al., 2010). It is likely that, during very fast precipitation of Mg-ACC from a highly supersaturated solution, $MgHCO_3^+$ and $MgCO_3°$, which account for 50-to-20% and 26-to-10% of total dissolved magnesium, respectively, are directly incorporated in the precipitating nanoporous solids together with $Mg(H_2O)_6^{2+}$. This is consistent with the results of Wang et al. (2012) documenting that ACC with a higher Mg content can be produced when conditions are biased to favor the formation of $MgCO_3°$ species. As a result, the actual Mg isotope fractionation occurring during Mg-ACC precipitation may be better approximated by $\Delta^{26}_{meas}Mg_{ACC-Mg(aq,tot)}$ = -1.0‰ than by

calculated values ($\Delta^{26}_{calc}Mg_{ACC-Mg^{2+}(aq)}$ = 2.0 to 0.0‰). Note, however, that the -1‰ fractionation value could not be considered as representing isotope equilibrium fractionation factor between Mg-ACC and the fluid because the formed Mg-ACCs, that may accommodate significant amount of water and Mg aqueous complexes, are highly metastable solids.

4.4.3 Magnesium isotope fractionation during direct Mg-calcite precipitation

A striking feature of our results is that Mg-calcite formation pathway – via an amorphous precursor or during direct precipitation - has a profound impact on the temporal evolution of the Mg content and isotope composition of the reacting fluids and the newly formed solid. During the formation of Mg-calcite in experiment MgCa8 which occurred in the absence of an ACC precursor no changes in Mg concentration and only small changes in the Mg isotope fractionation between calcite and fluid were observed once the titration of the (Ca,Mg)Cl_2 inlet solution had been stopped (see **Figs. 2** and **6**). In contrast, the formation of Mg-calcites via an initial Mg-ACC precursor in experiments MgCa4, MgCa5 and MgCa6 is accompanied by a profound evolution of (i) the Mg composition of reacting fluid and precipitated solids (**Fig. 2**) and (ii) of the isotope fractionation between Mg-calcites and the fluid (**Fig. 6**). Furthermore, in the absence of a Mg-ACC precursor, the extent of Mg isotope fractionation (- 2.0‰ ≤ $\Delta^{26}_{meas}Mg_{calcite-fluid}$ ≤ - 1.8‰) is significantly lower than that measured for Mg-calcites issued from ACC precursors (- 3.6‰ ≤ $\Delta^{26}_{meas}Mg_{calcite-fluid}$ ≤ - 3.2‰).

In experiment MgCa8 with a [Mg]/[Ca] ratio of 0.125 in the inlet solution, the Mg concentration is too low to enable the formation and/or stabilization of amorphous calcium carbonates. Moreover the higher Ca concentration together with the low [Mg]/[Ca] ratio in the inlet fluid (see **Table S1**) of this run induces faster apparent growth rates as it can be seen in **Fig. 1**. Consequently, the ~ 7-8 mol% Mg precipitated calcite records a strong isotopic shift from that expected for equilibrium conditions. Because the dehydration rate of $Mg(H_2O)_6^{2+}$ is ~ 5 orders of magnitude lower than that of $Ca(H_2O)_6^{2+}$, the very fast calcite precipitation rates result in the incorporation of only partially dehydrated Mg in the calcite lattice and thus in a lesser extent of isotopic fractionation between calcite and dissolved magnesium (Mavromatis et al., 2013). The Mg isotopic signatures acquired during the titration of the inlet solution exhibit small variations of -1.80 ≤ $\Delta^{26}_{meas}Mg_{calcite-fluid}$ ≤ -2.35‰ (**Fig. 6A**) during the full duration of the experiment (~ 200

hrs). This slow exchange is similar to that observed for oxygen isotopes between Mg-calcite and fluid at near equilibrium conditions that reported earlier by Mavromatis et al. (2012b). This likely happens because Mg-calcite precipitated directly in experiment MgCa8 consists of larger crystals and consequently offers a lower surface area to the reacting fluid compare to those precipitated via an amorphous precursor as it is illustrated in **Fig. 5**.

In contrast, the chemical and isotopic signatures of the Mg-ACC formed in experiments MgCa4, MgCa5, and MgCa6 during the initial titration of the Mg-rich inlet solutions are not preserved and continuously evolved with time during the full duration of the experiments. This likely occurs because the initially formed highly nanoporous ACC accommodates hydrated Ca and Mg within the interconnected/percolating channels that contain water with high carbonate and Mg concentrations. As a result, Mg-ACC is progressively converted into crystalline Mg-calcite via an exchange of carbonate and magnesium from the channels with hydrated calcium. This conversion requires only small movements within this nanoporous solid being intersected by a network of connected channels. The transformation from Mg-ACC to Mg-calcite is consequently easily achieved by small scale dissolution/precipitation and/or diffusion processes. This transition, occurring near chemical equilibrium (see $SI_{Mg\text{-}calcite}$ values listed in **Table S1**) from enriched Mg solutions (up to 27 mM Mg in experiment MgCa4), leads to the formation of Mg-calcites whose Mg content progressively increases with time (i.e. to near 20 mol% in experiment MgCa4) to approach equilibrium between the fluid and the two end-members of the crystalline solid-solution. Accordingly, $\Delta^{26}_{meas}Mg_{calcite-fluid}$ becomes progressively more negative (up to -3.6‰) as calcite Mg content increases (**Fig. 6A**). This observed evolution of the $\Delta^{26}_{meas}Mg_{calcite-fluid}$ value with increasing Mg content in calcite (**Fig. 7B**) can be explained by the increase of Mg content in calcite as it was earlier suggested by the *ab initio* calculations of Pinilla et al. (2015) and/or by the evolution of the forming crystalline solid-solutions to thermodynamically more stable phases as illustrated in run MgCa4 by the reduction of the excess free energy of mixing from 5.31 kJ/mol for the solid sampled after 60 min to 1.08 kJ/mol for the solid sampled at 14 days. The time evolution of $\Delta^{26}_{meas}Mg_{calcite-fluid}$ due to changes in the isotopic composition of Mg^{2+}(aq) can be excluded as the ratio [Mg^{2+}aq)]/[$\sum$Mg(aq)] does not change after 180 min of reaction (**Table S2**) and the evolution of $\delta^{26}Mg_{solid}$ is similar to that of δ^{26}Mg(aq).

4.4.4 Implication for marine biogenic carbonate archives

The results shown here have implications for the interpretation of Mg isotope from biogenic marine carbonate archives. In the case of the direct nucleation/precipitation of a crystalline Mg-calcite (experiment MgCa8), the Mg composition and isotopic signature acquired during precipitation remained quasi constant. This implies that the Mg isotope signatures of directly crystallized calcites reflect the chemical environment of their formation, with small changes in the isotopic composition of the solid over time to be attributed to re-equilibration between solid and fluid due to the high reactive surface area of the solid (**Fig. 5**). Similarly, Mavromatis et al. (2016b) have shown that the outer surfaces of precipitated witherite crystals are subject to isotopic re-equilibration. Actually the obtained results indicate that the isotopic composition of the Mg-calcites formed in the absence of an amorphous precursor is strongly affected by the fast precipitation kinetics with a shift of ~ +0.9‰ relative to the equilibrium fractionation (i.e. $\Delta^{26}_{meas}Mg_{calcite-Mg^{2+}(aq)}$ = -3.1‰). Such shifts have to be taken into account for environmental reconstructions (seawater chemistry, saturation state, pCO_2…), considering that in the case of ACC secreting organisms, also parameters such as pH, photosynthetic activity, complexation with organic ligands, enzymatic activity etc. - summarized under the generic term "vital effects" may affect the isotopic composition of the forming carbonate solid. Note also that Mg-rich calcites (> 10 mol% Mg) cannot be formed via the direct precipitation of crystalline calcite from aqueous solution at 25°C (Purgstaller et al., 2016).

At pH 8.3 and inlet fluid [Mg]/[Ca] ≥ 0.17, the formation of nanoporous hydrated Mg-ACCs that is progressively transforming into Mg-rich crystalline calcites (up to 20 mol% Mg) is observed in this study. This transformation takes place in near chemical and isotopic equilibrium conditions and proceeds via ion exchange and/or dissolution/re-precipitation processes. This leads to Mg isotope fractionation under isotopic equilibrium conditions, whose absolute value slightly increases with calcite Mg content. Because of the significant Mg isotope fractionation ($\delta\Delta^{26}_{meas}Mg_{calcite-fluid}$ = - 2‰) and fluid increase in δ^{26}Mg (by nearly 3‰) following the ACC-calcite transformation (**Fig. 6A**), the final Mg-calcite isotopic composition does not reflect the fluid isotopic composition at the onset of Mg-ACCs precipitation. It can thus be inferred that due to the pronounced change in $\Delta^{26}_{meas}Mg_{calcite-fluid}$ accompanying the transformation of Mg-ACC to crystalline Mg-calcite, the bulk isotopic compositions of skeletons where amorphous and

crystalline $CaCO_3$ coexist are potentially compromised as archives of their formation environment. Specifically, the Mg isotope fractionation during the formation of ACC as documented herein suggests that the interpretation of the isotopic signature of stabilized ACC may not be straightforward. Indeed the large shift observed between the calculated $\Delta^{26}_{calc}Mg_{ACC-Mg^{2+}(aq)}$ (i.e. 0.0‰ ≤ Δ^{26}Mg ≤ +2.0‰) and the measured $\Delta^{26}_{meas}Mg_{ACC-Mg(aq,tot)}$ (i.e. Δ^{26}Mg = -1.0±0.1‰) may reflect (i) a shorter average Mg-O bond in Mg-ACC compared to the Mg aquo ion, within a scenario assuming that only Mg^{2+}(aq) is incorporated in the solids; (ii) a simple calculation artifact if all Mg aqueous species (including $MgHCO_3^+$ and $MgCO_3$°) are incorporated in the forming Mg-ACCs and (iii) a combination of the two above processes. Consequently only the spatial isotope analyses of crystalline calcite domains could provide information on the confined fluids. But even then, kinetic effects might compromise these results. If this holds true in a general manner for major groups of carbonate secreting organisms, then the interpretation of proxy data requires a critical re-assessment (Weiner et al., 2009; Immenhauser et al., 2016). Note here that not all carbonate biomineralizers secrete their skeletal hardparts via amorphous precursor phases (Brown, 1982). Some apply this biomineralization strategy mainly during their larval stage (Weiss et al., 2002), whilst others might apply direct mineralization combined with an amorphous strategy (Aizenberg et al., 2002, 2003; Nassif et al., 2005; Jacob et al., 2008; Griesshaber et al., 2009). This includes the storage of amorphous calcium carbonate phases in vesicles for extended time periods (Brown, 1982; Griesshaber et al., 2009; Weiner et al., 2009; Immenhauser et al., 2016). Another crucial issue in using the Mg isotope composition of biominerals formed, at whole or partly, via an Mg-ACC precursor phase are the environmental conditions occurring during this transformation. Indeed transformation in an open or closed system with respect to aqueous Mg may alter the interpretation of isotopic signatures. In a closed system (no external Mg source) the Mg isotope composition of the Mg-ACC is fixed in the Mg calcite, whereas is an open system equilibration between solid and fluid is determined by aqueous Mg prior to achievement of isotopic equilibrium. Likewise a change in the fluid pH in both closed and open system environments may alter the interpretation of isotopic signatures as the abundance of aqueous species (e.g. $MgHCO_3^+$ and $MgCO_3$°) is pH dependent and the isotopic shifts they induce somewhat different.

4.5. CONCLUSIONS

We investigated the magnesium isotope composition of reacting fluids and precipitated carbonates at 25°C and pH 8.3 in a 1M $NaHCO_3$ solution. For a titrated solution with [Mg]/[Ca] = 0.125, a crystalline Mg-calcite directly precipitates without the measurable formation of an amorphous $CaCO_3$ precursor. This Mg-calcite phase exhibits a kinetic isotopic signature ($\Delta^{26}_{meas}Mg_{calcite-fluid}$ = -2.3‰) which was acquired during its precipitation. For 0.125 < [Mg]/[Ca] ≤ 0.25, the initial precipitation of a Mg-rich amorphous calcium carbonate acts as a precursor for Mg-calcite formation with up 20 mol % Mg in the crystal lattice. The weak Mg isotope fractionation between Mg-ACCs and the fluid $\Delta^{26}_{meas}Mg_{ACC-fluid}$ = -1.0‰) is not preserved during conversion of the Mg-ACC into Mg-calcite. After a pronounced isotopic shift accompanying the transformation of Mg-ACC into Mg-calcites, $\Delta^{26}_{meas}Mg_{calcite-fluid}$ progressively decreases with reaction progress from ~ -3.0‰ to -3.6‰, reflecting both the approach of isotopic equilibrium and the increase of calcites Mg content.

The significantly different values of Mg isotope fractionation between Mg-ACC and the fluid ($\Delta^{26}_{meas}Mg_{ACC-fluid}$ = -1.0‰) and between Mg-ACC and $Mg^{2+}_{(aq)}$ ($\Delta^{26}_{calc}Mg_{ACC-fluid}$ = +2.0‰) determined at the onset of Mg-ACC precipitation are consistent with the formation of a hydrated Ca nanoporous solid accommodating Mg bicarbonate/carbonate species combined with hydrated magnesium. This solid, crossed by a connected system of channels filled with the reacting fluid, easily converts to Mg-rich calcites via exchange and/or dissolution-precipitation reactions in a closed system.

The implication of these results for reconstructions of past seawater δ^{26}Mg signatures are significant. Abiogenic marine carbonate cements primarily reflect the Mg isotope signature of their aquatic environment but isotope values are potentially influenced by their precipitation kinetics. In contrast, in biogenic carbonates secreted by organisms that apply (at least in part) amorphous precursor strategies, the Mg calcite isotopic signatures of stabilized biominerals are not representative of the fluid isotopic composition at the onset of ACC precipitation. Pending a detailed understanding of biomineralization pathways, this implies that Mg isotope values of biogenic carbonates are potentially compromised as archives of their marine environment.

4.6. SUPPLEMENTARY DATA

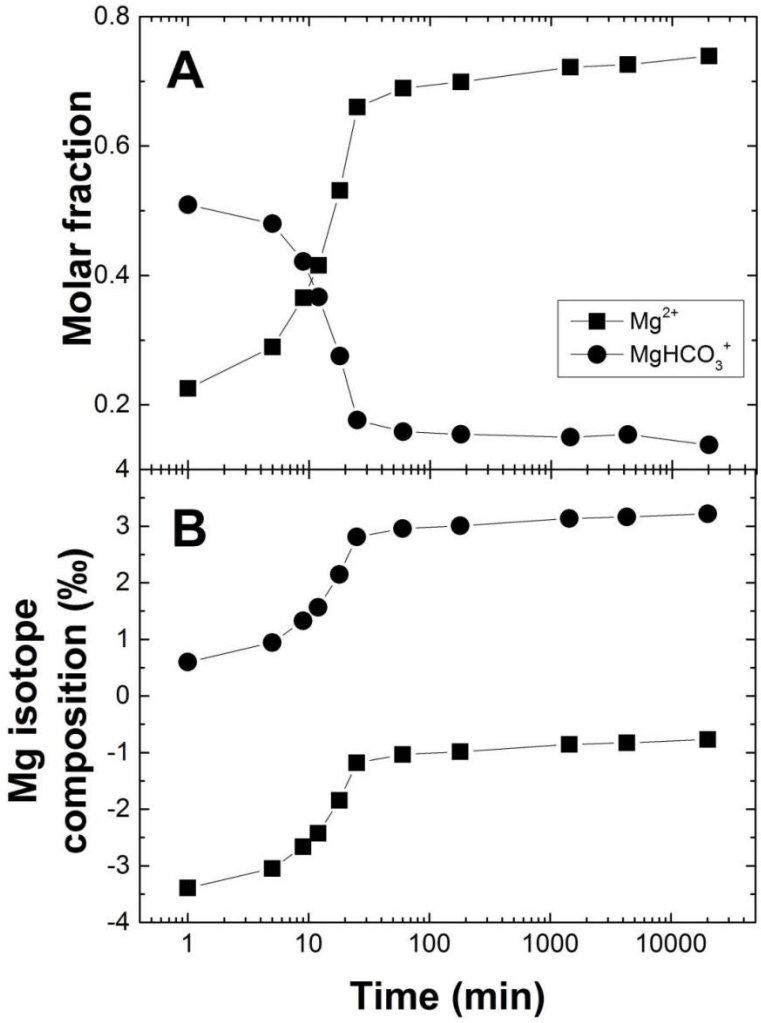

Fig. S1. Example of the temporal evolution of (**A)** the molar fraction of Mg^{2+} and $MgHCO_3^+$ aqueous species to Mg (tot) and (**B)** their isotopic composition for experiment MgCa4 assuming that the isotopic composition of aqueous Mg (tot) is equal to zero ‰ at any given time.

Table S1

Temporal evolution of pH and Ca, Mg and alkalinity concentrations and solution saturation index with respect to Mg-calcite during the experimental runs. The $SI_{Mg\text{-}calcite}$ were calculated assuming the precipitated solid-solutions are ideal.

Experiment	t (min)	pH	Alkalinity (mM)	Ca (mM)	Mg (mM)	$SI_{Mg\text{-}calcite}$
MgCa4						
	0	8.37	1020	*480**	*120**	
	1	8.37	977.2	2.78	4.00	2.25
	5	8.31	707.0	3.69	14.97	2.28
	9	8.30	491.1	3.66	20.68	2.24
	12	8.35	380.1	3.84	24.42	2.25
	18	8.36	226.5	4.15	26.96	2.20
	25	8.36	119.2	6.18	27.23	2.18
	60	8.33	94.1	0.39	12.06	0.93
	180	8.30	88.9	0.20	8.89	0.61
	1440	8.16	81.4	0.14	6.08	0.30
	4320	8.07	81.7	0.13	4.32	0.15
	20160	8.13	71.8	0.16	1.89	0.19
MgCa5						
	0	8.32	1016	*500**	*100**	
	1	8.32	971.6	0.36	2.89	1.30
	5	8.31	704.8	0.43	11.55	1.38
	9	8.29	499.7	0.39	15.90	1.28
	12	8.33	398.7	0.52	18.42	1.44
	18	8.31	236.7	0.61	19.91	1.39
	25	8.32	129.9	0.67	21.87	1.32
	60	8.37	113.8	0.39	11.38	1.05
	180	8.40	111.3	0.39	9.79	1.05
	1440	8.17	108.3	0.14	6.79	0.44
	4320	8.12	101.8	0.18	5.15	0.45
	20160	8.18	95.7	0.18	2.77	0.43
MgCa6						
	0	8.33	1015	*514,3**	*85,7**	
	1	8.33	967.56	1.62	2.90	1.97
	5	8.30	683.95	0.15	9.83	0.93
	9	8.31	478.56	0.53	14.31	1.46
	12	8.31	378.28	0.11	15.83	0.77
	18	8.25	216.76	0.35	17.43	1.12
	25	8.31	112.93	0.19	18.53	0.77
	60	8.31	95.51	0.33	8.24	0.89
	180	8.30	91.58	0.23	6.62	0.71
	1440	8.17	89.84	0.06	5.34	0.09
	4320	8.12	85.55	0.08	5.25	0.17
	20160	8.12	86.73	0.12	4.07	0.26
MgCa8						
	0	8.32	1015	*525**	*75**	
	1	8.32	1015.30	0.92	1.99	1.73
	5	8.30	674.20	0.12	4.32	0.82
	9	8.30	450.20	0.14	5.05	0.84
	12	8.34	359.70	0.14	5.54	0.85
	18	8.31	186.30	0.33	6.32	1.07
	25	8.34	88.30	0.64	8.10	1.18
	60	8.27	55.10	0.45	9.35	0.86
	180	8.31	48.30	0.28	9.38	0.66
	1440	8.35	56.90	0.14	9.60	0.47
	4320	8.32	61.40	0.13	9.25	0.44
	20160	8.41	54.60	0.14	7.59	0.49

*Estimated values based on the Mg/Ca ratio of the titrant.

Table S2
Temporal distribution of the fraction of aqueous Mg species and Mg isotope composition of bulk reactive fluid as it was measured and estimated by **Eq.3** as well as the Mg isotope composition of Mg^{2+}(aq) calculated by aqueous Mg speciation together with density functional theory estimates that reported earlier by Schott et al. (2016).

			Mole fraction					δ^{26}Mg (‰)	
Experiment	Time (min)	Mg (mM)	Mg^{2+}	$MgCO_3^o$	$MgHCO_3^+$	$MgOH^+$	$MgCl^+$	$\delta^{26}Mg_{fluid}$ (measured)	$\delta^{26}Mg_{fluid}$ (estimated)
MgCa4									
	1	4.00	0.23	0.26	0.51	<0.01	<0.01		
	5	14.97	0.29	0.22	0.48	<0.01	0.01	0.69	
	9	20.68	0.37	0.19	0.42	<0.01	0.02		
	12	24.42	0.42	0.19	0.37	<0.01	0.03	0.81	
	18	26.96	0.53	0.14	0.28	<0.01	0.05		
	25	27.23	0.66	0.09	0.18	<0.01	0.07	0.94	0.98
	60	12.06	0.69	0.08	0.16	<0.01	0.07	2.44	2.65
	180	8.89	0.70	0.07	0.15	<0.01	0.07		3.00
	1440	6.08	0.72	0.05	0.15	<0.01	0.08	3.6	3.31
	4320	4.32	0.73	0.04	0.15	<0.01	0.08	3.77	3.50
	20160	1.89	0.74	0.04	0.14	<0.01	0.08	3.84	3.77
MgCa5									
	1	2.89	0.23	0.24	0.52	<0.01	<0.01		
	5	11.55	0.29	0.22	0.48	<0.01	0.01		
	9	15.90	0.36	0.19	0.43	<0.01	0.02		
	12	18.42	0.40	0.19	0.38	<0.01	0.03	0.83	
	18	19.91	0.52	0.14	0.29	<0.01	0.05		
	25	21.87	0.64	0.10	0.20	<0.01	0.07	0.96	0.98
	60	11.38	0.65	0.10	0.18	<0.01	0.07		2.42
	180	9.79	0.65	0.10	0.18	<0.01	0.07		2.64
	1440	6.79	0.68	0.06	0.19	<0.01	0.07	3.41	3.05
	4320	5.15	0.69	0.06	0.18	<0.01	0.07		3.27
	20160	2.77	0.69	0.06	0.17	<0.01	0.07	3.5	3.60
MgCa6									
	1	2.90	0.23	0.25	0.52	<0.01	<0.01		
	5	9.83	0.30	0.21	0.48	<0.01	0.01		
	9	14.31	0.37	0.19	0.42	<0.01	0.03		
	12	15.83	0.42	0.17	0.38	<0.01	0.04	0.89	
	18	17.43	0.54	0.12	0.29	<0.01	0.06		
	25	18.53	0.66	0.08	0.18	<0.01	0.08	1.03	0.98
	60	8.24	0.68	0.08	0.16	<0.01	0.08		2.65
	180	6.62	0.69	0.07	0.16	<0.01	0.08		2.91
	1440	5.34	0.70	0.05	0.16	<0.01	0.08		3.12
	4320	5.25	0.71	0.05	0.16	<0.01	0.09		3.13
	20160	4.07	0.71	0.05	0.16	<0.01	0.09	3.5	3.32
MgCa8									
	1	1.99	0.22	0.24	0.53	<0.01	<0.01		
	5	4.32	0.30	0.21	0.48	<0.01	0.01		
	9	5.05	0.38	0.19	0.41	<0.01	0.02		
	12	5.54	0.42	0.18	0.37	<0.01	0.03		
	18	6.32	0.57	0.12	0.26	<0.01	0.05		
	25	8.10	0.70	0.08	0.15	<0.01	0.07		
	60	9.35	0.77	0.05	0.10	<0.01	0.08		
	180	9.38	0.78	0.04	0.09	<0.01	0.08		
	1440	9.60	0.76	0.06	0.11	<0.01	0.08		
	4320	9.25	0.75	0.06	0.11	<0.01	0.08		
	20160	7.59	0.76	0.06	0.10	<0.01	0.08	2.04	

5. Control of Mg^{2+}/Ca^{2+} Activity Ratio on the Formation of Crystalline Carbonate Minerals via an Amorphous Precursor

Bettina Purgstaller[1], Florian Konrad[1], Martin Dietzel[1], Adrian Immenhauser[3], Vasileios Mavromatis[1,2]

[1]*Institute of Applied Geosciences, Graz University of Technology, Rechbauerstrasse 12, 8010 Graz, Austria*
[2] *Géosciences Environnement Toulouse (GET), CNRS, UMR 5563, Observatoire Midi-Pyrénées, 14 Av. E. Belin, 31400 Toulouse, France*
[3]*Institute of Geology, Mineralogy and Geophysics, Bochum, Universitätsstraße 150, 44801 Bochum, Germany*

Published in Crystal Growth and Design 17 (2017) 1069-1078

ABSTRACT

The formation of amorphous calcium carbonate (ACC) and its transformation to crystalline phases plays a key role on the formation of carbonate minerals on Earth's surface environments. Nonetheless, the pysichochemical parameters controlling the formation of crystalline $CaCO_3$ via an amorphous precursor are still under debate. In the present study we examine whether crystalline $CaCO_3$ formation occurs via an ACC precursor in the pH range from 7.8 to 8.8 and at initial Mg/Ca ratios from 1/3 to 1/8. The obtained results document that the transformation of Mg-rich ACC (Mg-ACC) to a crystalline phase is strictly controlled by the prevailing ratio of the Mg^{2+} to Ca^{2+} activity, $a_{Mg^{2+}}/a_{Ca^{2+}}$, of the reactive solution after Mg-ACC was synthesized: Mg-ACC transformed to (i) Mg-calcite at $5 \leq a_{Mg^{2+}}/a_{Ca^{2+}} \leq 8$ and to (ii) monohydrocalcite at $8 \leq a_{Mg^{2+}}/a_{Ca^{2+}} \leq 12$. Our findings suggest that the formation of the crystalline phase induces undersaturation of the reactive solution with respect to the ACC and triggers its dissolution. Thus, the metastability of Mg-ACC in the reactive solution is not determined by its Mg content, but is related to the formation kinetics of the less soluble crystalline phase. The experimental results highlight the importance of prevailing physicochemical conditions of the reactive solution on Mg-ACC transformation pathways.

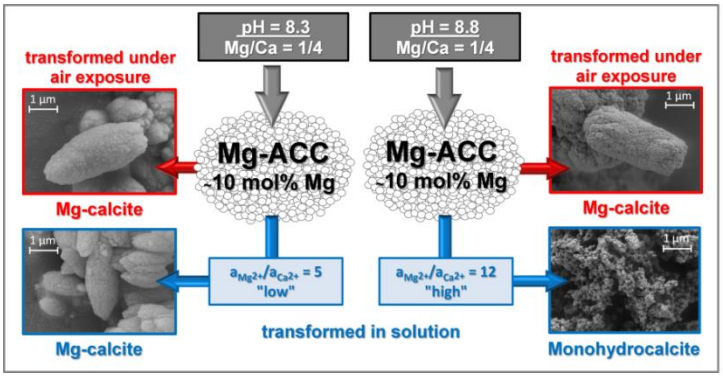

5.1. INTRODUCTION

Calcium carbonate ($CaCO_3$) occurs in three anhydrous crystalline forms, calcite, aragonite and vaterite, and two hydrous crystalline forms, monohydrocalcite ($CaCO_3 \cdot H_2O$) and ikaite ($CaCO_3 \cdot 6H_2O$). Of these calcium carbonate minerals, the geological occurrence of the less stable vaterite, monohydrocalcite, and ikaite is rare (Lowenstam, 1981; Ito, 1993; Burchardt et al., 2001; Lu et al., 2012). In contrast, calcite and aragonite are deposited readily in marine and terrestrial environments (Morse and Mackenzie, 1990). Many biogenic and non-biogenic calcites contain significant amounts of magnesium (Mackenzie et al., 1983; Long et al., 2011) . Calcites with more than 4 mol% magnesium are generally referred to as Mg-calcites.

As early as the 19th century, it has been observed that biominerals can be formed via an amorphous calcium carbonate (ACC) phase (Krukenberg, 1882; Michin, 1989). Since then, the presence of an ACC precursor has been observed in the skeletons of sea urchins (Beniash et al., 1997; Politi et al., 2004), freshwater snails (Hasse et al., 2000; Khairoun et al., 2002), bivalves (Jacob et al., 2008), brachiopods (Griesshaber et al., 2009), ascidians (Aizenberg et al., 2002), sponges (Sethmann et al., 2006), and crustaceans (Tao et al., 2009). More recently, amorphous carbonate phases were found in intracellular inclusions in modern microbialites in Lake Alchichica (Couradeau et al., 2012) and in the mucilaginous matrix embedding planktonic cells in Lake Geneva (Jaquet et al., 2013). With respect to abiotic precipitation environments, ACC formation and its transformation to calcite was for instance associated with speleothem formation in caves (Demény et al., 2016) and found to be applicable for medical product development (Meiron et al., 2011; Zhao et al., 2015).

By mixing concentrated solutions of $CaCl_2$ and Na_2CO_3, Brečević and Nielsen showed that ACC is highly soluble ($K_{sp\text{-}ACC} = 10^{-6.39}$ at 25°C); and that it rapidly transforms to crystalline calcium carbonate polymorphs. In this context, it has been observed that organic molecules and magnesium ions stabilize both biogenic and inorganic ACC (Raz et al., 2003; Loste et al., 2003; Lam et al., 2007; Han and Aizenberg, 2008; Politi et al., 2010; Mavromatis et al., 2012; Radha et al., 2012, Rodriguez-Blanco et al., 2012). In the latter case, the elevated metastability of Mg enriched amorphous calcium carbonate (Mg-ACC) was attributed to the structural water bound to Mg ions that retards the process of dehydration and transformation.

Despite the fact that numerous studies have focused on ACC formation, the mechanisms controlling its transformation into, for instance, (Mg-)calcite and/or aragonite is poorly

understood. The literature of the last decade has revealed that the crystallization pathways of the amorphous phase depend on physicochemical parameters including temperature (Ogino et al., 1987), pH (Rodriguez-Blanco, 2012; Gebauer et al., 2008), solution additives like magnesium ions (Loste et al., 2003; Lam et al., 2007; Rodriguez-Blanco, 2012) and organic molecules Lam et al., 2007). For example, when ACC was synthesized from a solution with a high initial pH (> 9.5), it transformed to calcite via metastable vaterite (Rodriguez-Blanco, 2012; Bots et al., 2012). Conversely, by using Mg in the initial solution (Mg/Ca = 1/9) ACC crystallized directly to (Mg-)calcite (Rodriguez-Blanco, 2012). On the other hand, by mixing solutions with molar Mg/Ca ratios ≥ 1/5.6 and CO_3/Ca ratios > 1, monohydrocalcite formation was reported to proceed through an ACC precursor (Kimura et al., 2011; Nishiyama et al., 2013). In this context, it has been suggested that ACC crystallizes through a nucleation controlled dissolution-reprecipitation reaction (Bots et al., 2012; Rodriguez-Blanco et al., 2014; Rodriguez-Navarro et al., 2015). In contrast, many studies suggested that the short-range structure or the composition of ACC (e.g. Mg content) controls its crystallization to a distinct crystalline carbonate phase (Loste et al., 2003; Lam et al., 2007; Gebauer et al., 2008).

Most of the former studies dealing with (Mg-)ACC formation were conducted at solution pH > 9.5 (Rhada et al., 2012; Rodriguez-Blanco et al., 2012; Bots et al., 2012; Kimura and Koga, 2011; Rodriguez-Navarro et al., 2015), a value that is significantly higher than the pH of most natural aquatic environments. Moreover, (Mg-)ACC was synthesized by batch methods with $CaCl_2$/$MgCl_2$ and $NaHCO_3$/Na_2CO_3 solutions, where the pH decreased from ~11 to ~8 during mixing and subsequent (Mg-)ACC crystallization (Rodriguez-Blanco et al., 2012; Bots et al., 2012). In the context of this study, we conducted experiments under controlled physicochemical conditions (constant T and pH) in order to shed light on the role of circum-neutral pH regimes and effects of Mg/Ca ratios during the (trans-)formation of Mg-ACC to crystalline phases. Specifically, the transformation pathways of Mg-ACC were systematically examined from pH 7.8 to 8.8 at distinct Mg/Ca ratios (1/3 to 1/8) and discussed together with our previous study at pH 8.3 (Purgstaller et al., 2016). The aim of the present paper is to provide a more detailed understanding on the mechanisms controlling the formation of crystalline carbonate phases via a Mg-ACC precursor.

5.2. METHODS

5.2.1 Experimental setup and analytical procedures

The synthesis of a solid $Ca_{1-x}Mg_xCO_3$ phase was carried out under controlled physicochemical conditions (T and pH = constant) using the experimental setup described in Purgstaller et al. (2016). Hereafter, only the most important features are described. The precipitation of $Ca_{1-x}Mg_xCO_3$ was induced by the titration (702 SM Titrino titrator; Methrom) of 50 ml of a 0.6 M $(Ca,Mg)Cl_2$ solution with distinct Mg/Ca ratios (1/3, 1/4, 1/6 and 1/8) at a rate of 2 ml/min into 50 ml of a 1 M $NaHCO_3/Na_2CO_3$ solution at 25.00 ±0.03°C (Easy Max^{Tm} 102; Mettler Toledo). The pH of the reactive solution was kept constant at values of 7.8, 8.3, or 8.8 ±0.1 by the automatic titration of a 1 M NaOH solution (Schott; TitroLine alpha plus), with titration steps of 0.1 ml. Experiments conducted with the Mg/Ca ratios 1/4, 1/6 and 1/8 are labeled as A1, A2 and A3 at pH 7.8 and as C1, C2 and C3 at pH 8.8, respectively (**Table 1**). A replicate experiment of C1 is labeled as C1_2. One experiment was carried out at pH 8.3 with a Mg/Ca ratio of 1/3 (exp. MgCa3, **Table 1**). Prior to each experiment the pH of the carbonate buffer solution was adjusted to the required experimental pH (±0.07) using a 1 M NaOH or a 1 M HCl solution.

During the experimental run, the temporal evolution of mineral precipitation was monitored by *in situ* Raman spectroscopy (Raman RXN2^{TM} analyzer, Kaiser Optical Systems). After 180 min of reaction time, the reactive solution was transferred into a 150 ml glass bottle and placed air-tight on a compact shaker (Edmund Bühler GmbH; KS-15) operating at 150 rpm in a temperature controlled room at 25 ±1°C. In each experiment, 5 ml of the reactive solution were sampled after selected time steps for solid and solution analysis. Immediately after sampling the solids were separated by a 0.2 µm cellulose acetate filter using a suction filtration unit and were analyzed using Attenuated Total Reflectance - Fourier Transform Infrared Spectroscopy (ATR-FTIR; Perkin Elmer Spektrum 100). The solids were subsequently dried at room temperature in a desiccator using silica gel. The mineralogy of the dried precipitates was determined using X-ray diffraction (PANalytical X´Pert PRO) and the mineral phases were quantified using Rietveld refinement (software HighScore Plus, PANalytical, PDF-2 database). Selected precipitates were gold coated and imaged using a scanning electron microscope (SEM, ZEISS DSM 982 Gemini). The aqueous cation concentrations were determined using ion chromatography (Dionex IC S 3000, IonPac®, AS19 and CS16 column), with an analytical precision of ±3%. The total

alkalinity of the solutions was measured by a Schott TitroLine alpha plus titrator using a 0.02 M HCl solution with a precision better than ±2% and a detection limit of 5 x 10^{-6} M.

The Mg content of the solids (in mol%) sampled at a given reaction time was calculated according to the equation:

$$[Mg]_{solid} = \frac{[Mg]_{add} - [Mg]_{aq}}{[Mg]_{add} - [Mg]_{aq} + [Ca]_{add} - [Ca]_{aq}} \cdot 100 \quad (1)$$

where $[Mg]_{add}$ and $[Ca]_{add}$ are the concentrations of added Mg and Ca by titration into the reactive solution given in mol L^{-1} considering at any time volume change in the reaction solutions. $[Mg]_{aq}$ and $[Ca]_{aq}$ are the measured molar concentrations of Mg and Ca in the reactive solutions. The calculated $[Mg]_{solid}$ values obtained from Eq. 1 are in excellent agreement (R^2 = 0.96) with the Mg contents of the bulk digested solids analyzed by inductively coupled plasma optical emission spectrometry (Perkin Elmer Optima 8300 DV) (**Fig. S1**). The analytical error was calculated to be < ±3% for Ca and Mg.

Table 1
Initial compositions of the experimental solutions for ACC (trans)formation. Mg/Ca denotes molar ratio referred to total concentration (Mg + Ca) of 0.6 M.

Experiment	pH	Mg/Ca
A1	7.8	1/4
A2	7.8	1/6
A3	7.8	1/8
C1	8.8	1/4
C1_2	8.8	1/4
C2	8.8	1/6
C3	8.8	1/8
MgCa3	8.3	1/3

2.2 Hydrochemical modeling

The aqueous speciation and ion activities of the reactive solutions were calculated using the PHREEQC software (minteq.v4 database). The saturation Index (SI) of the reactive solution with respect to ACC was calculated using the equation

$$SI_{ACC} = \log\left[\frac{(a_{Ca^{2+}}) \cdot (a_{CO_3^{2-}})}{K_{sp}}\right] \quad (2)$$

where a denotes the activity of the *i*th species in solution and the solubility product (K_{sp}) is $10^{-6.39}$ at 25°C (Brečević and Nielsen, 1989).

5.3. RESULTS

5.3.1 Solid phase characterization

The *in situ* Raman spectra of experiments A1, A2, and A3 carried out at pH 7.8 showed that Mg-calcite is present right after the onset of the experiments within 1 min, as it was indicated by the increase of intensity of the carbonate stretching band (v_1) at ~1087 cm^{-1} (exp. A1, **Fig. 1A**) and of the libration mode of Mg-calcite at ~282 cm^{-1} (see values in **Table 2**) (Bischoff et al., 1985). The intensity of the Raman v_1 band for Mg-calcite was constant over time as soon as the titration of the (Ca,Mg)Cl_2 solution was stopped (exp. A1, **Fig. 1A**). In experiments A2 and A3, aragonite was identified in addition to Mg-calcite after 180 min of reaction time detectable through the presence of the libration mode at ~205 cm^{-1} in the Raman spectra (**Table 2**) (Edwards et al., 2005). The results obtained by Raman spectroscopy are in good agreement with the ATR-FTIR analysis, showing the characteristic vibration band of Mg-calcite at ~711 cm^{-1} (v_4) (Böttcher et al., 1997) in all precipitates and the presence of aragonite by the ATR-FTIR bands at ~699 cm^{-1} (v_4) and ~856 cm^{-1} (v_2) (Kontoyannis and Vagenas, 2000) after 25 min of reaction time in experiments A2 and A3 (**Table 2**). Moreover, the ATR-FTIR spectra of the precipitates that were sampled between 13 and 25 min and between 13 and 180 min in experiments A2 and A3, respectively, showed vibration bands at ~743 cm^{-1} (v_4) corresponding to vaterite (**Table 2**) (Kontoyannis and Vagenas, 2000). The discrepancy of the analyzed mineralogy at certain reaction times within a single experiment (**Table 2**) is attributed to the higher sensitivity of the ATR-FTIR analysis of the collected solids compared to that of the *in situ* Raman spectroscopy of the reactive solution/suspension.

Quantitative XRD results (**Table 3**) showed that the dried precipitates of experiment A1 mainly consist of Mg-calcite (96 ±2 wt. %) and traces of aragonite (4 ±2 wt. %). In experiments A2 and A3 vaterite (up to 21 wt. %) and aragonite (13-33 wt. %) can be found additionally to Mg-calcite, which is abundant in the bulk precipitate (61-75 wt. %).

The SEM images of the precipitates of experiments A1, A2 and A3, sampled after 1 day of reaction time, showed aggregates (~4 μm) of rhombohedral Mg-calcite crystals (**Fig. 2A-C**), which are similar in texture to those obtained in experiment MgCa8 from Purgstaller et al. (2016) (**Fig. 2F**). The Mg-calcite crystals are smaller in size (< 0.1 μm) in experiment A1 compared to those from experiments A2 (~0.3 μm) and A3 (~1 μm). Moreover, in experiment A1 Mg-calcite crystal habits are more elongated (**Fig. 2A**) compared to those from experiments A2 (**Fig. 2B**) and A3 (**Fig. 2C**). Finally, in the A2 and A3 experiments, pseudo-hexagonal crystals of aragonite (~1 μm) were observed (exp. A3 in **Fig. S2A**).

In experiments C1, C2, and C3 carried out at pH 8.8 the collected *in situ* Raman spectra revealed the presence of only Mg-ACC within 58, 40, and 36 min of reaction time, respectively. The Raman spectra of Mg-ACC are characterized by a single broad v_1 band at 1082 ±1 and by the absence of lattice modes (exp. C1 in **Fig. 1B**; **Table 2**) (Wang et al., 2012). These results were confirmed by ATR-FTIR analyses of sampled precipitates (exp. C1 in **Fig. 1B**, **Table 2**). The lack of the v_4 vibration band and the presence of vibration bands at 860-861 cm^{-1} and 1073 ±1 cm^{-1} in the ATR-FTIR spectra are characteristic of Mg-ACC (Loste et al., 2003). In the experiment conducted with the highest Mg/Ca ratio (exp. C1), a Raman band at ~1068 cm^{-1} corresponding to the v_1 band of monohydrocalcite (Coleyshaw et al., 2003) evolved after 58 min of reaction time, while the characteristic band of Mg-ACC at ~1083 cm^{-1} decreased (**Fig. 1B**). ATR-FTIR spectra of the precipitates collected after 180 min of reaction time showed vibration bands at ~697/~726 cm^{-1}, ~755 cm^{-1}, ~871 cm^{-1}, ~1068 cm^{-1} and ~1395/~1474 cm^{-1} (**Fig. 1B**). These ATR-FTIR bands are in good agreement with wavenumber values for synthetic monohydrocalcite from Neumann and Epple (2007). Similar *in situ* Raman and ATR-FTIR results were obtained in the replicate experiment C1_2 (**Table S1**). After 1 day of reaction time, the *in situ* Raman spectra indicated the presence of a second v_1 band at ~1100 cm^{-1} (**Table 2**), corresponding to nesquehonite (Coleyshaw et al., 2003). In contrast to the *in situ* Raman spectroscopic observations, the presence of nesquehonite was not detectable by ATR-FTIR analysis due to similarities of the vibration bands of monohydrocalcite and nesquehonite at higher wavenumbers in the ATR-FTIR spectra. The XRD results showed that the dried precipitate consists of Mg-calcite at 25 min of reaction time, whereas monohydrocalcite was found in the precipitate sampled at 180 min of reaction time (**Table 3**). After 1 day of reaction time nesquehonite (14 wt. %) was detected beside monohydrocalcite (86 wt. %, **Table 3**).

In contrast, in experiments conducted with the Mg/Ca ratios 1/6 and 1/8 (exp. C2 and C3), *in situ* Raman spectroscopy revealed the transformation of Mg-ACC to Mg-calcite (exp. C3 in **Fig. S3**). The formation of Mg-calcite was indicated by the rise of the translation mode of Mg-calcite at ~283 cm^{-1} (**Table 2**) and the rise of the intensity of the v_1 Raman vibration band at 1088 cm^{-1} (Purgstaller et al., 2016). The results obtained by *in situ* Raman spectroscopy are in good agreement with those obtained by ATR-FTIR analysis (**Table 2**). As reported in **Table 3** the XRD patterns of all dried precipitates in experiments C2 and C3 showed only Mg-calcite.

The monohydrocalcite obtained in experiment C1 forms non-aggregated nano-spheres (exp. C1, **Fig. 2G**), whereas the nesquehonite precipitates of experiment C1 are rod-shaped with individual rods reaching lengths of up to 40 μm (**Fig. S2B**). The Mg-calcites of experiments C2 (**Fig. 2H**) and C3 (**Fig. 2I**) display aggregates composed of nanoparticles (~ 80 nm) that agglomerated to larger clusters. These particles are significantly smaller in size than the Mg-calcite crystals resulting from experiments conducted at pH 7.8 (**Fig. 2A-C**). The Mg-calcite aggregates however are similar in texture to those observed in experiments MgCa4 (**Fig. 2D**) and MgCa6 (**Fig. 2E**) conducted at pH 8.3 by Purgstaller et al. (2016) where Mg-calcite was formed via Mg-ACC.

The collected *in situ* Raman spectra of experiment MgCa3 conducted at pH 8.3 (Mg/Ca = 1/3) showed that Mg-ACC was present during the titration of the $(Ca,Mg)Cl_2$ solution (**Table 2**). After about 50 min of reaction time the presence of a second v_1 band at ~1069 cm^{-1} corresponding to monohydrocalcite was observed in the *in situ* Raman spectra (**Table 2**). Similar results were obtained by ATR-FTIR analysis, showing the characteristic vibration bands of monohydrocalcite beside the vibration bands of ACC after 60 min of reaction time (**Table 2**). After 180 min of reaction time only vibration bands of monohydrocalcite and a weak band at 1088 cm^{-1} were observed in ATR-FTIR spectra (**Table 2**). The XRD pattern showed that the dried precipitates produced in experiment MgCa3 at 25 min of reaction time consist of Mg-calcite (**Table 3**). In contrast, the precipitate collected at 180 min of reaction time consists of monohydrocalcite (87 wt.%) and minor amounts of Mg-calcite (13 wt.%, **Table 3**). After 1 day of reaction time nesquehonite (13 wt.%) was found in addition to monohydrocalcite (79 wt. %) and Mg-calcite (8 wt. %, **Table 3**).

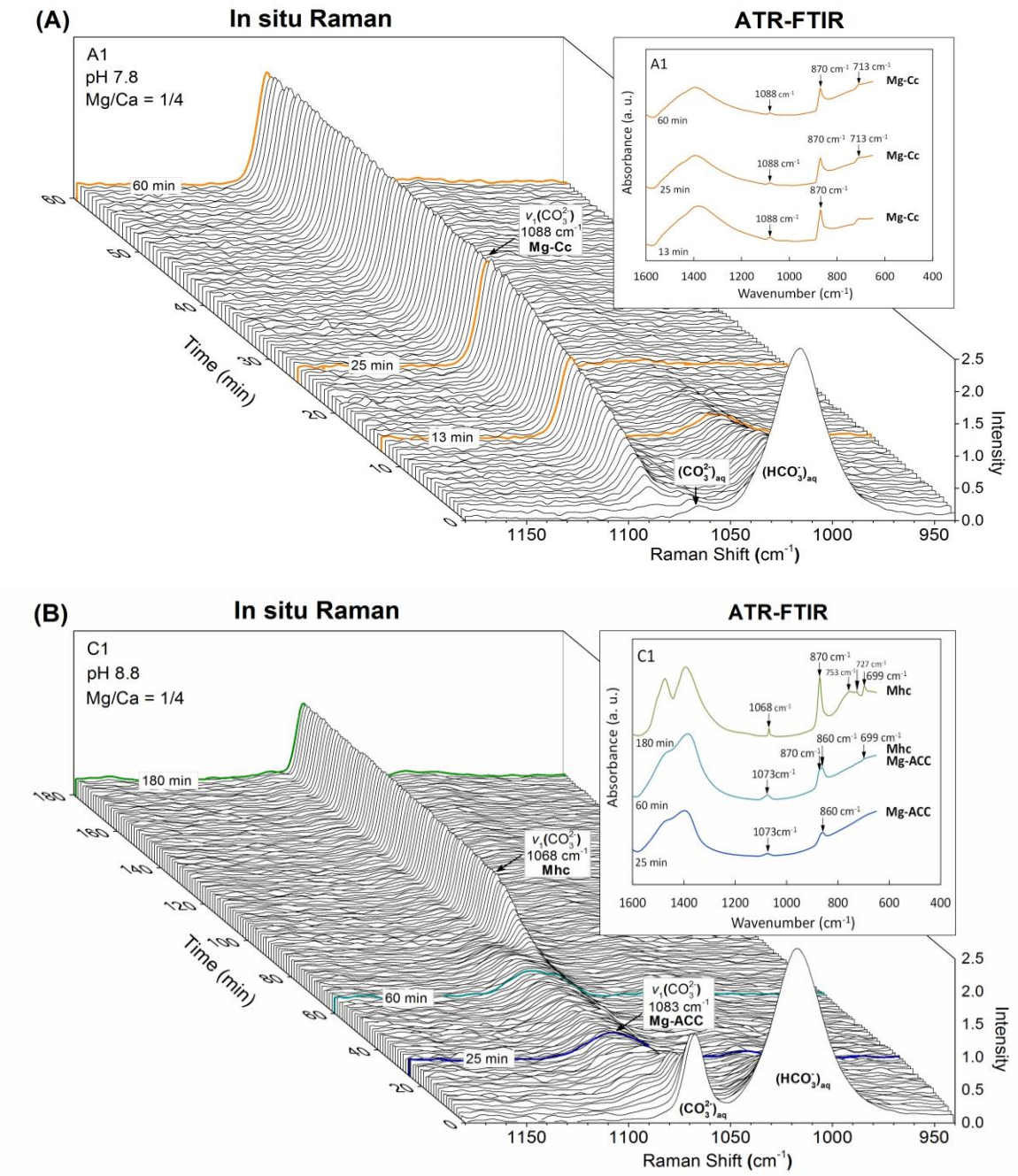

Fig. 1. Waterfall plot of *in situ* Raman spectra showing the vibration band of aqueous HCO_3^- and CO_3^{2-} as well as of ν_1 band of CO_3^{2-} related to Mg-ACC, Mg-calcite (Mg-Cc) and monohydrocalcite (Mhc) and ATR-FTIR spectra of precipitates sampled during certain reaction times of the experiment A1 **(A)** and C1 **(B)**.

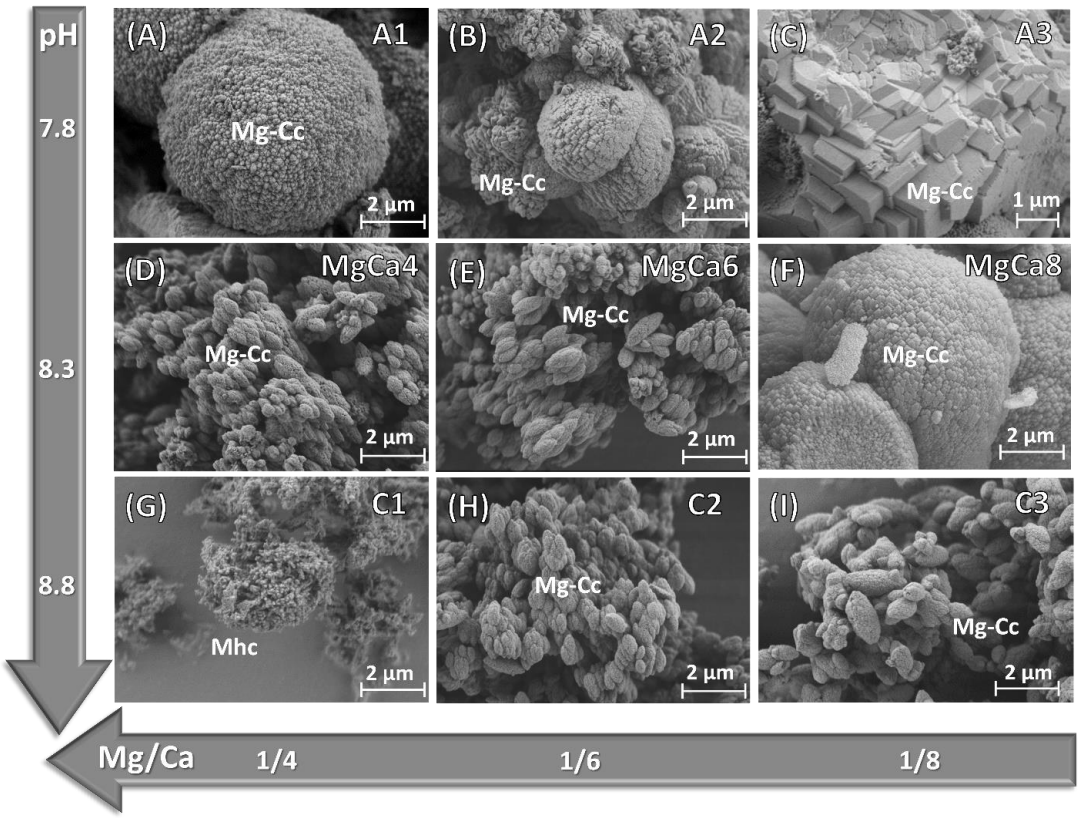

Fig. 2. SEM images of precipitates sampled after 1 day of reaction time from experiments of the present study and from experiments MgCa4, MgCa6 and MgCa8 of Purgstaller et al. (2016) showing Mg-calcite (Mg-Cc), aragonite (Arg) and monohydrocalcite (Mhc) crystals.

Table 2
Frequencies (cm^{-1}) of observed carbonate vibration bands from *in situ* Raman and ATR-FTIR spectra and identified mineralogy of the precipitates at certain reaction times. Note that in experiment MgCa3 *in situ* Raman spectra of reactive solution were not obtained after 60 min (n.a.). Mg-Cc: Mg-calcite, Arg: aragonite, Vtr: vaterite, Mhc: monohydrocalcite, Nesq: nesquehonite.

Experiment	time	Raman		Mineralogy	ATR-FTIR			Mineralogy
		ν_1	libration mode		ν_1	ν_2	ν_4	
A1	13 min	1088	282	Mg-Cc	1082	870	713	Mg-Cc
	25 min	1088	283	Mg-Cc	1083	870	713	Mg-Cc
	60 min	1088	283	Mg-Cc	1083	871	712	Mg-Cc
	180 min	1088	283	Mg-Cc	1083	870	712	Mg-Cc
	1d	1088	283	Mg-Cc	1083	870	712	Mg-Cc
A2	13 min	1087	283	Mg-Cc	1082	871	743/712	Mg-Cc, Vtr
	25 min	1087	283	Mg-Cc	1082	870	743/712/700	Mg-Cc, Arg, Vtr
	60 min	1087	283	Mg-Cc	1083	870/856	712/700	Mg-Cc, Arg
	180 min	1086	283/205	Mg-Cc, Arg	1082	870/855	711/700	Mg-Cc, Arg
	1d	1086	283/205	Mg-Cc, Arg	1083	871/855	712/700	Mg-Cc, Arg
A3	13 min	1087	282	Mg-Cc	1082	871	743/712	Mg-Cc, Vtr
	25 min	1087	282	Mg-Cc	1082	870/856	743/712/699	Mg-Cc, Arg, Vtr
	60 min	1087	282	Mg-Cc	1082	870/856	743/712/699	Mg-Cc, Arg, Vtr
	180 min	1086	282/205	Mg-Cc, Arg	1082	870/855	743/712/699	Mg-Cc, Arg, Vtr
	1d	1086	282/205	Mg-Cc, Arg	1082	870/854	712/699	Mg-Cc, Arg
C1	13 min	1083	-	Mg-ACC	1073	860	-	Mg-ACC
	25 min	1083	-	Mg-ACC	1074	860	-	Mg-ACC
	60 min	1083/1068	-	Mg-ACC, Mhc	1073	870 /860	697	Mg-ACC, Mhc
	180 min	1068	-	Mhc	1068	870	753/726/697	Mhc
	1d	1100/1068	-	Mhc, Nesq	1068	871	751/726/697	Mhc
C2	13 min	1081	-	Mg-ACC	1072	860	-	Mg-ACC
	25 min	1081	-	Mg-ACC	1074	860	-	Mg-ACC
	60 min	1087	282	Mg-Cc	1085	871	711	Mg-Cc
	180 min	1088	283	Mg-Cc	1085	870	712	Mg-Cc
	1d	1088	283	Mg-Cc	1083	870	711	Mg-Cc
C3	13 min	1082	-	Mg-ACC	1073	861	-	Mg-ACC
	25 min	1082	-	Mg-ACC	1073	860	-	Mg-ACC
	60 min	1088	282	Mg-Cc	1084	871	712	Mg-Cc
	180 min	1088	282	Mg-Cc	1084	871	712	Mg-Cc
	1d	1088	282	Mg-Cc	1084	871	712	Mg-Cc
MgCa3	13 min	1082	-	Mg-ACC	1073	860	-	Mg-ACC
	25 min	1083	-	Mg-ACC	1073	859	-	Mg-ACC
	60 min	1083/1069	-	Mg-ACC, Mhc	1073	871/860	697	Mg-ACC, Mhc
	180 min	n.a.	n.a.	n.a	1068/1088	870	755/727/697	Mhc, Mg-Cc
	1d	n.a	n.a.	n.a	1068/1088	872	761/728/699	Mhc, Mg-Cc

Table 3
Mineralogical composition from XRD-patterns of precipitates sampled at certain reaction times. The compositions refer to precipitates, which are completely transformed to crystalline solids after sampling. Quantifications were realized by Rietveld refinement. Mg-Cc: Mg-calcite, Arg: aragonite, Vtr: vaterite; Mhc: monohydrocalcite; Nesq: nesquehonite.

Experiment	time min/d	Mg-Cc wt. %	Arg wt. %	Vtr wt. %	Mhc wt. %	Nesq wt. %
A1	25 min	97	3	-	-	-
	180 min	96	4	-	-	-
	1 d	95	5	-	-	-
A2	25 min	74	13	14	-	-
	180 min	72	18	9	-	-
	1 d	75	25	-	-	-
A3	25 min	61	18	21	-	-
	180 min	61	24	15	-	-
	1 d	61	33	6	-	-
C1	25 min	100	-	-	-	-
	180 min	-	-	-	100	-
	1 d	-	-	-	86	14
C2	25 min	100	-	-	-	-
	180 min	100	-	-	-	-
	1 d	100	-	-	-	-
C3	25 min	100	-	-	-	-
	180 min	100	-	-	-	-
	1d	100	-	-	-	-
MgCa3	25 min	100	-	-	-	-
	180 min	13	-	-	87	-
	1d	8	-	-	79	13

5.3.2 Chemical evolution of the reactive solutions

The initial carbonate solutions are characterized by a carbonate alkalinity of 0.99 ±0.02 M at pH 7.8, 1.02 ±0.01 M at pH 8.3 and 1.15 ±0.02 M at pH 8.8. In all experiments, the carbonate alkalinities decreased to a value of 0.11 ±0.03 M during the titration of the $(Ca,Mg)Cl_2$ solutions (**Table S2-S4**).

The titration of the $(Ca,Mg)Cl_2$ solutions into the carbonate buffer solutions caused instant nucleation/precipitation of $Ca_{1-x}Mg_xCO_3$ within 1 min of reaction time. The $[Ca]_{aq}$ of the reactive solutions did not exceed 0.007 M during all experimental runs (**Table S1-4**). After 25 min of reaction time about 98 % of the $n_{Ca_{add}}$ was removed from the reactive solutions due to mineral precipitation. The temporal evolution of the $[Mg]_{aq}$ of the reactive solutions of experiments conducted at pH 8.3 and 8.8 is displayed in **Fig. 3A-B**, while the obtained $[Mg]_{aq}$ values of experiment MgCa3 are displayed in **Fig. S4A**. The $[Mg]_{aq}$ of the reactive solutions increased during the titration of the $(Ca,Mg)Cl_2$ solutions. In experiments A1 to A3 the $[Mg]_{aq}$ remained

nearly constant between 25 min and 1 day of reaction time (**Fig. 3A**), whereas in experiments C2, and C3 a significant decrease of the $[Mg]_{aq}$ (up to 0.015 M) was observed for the same time interval (**Fig. 3B**). In experiments C1 and MgCa3 on the other hand, the $[Mg]_{aq}$ remained constant at 0.026 and 0.036 M , respectively, between 25 and 60 min of reaction time, before it increased to about 0.040 M in both experiments (180 min, **Fig. 3A** and **Fig. S4A**). Subsequently, the $[Mg]_{aq}$ decreased again to 0.019 M and 0.035 M in experiments C1 and MgCa3, respectively, between 180 min and 1 day of reaction time. A similar $[Mg]_{aq}$ trend as in experiment C1 was observed in the replicate experiment C1_2 (**Fig. 3B**).

5.3.3 Temporal evolution of Mg content in precipitates

During the titration of the $(Ca,Mg)Cl_2$ solutions, the $[Mg]_{solid}$ increased in all experiments (**Fig. 3C-D**). The highest $[Mg]_{solid}$ content after 25 min of reaction time was 10.2 ±0.5 mol% present in the solids of experiments A1 and C1. In experiments A2 and C2 the precipitates contained 7.6 ±0.6 mol% Mg, whereas those in experiments A3 and C3 contained 6.7 ±1.2 mol% Mg after 25 min of reaction time. In experiment MgCa3 the $[Mg]_{solid}$ obtained after 25 min of reaction time is 11.4 mol%.

In experiments A1 to A3 (**Fig. 3C**), the $[Mg]_{solid}$ remained nearly constant between 25 min and 1 day of reaction time, while in experiments C2 and C3 the $[Mg]_{solid}$ increased significantly between 25 and 60 min of reaction time (**Fig. 3D**). In the case of experiments C1 and MgCa3, the $[Mg]_{solid}$ remained constant between 25 and 60 min of reaction time and then decreased from 10 to 4 mol% in experiment C1 (180 min, **Fig. 3D**) and from 12 to 9 mol% in experiment MgCa3 (180 min, **Fig. S4B**). However, between 180 min and 1 day of reaction time, the $[Mg]_{solid}$ increased significantly in both experiments (**Fig. 3D** and **Fig. S4B**), which is also the case for the replicate experiment C1_2, where the evolution of the $[Mg]_{solid}$ is similar to experiment C1.

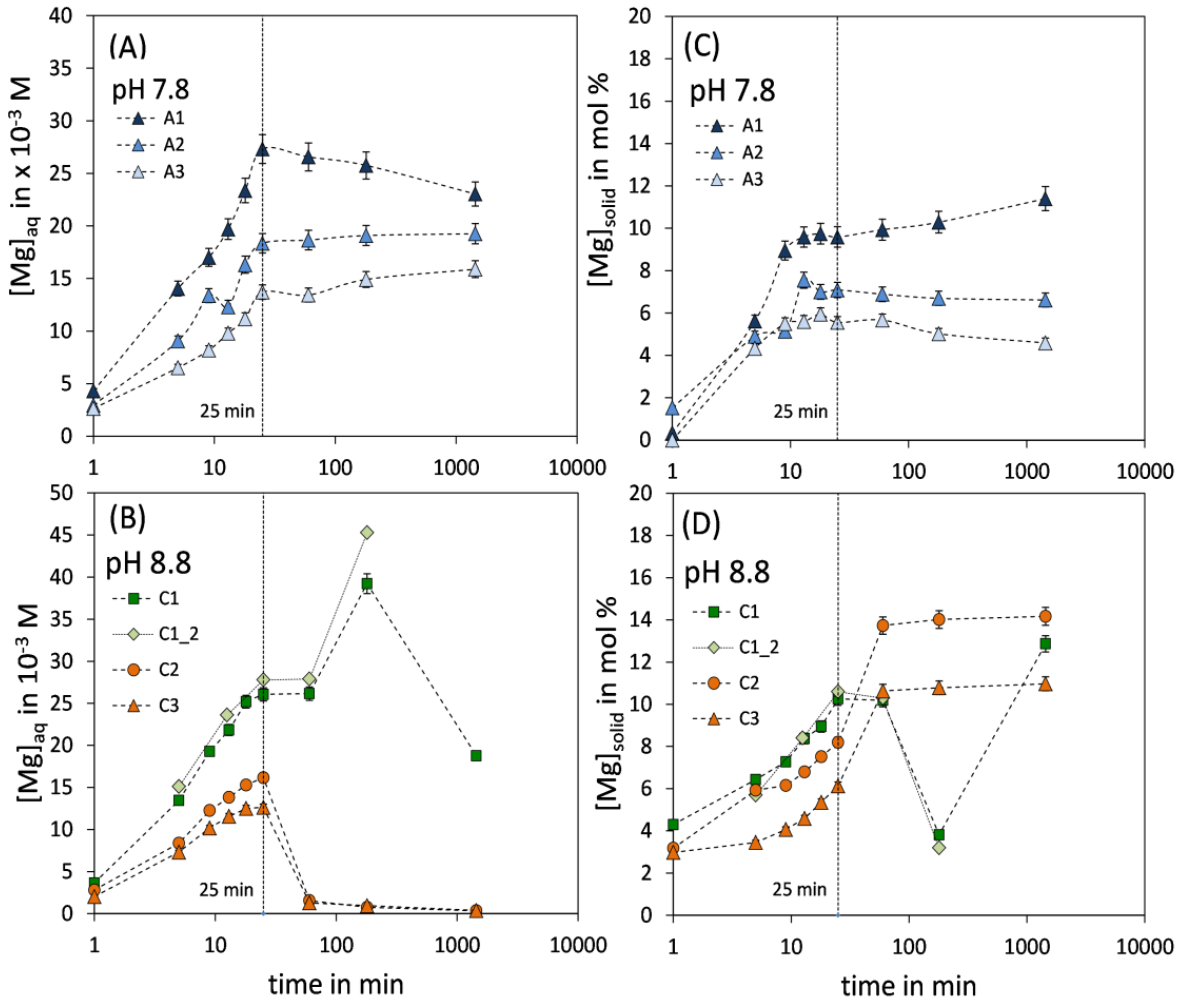

Fig. 3. (Left) Concentration of dissolved Mg ions of the reactive solution, $[Mg]_{aq}$, versus experimental run time of experiments conducted at pH 7.8 **(A)** and pH 8.8 **(B)**. (Right) Mg content of the precipitated solid, $[Mg]_{solid}$, calculated according to Eq. 1 versus experimental run time of experiments conducted at pH 7.8 **(C)** and pH 8.8 **(D)**. Titration of the $(Ca,Mg)Cl_2$ solutions into the $NaHCO_3$ solutions was stopped at 25 min of experimental time (dashed line). When not visible, error bars are smaller than the symbols.

5.4. DISCUSSION

5.4.1 Effect of pH on the formation of amorphous calcium carbonate

The presence of Mg-rich ACC was observed in all experiments conducted at pH 8.8 (e.g. experiment C1 in **Fig. 1B**, **Table 2**). In contrast, in experiments conducted at pH 7.8 the *in situ* Raman spectra showed that Mg-calcite is present within 1 min after the onset of the experiments and in absence of an amorphous precursor (e.g. experiment A1 in **Fig. 1A**; **Table 2**). Note here that the resolution of *in situ* Raman spectra at the initial stage of the experiments (< 5 min) is low due to the low amount of solid suspended in the reactive solution. Moreover, the Raman v_1 band

of ACC is significantly broadened compared to that of crystalline $CaCO_3$ owing to its poorly ordered structure (Wang et al., 2012). Thus, the presence of ACC within this time frame cannot be completely excluded. In order to evaluate the metastability conditions of ACC in the present experiments, the saturation index of the reactive solutions with respect to ACC (SI_{ACC}) was calculated according to Eq. (2). Reactive solutions exhibit SI_{ACC} slightly above 0 within at least 25 min of reaction time in the experiments conducted at pH 8.8 (**Fig. 4**). In contrast, in experiments conducted at pH 7.8 reactive solutions exhibit $SI_{ACC} < 0$ during the titration of the $(Ca,Mg)Cl_2$ solution (**Fig. 4**). The concentrations and activities of the two dissolved inorganic carbon species (e.g. HCO_3^- and CO_3^{2-}) depend on the pH of the reactive solution. For example, after 1 min of reaction time in experiments conducted at pH 8.8, the ratio of CO_3^{2-} to HCO_3^- activities in the reactive solutions, $a_{CO_3^{2-}}/a_{HCO_3^-}$, was $\sim 3 \cdot 10^{-2}$, whereas in experiments conducted at pH 7.8 the $a_{CO_3^{2-}}/ a_{HCO_3^-}$ was significant lower at $\sim 3 \cdot 10^{-3}$ (**Table S5**). In the latter case, Mg-ACC was likely not formed due to the limited concentration and activity of CO_3^{2-} in the reactive solutions at lower pH (**Table S5**).

The direct formation of Mg-calcite in experiments conducted at pH 7.8 could be followed by SEM images displaying Mg-calcite aggregates of aligned rhombohedral crystals, which are significantly larger in size (**Fig. 2A-C**) compared to the Mg-calcite nanoparticles formed in experiments, where Mg-ACC transformation was detected (**Fig. 2H-I**). These polycrystalline Mg-calcite aggregates (**Fig. 2A-C**) were likely formed via a spherulitic growth mechanism, where the spherical particles grow from a central nucleation site or seed by incorporation of ions from the solution (Andreassen et al., 2010). This occurred in experiments A1 to A3 as a consequence of high superstation levels of the reactive solution with respect to calcite ($SI_{calcite}$ = 1.9 ±0.2 after 1 min of reaction time). In experiment A2 and A3, XRD results indicated the presence of vaterite and aragonite beside Mg-calcite (**Table 3**). Between 25 min and 1 day of reaction time the proportion of vaterite decreased while the proportion of aragonite increased (**Table 3**). In most cases, metastable vaterite transforms to calcite via a dissolution-reprecipitation mechanism (Ogino et al., 1987; Rodriguez-Blanco et al., 2012; Bots et al., 2012). In the present study, the ongoing formation of aragonite rather than of Mg-calcite is at first documented at 25°C and is suggested to be caused by the high molar Mg/Ca ratio in the reactive solution after 25 min of reaction time (> 46), inhibiting calcite formation (Lippmann, 1973; Falini et al., 1994; Fernández-Díaz et al., 1996).

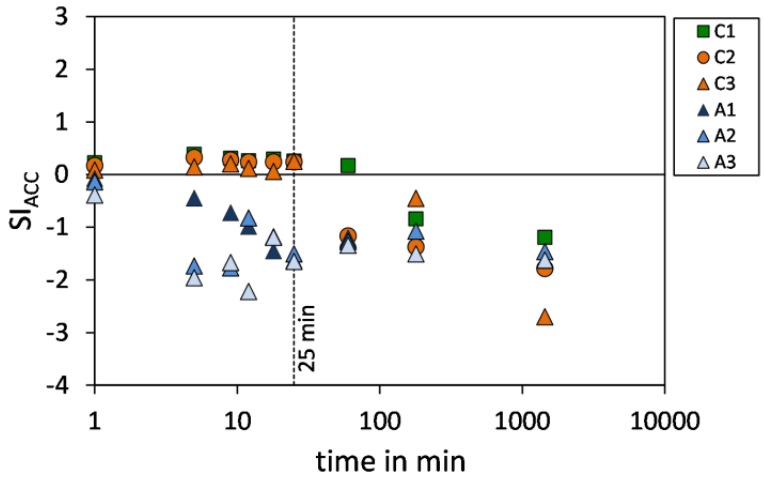

Fig. 4. Evolution of the saturation index with respect to ACC (SI_{ACC}) over the experimental time of the reactive solutions of experiments conducted at pH 7.8 (exp. A1 to A3), and 8.8 (exp. C1 to C3).

5.4.2 Effect of pH and aqueous Mg^{2+}/Ca^{2+} ratio on the transformation pathways of ACC

The experimental results revealed two pathways of Mg-ACC transformation in the reactive solutions (**Fig. 5A**). Mg-ACC transformed into (i) Mg-calcite in experiments conducted at pH 8.3 with the Mg/Ca ratios of 1/6 to 1/4 (exp. MgCa4, MgCa5 and MgCa6 conducted by Purgstaller et al. (2016) as well as in experiments conducted at pH 8.8 with the Mg/Ca ratios 1/6 and 1/8 (exp. C2 and C3), and (ii) monohydrocalcite in experiments conducted at pH 8.3 and 8.8 with the Mg/Ca ratios 1/3 (exp. MgCa3) and 1/4 (exp. C1), respectively. Note that in experiment MgCa3 small amounts of Mg-calcite (13 wt. %) were detected beside monohydrocalcite (**Table 3**).

It has been recently suggested that the crystalline phase forming from ACC is defined by the Mg/Ca ratio of the initial solution: ACC with 10 mol% Mg precipitated from a solution with an initial Mg/Ca ratio of 1/9 crystallized to Mg-calcite (Rodriguez-Blanco et al., 2012), whereas ACC with 30 mol% Mg precipitated from a solution with an initial Mg/Ca ratio of 3/7 crystallized to monohydrocalcite (Rodriguez-Blanco et al., 2014). A different pattern is documented in experiments of the present study conducted with the initial Mg/Ca ratio of 1/4 (exp. MgCa4 and C1). Although in both experiments formed ACC has a similar Mg content (10.1 ±0.2 mol% Mg), the *in situ* Raman spectroscopy revealed the formation of Mg-calcite in experiment MgCa4 and of monohydrocalcite in experiment C1. The formation of monohydrocalcite versus Mg-calcite from Mg-ACC could be attributed to the higher pH of the reactive solution in experiment C1 (pH 8.8) compared to that in experiment MgCa4 (pH 8.3, **Fig.**

5A). However, considering that monohydrocalcite was formed at pH 8.8 only in the experiment conducted with the highest initial Mg/Ca ratio (exp. C1, **Fig. 5A**), a coupled effect of pH and aqueous Mg concentration on the transformation pathways of Mg-ACC is indicated.

In the experiments conducted in this study at the end of the $(Ca,Mg)Cl_2$ solution titration and before the transformation of the amorphous to the crystalline phase took place, the ratio of the Ca^{2+} to CO_3^{2-} activities in the reactive solution, $a_{Ca^{2+}}/a_{CO_3^{2-}}$, is lower (0.2 ±0.1) in experiments conducted at pH 8.8 compared to that in experiments conducted at pH 8.3 (1.7 ±0.4, **Fig. 5B**). In the latter case, the $a_{CO_3^{2-}}$ is lower, owing to the predominance of aqueous HCO_3^- versus CO_3^{2-} ions. In order to maintain a solution that is saturated with respect to ACC, the $a_{Ca^{2+}}$ is thus higher at pH 8.3 than at pH 8.8 (**Fig. 5B**). This affects the prevailing ratio of Mg^{2+} to Ca^{2+} activities in the reactive solution after Mg-ACC was synthesized ($a_{Mg^{2+}}/a_{Ca^{2+}}$, **Fig. 5C**). For example, although the initial Mg/Ca ratio was similar in both experiments, the $a_{Mg^{2+}}/a_{Ca^{2+}}$ is significantly higher in experiment C1 compared to that in experiment MgCa4 after 25 min of reaction time (**Fig. 5C**), due to the lower $a_{Ca^{2+}}$ at high versus low pH (**Fig. 5B**). Overall, the results obtained revealed that in experiments where Mg-ACC transformed to Mg-calcite (exp. MgCa4, C2 and C3), the $a_{Mg^{2+}}/a_{Ca^{2+}}$ is significant lower compared to that in experiment C1, where transformation of Mg-ACC to monohydrocalcite was observed (**Fig. 5C**). In experiment MgCa3, where Mg-ACC transformed to monohydrocalcite and Mg-calcite (13 wt.%), the $a_{Mg^{2+}}/a_{Ca^{2+}}$ is equal to 8 and this value likely defines the boundary conditions for the transformation of Mg-ACC to either Mg-calcite or monohydrocalcite (**Fig. 5C**). These observations suggest that the formation of the distinct crystalline phase is controlled by the prevailing $a_{Mg^{2+}}/a_{Ca^{2+}}$ of the reactive solution after Mg-ACC was formed: Mg-ACC transformed to (i) Mg-calcite at $5 \leq a_{Mg^{2+}}/a_{Ca^{2+}} \leq 8$ and to (ii) monohydrocalcite at $8 \leq a_{Mg^{2+}}/a_{Ca^{2+}} \leq 12$.

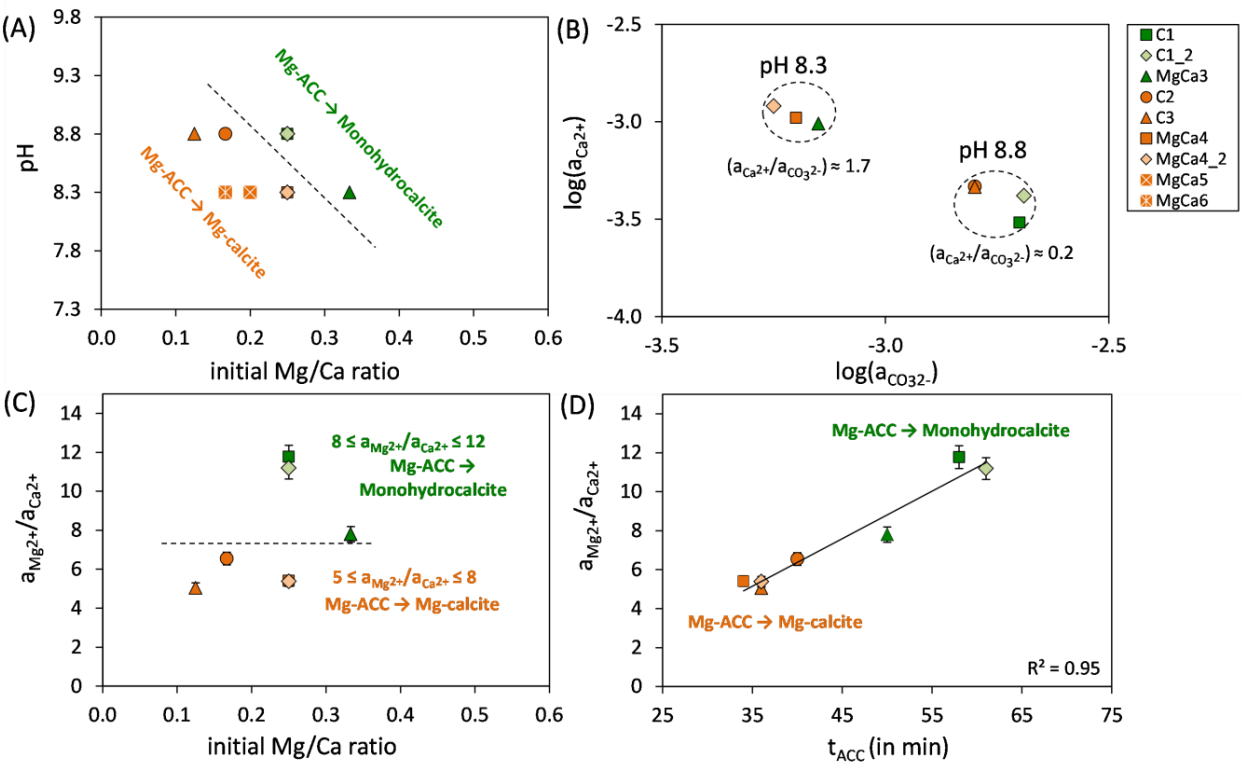

Fig. 5. (A) Pathways of Mg-ACC transformation in the reactive solutions depending on pH and initial Mg/Ca ratio. **(B)** Activities of Ca^{2+} and CO_3^{2-} in reactive solutions after the titration of the $(Ca,Mg)Cl_2$ solution was stopped and before transformation of the amorphous to the crystalline phase took place. **(C)** Initial Mg/Ca ratio versus the prevailing ratio of Mg^{2+} to Ca^{2+} activities of reactive solutions, $a_{Mg^{2+}}/a_{Ca^{2+}}$, after the titration of the $(Ca,Mg)Cl_2$ solution was stopped and before the transformation of the amorphous to the crystalline phase took place **(D)** Reaction time at which Mg-ACC transformation was indicated by *in situ* Raman spectroscopy (t_{ACC}) versus $a_{Mg^{2+}}/a_{Ca^{2+}}$. Note that, except for experiment MgCa4, the $a_{Mg^{2+}}/a_{Ca^{2+}}$ values obtained in experiments MgCa5 and MgCa6 conducted at pH 8.3 by Purgstaller et al.(2016) could not be displayed in Figure 5C-D because the transformation of crystalline carbonate minerals took place before the titration of the $(Mg,Ca)Cl_2$ solution was stopped.

5.4.3 Mechanism of Mg-calcite and monohydrocalcite formation via metastable ACC

The experiments conducted in this study document that the reactive solutions are slightly supersaturated with respect to ACC up to at least 25 min of reaction time (**Fig. 4**). During this timeframe, the reactive solutions are highly supersaturated with respect to calcite (SI ≈ 2.3) and monohydrocalcite (SI ≈ 1.0), which is provoking formation of these phases in the reactive solutions. In experiment C1, the formation of monohydrocalcite instead of thermodynamically more stable calcite can be explained by the inhibition of the latter (Lippmann, 1973; Falini et al., 1994; Fernández-Díaz et al., 1996) due to the elevated prevailing $a_{Mg^{2+}}/a_{Ca^{2+}}$ (**Fig. 5C**). The inhibiting effect of aqueous Mg^{2+} is already indicated in experiment MgCa3, where only small

amounts of Mg-calcite were formed besides monohydrocalcite (**Table 3**). As soon as precipitation of a less soluble crystalline phase (Mg-calcite and/or monohydrocalcite) takes place, the solution reaches undersaturation with respect to ACC (**Fig. 4**). Thus, it is likely that the transformation of the amorphous to the crystalline phase occurred via a dissolution- and re-precipitation mechanism. This mechanism is further supported by the observation that Mg ions are released into the reactive solution throughout Mg-ACC transformation to monohydrocalcite (exp. C1 and C1_2, between 60 and 180 min in **Fig. 3B**). In this context, the Mg content of the solid decreased significantly from 10 to 4 mol%, which strongly suggests a partial dissolution/re-precipitation of Mg-rich ACC (**Fig. 3D**). The prevailing $a_{Mg^{2+}}/a_{Ca^{2+}}$ ratio of the reactive solutions and thus the formation of Mg-calcite or monohydrocalcite are suggested to determine the period of Mg-ACC metastability in the reactive solutions (t_{ACC}). As it can be seen in **Fig. 5D**, t_{ACC} is longer in experiments where monohydrocalcite formation was observed (at higher $a_{Mg^{2+}}/a_{Ca^{2+}}$) compared to experiments with Mg-calcite as the reaction product (at lower $a_{Mg^{2+}}/a_{Ca^{2+}}$). In that sense, it has been documented that elevated Mg contents in ACC increase the metastability of the amorphous phase in a solution (Loste et al., 2003; Rodriguez-Blanco et al., 2012; Purgstaller et al., 2016). In contrast, results of the present study showed that the t_{ACC} is much longer in experiment C1 (~58 min) compared to that in experiment MgCa4 (~34 min) (**Fig. 5D**), although the Mg content of ACC is about the same in both experiments (10.1 ±0.2 mol%). It is concluded that the metastability of the amorphous phase in the reactive solution is not determined by its Mg content, but is related to the prevailing $a_{Mg^{2+}}/a_{Ca^{2+}}$ ratio of the reactive solution and formation behavior of the less soluble crystalline phases, initiating the dissolution of Mg-ACC.

Previous experimental studies on calcite formation documented that the nucleation/growth of calcite is retarded at higher aqueous Mg/Ca molar ratios (Fernández-Díaz et al., 1996; Niedermayr et al., 2013). Indeed, in the present study, transformation of Mg-ACC to Mg-calcite was observed earlier in reactive solutions at low compared to high $a_{Mg^{2+}}/a_{Ca^{2+}}$ ratios (**Fig. 5D**). Moreover, the *in situ* Raman results obtained in our previous study (Purgstaller et al., 2016) showed that the time of Mg-ACC transformation to Mg-calcite is delayed when higher Mg/Ca ratios in the $(Ca,Mg)Cl_2$ solution were used: at initial Mg/Ca ratios of 1/6, 1/5, and 1/4 the transformation of Mg-ACC to Mg-calcite was observed after about 15, 25 and 36 min of reaction time, respectively. We attributed the prolonged presence of Mg-ACC in the reactive solution to its higher Mg content, but it could also be explained by retarded formation kinetics of Mg-calcite

at higher Mg concentrations in the reactive solution. In experiment C1, the presence of Mg-ACC is prolonged due to (i) the inhibition of calcite formation by high $a_{Mg^{2+}}/a_{Ca^{2+}}$ values (**Fig. 5D**) and (ii) the slow formation kinetics of monohydrocalcite. Distinct precipitation rates can be followed by *in situ* Raman spectroscopy, where the formation of monohydrocalcite required ~ 25 min in experiment C1 (**Fig. 1B**). In contrast, the formation of Mg-calcite is significantly faster (~ 8 min, exp. C3 in **Fig. S3**; cf. Purgstaller et al., 2016).

Evidence for the control of the fluid composition (i.e. aqueous Mg/Ca ratio) on the formation of Mg-calcite or monohydrocalcite from Mg-ACC comes also from X-ray diffraction results. Our findings showed that Mg-ACC separated rapidly from reactive solutions of experiments C1 and MgCa3 by membrane filtration transformed to Mg-calcite under air exposure (**Table 3**), despite the fact that the same Mg-ACC transformed to monohydrocalcite when it remained in the reactive solutions (e.g. exp. C1 in **Fig. 1B**). Under ambient atmospheric conditions H_2O molecules are adsorbed onto the ACC phase, forming a water layer, which promotes its dissolution and re-precipitation (Xu et al., 2006; Konrad et al., 2016). The only source of cations in this water layer is that released during the dissolution of Mg-ACC. In the present case, the $[Mg]_{aq}/[Ca]_{aq}$ ratio of the water layer is most likely close to that of the Mg-ACC; in experiments C1 and MgCa3 the Mg/Ca of Mg-ACC is 1/9 and 1/8, respectively. These values are much lower compared to those in the reactive solutions of experiments C1 ($[Mg]_{aq}/[Ca]_{aq}$ = 9/1) and MgCa3 ($[Mg]_{aq}/[Ca]_{aq}$ = 6/1), inducing nucleation and growth of Mg-calcite rather than monohydrocalcite. The different reaction products observed during the transformation of the same Mg-ACC precursor either in contact with a reactive fluid or in air indicate that the crystallization of Mg-ACC in our experiments is significantly affected by the physicochemical conditions of the transformation environment (prevailing $[Mg]_{aq}/[Ca]_{aq}$ ratio of the fluid, ions released during Mg-ACC dissolution etc.) and to a lesser extent by a potential proto-crystalline pre-structuring (Gebauer et al., 2008) of the primary Mg-ACC.

5.5. SUMMARY AND CONCLUSIONS

Despite the fact that Mg-rich amorphous calcium carbonate was precipitated at different pH values (8.3 to 8.8) and initial Mg/Ca ratios (1/3 to 1/8) our findings revealed two pathways of Mg-ACC transformation in aqueous solution, which strictly depend on the prevailing $a_{Mg^{2+}}/a_{Ca^{2+}}$ of the reactive solution after Mg-ACC was synthesized: (i) at $5 \leq a_{Mg^{2+}}/a_{Ca^{2+}} \leq 8$ Mg-calcite is

formed via intermediate Mg-ACC. (ii) Conversely, at $8 \leq a_{Mg^{2+}}/a_{Ca^{2+}} \leq 12$, Mg-ACC transformed to monohydrocalcite.

Independent of the Mg content in ACC, the *in situ* Raman monitoring indicated a significantly extended metastability of Mg-ACC in the reactive solution in experiments where Mg-ACC transformed to monohydrocalcite at higher $a_{Mg^{2+}}/a_{Ca^{2+}}$ (~ 58 min) compared to experiments where Mg-ACC transformed to Mg-calcite at lower $a_{Mg^{2+}}/a_{Ca^{2+}}$ (~ 36 min). Moreover, the formation of monohydrocalcite is shown to be a slow process (~ 25 min), whereas the formation of Mg-calcite was comparable fast (~ 8 min). These observations suggest that the formation time of the less soluble crystalline phase formed under the prevailing physicochemical condition of the reactive solution is the rate-limiting process in the dissolution/transformation of Mg-ACC. At higher $a_{Mg^{2+}}/a_{Ca^{2+}}$ the presence of Mg-ACC in the reactive solution is prolonged due to the inhibition of calcite formation and the slow precipitation kinetics of monohydrocalcite. Our experimental results documented a different transformation product when Mg-ACC was separated from the Mg-rich reactive solution. In this case, the formation of the crystalline phase is determined by the ions released through Mg-ACC dissolution in present adsorbed water layer under atmospheric conditions. These observations clearly highlight the importance of the physicochemical conditions of the transformation environment on the formation of distinct crystalline carbonate phases via metastable Mg-ACC.

5.6. SUPPLEMENTARY DATA

Table S1
Frequencies (cm^{-1}) of observed carbonate vibration bands from *in situ* Raman and ATR-FTIR spectra and identified mineralogy of the precipitates obtained at certain reaction times from experiments C1_2. Mhc: monohydrocalcite

Experiment	time	Raman		ATR-FTIR			Mineralogy
		ν_1	libration mode	ν_1	ν_2	ν_4	
C1_2	13 min	1080	-	1073	860	-	Mg-ACC
	25 min	1081	-	1074	860	-	Mg-ACC
	60 min	1082	-	1074	860	-	Mg-ACC
	180 min	1068	-	1068	870	752/728/697	Mhc

Table S2
Chemical composition of experimental solutions and solids from experiments A1, A2 and A3, time: reaction time during the experimental run; pH: pH of the reactive solution, $[Ca]_{aq}$, $[Mg]_{aq}$: Ca and Mg concentration of the reactive solution; Alkalinity: carbonate alkalinity concentration of the reactive solution; $[Mg]_{solid}$: Mg content of the solid calculated according to **Eq. (1)**.

Exp.	time min/d	pH	$[Ca]_{aq}$ x 10^{-3} M	$[Mg]_{aq}$ x 10^{-3} M	Alkalinity x 10^{-3} M	$[Mg]_{solid}$ mol%
A1	0 min		-	-	1006	-
	5 min	7.80	2.0	14.0	648	5.6
	13 min	7.79	0.7	19.7	354	9.6
	25 min	7.77	0.3	27.3	107	9.6
	60 min	7.86	0.7	26.6	102	9.9
	180 min	7.88	0.9	25.8	101	10.3
	1 d	7.80	0.3	23.0	98	11.4
A2	0 min	7.80	-	-	976	-
	5 min	7.81	0.1	9.1	655	4.9
	13 min	7.80	1.0	12.3	356	7.6
	25 min	7.80	0.4	18.3	100	7.1
	60 min	7.88	0.6	18.7	98	6.9
	180 min	8.00	0.3	19.1	92	6.7
	1 d	8.10	0.1	19.3	99	6.6
A3	0 min	7.84	-	-	985	-
	5 min	7.84	0.1	6.5	509	4.3
	13 min	7.80	0.0	9.8	350	5.6
	25 min	7.80	0.3	13.7	95	5.6
	60 min	7.90	0.5	13.4	99	5.7
	180 min	7.97	0.3	14.9	97	5.0
	1 d	8.26	0.1	15.9	97	4.6

Table S3
Chemical composition of experimental solutions and solids from experiments C1, C2 and C3, time: reaction time during the experimental run; pH: pH of the reactive solution¸ $[Ca]_{aq}$, $[Mg]_{aq}$: Ca and Mg concentration of the reactive solution; Alkalinity: carbonate alkalinity concentration of the reactive solution; $[Mg]_{solid}$: Mg content of the solid calculated according to **Eq. (1)**.

Exp.	time min/d	pH	$[Ca]_{aq}$ x 10^{-3} M	$[Mg]_{aq}$ x 10^{-3} M	Alkalinity x 10^{-3} M	$[Mg]_{solid}$ mol%
	0 min	8.80	-	-	1151	-
	5 min	8.82	2.7	13.4	776	6.4
	13 min	8.83	2.2	21.8	442	8.4
	25 min	8.85	3.0	26.1	141	9.9
C1	60 min	8.87	2.4	26.2	140	10.2
	180 min	8.99	0.2	39.2	154	3.8
	1 d	8.88	0.1	18.8	145	12.9
	0 min	8.82	-	-	1170	-
	5 min	8.81	2.4	8.4	785	5.9
	13 min	8.81	2.1	13.8	424	6.8
	25 min	8.81	3.2	16.2	120	8.2
C2	60 min	8.81	0.1	1.6	104	13.7
	180 min	8.82	0.1	0.8	99	14.0
	1 d	8.82	0.0	0.3	96	14.2
	0 min	8.81	-	-	1123	-
	5 min	8.80	1.6	7.3	733	3.5
	13 min	8.83	1.6	11.6	412	4.6
	25 min	8.81	3.3	12.6	119	6.2
C3	60 min	8.90	0.1	1.3	102	10.6
	180 min	8.84	0.1	1.0	102	10.8
	1 d	8.80	0.0	0.4	99	11.0

Table S4
Chemical composition of experimental solutions and solids from experiments MgCa3, MgCa4_2 and C1_2, time: reaction time during the experimental run; pH: pH of the reactive solution, $[Ca]_{aq}$, $[Mg]_{aq}$: Ca and Mg concentration of the reactive solution; Alkalinity: carbonate alkalinity concentration of the reactive solution; $[Mg]_{solid}$: Mg content of the solid calculated according to **Eq. (1)**.

Exp.	time min/d	pH	$[Ca]_{aq}$ x 10^{-3} M	$[Mg]_{aq}$ x 10^{-3} M	Alkalinity x 10^{-3} M	$[Mg]_{solid}$ mol%
	0 min		-	-	1018	-
	5 min	8.31	3.6	19.0	706	5.3
MgCa3	13 min	8.34	4.0	31.0	397	8.4
pH 8.3	25 min	8.36	6.0	37.2	136	11.4
Mg/Ca = 1/3	60 min	8.38	3.6	36.3	124	11.7
	180 min	8.42	0.4	40.9	143	9.4
	0 min	8.37	-	-	1082	-
MgCa4_2	5 min	8.30	2.1	16.5	722	4.1
pH 8.3	13 min	8.34	4.0	25.5	409	6.9
Mg/Ca = 1/4	25 min	8.31	7.0	30.8	121	9.1
	60 min	8.32	0.4	13.5	69	15.4
	180 min	8.33	0.1	9.8	89	16.7
	0 min	8.80	-	-	1160	-
C1_2	5 min	8.82	0.5	15.1	795	5.7
pH 8.8	13 min	8.80	2.5	23.6	450	8.4
Mg/Ca = 1/4	25 min	8.85	3.4	27.8	153	10.6
	60 min	8.82	3.1	27.9	135	10.3
	180 min	9.05	0.3	45.3	179	3.2

Table S5

Concentrations and activities of HCO_3^- and CO_3^{2-} species at 1 min of reaction time in experiments conducted at pH 7.8 and 8.8 calculated using the PHREEQC software (minteq.v4 database). [HCO_3^-], [CO_3^{2-}]: bicarbonate and carbonate concentration of the reactive solution; aHCO_3^-, aCO_3^{2-}: activity of bicarbonate and carbonate species in the reactive solution; $a_{CO_3^{2-}}$/ $a_{HCO_3^-}$: ratio of carbonate to bicarbonate activities in the reactive solution

Exp.	[HCO_3^-] x 10^{-3} M	[CO_3^{2-}] x 10^{-3} M	$a_{HCO_3^-}$, x 10^{-3} M	$a_{CO_3^{2-}}$ x 10^{-3} M	$a_{CO_3^{2-}}/a_{HCO_3^-}$
A1	708	4.8	471	1.6	3.48E-03
A2	696	4.1	464	1.4	2.95E-03
A3	674	4.2	451	1.4	3.03E-03
C1	601	30.5	394	11.9	3.03E-02
C2	587	30.8	385	11.9	3.09E-02
C3	594	30.1	390	11.5	2.95E-02

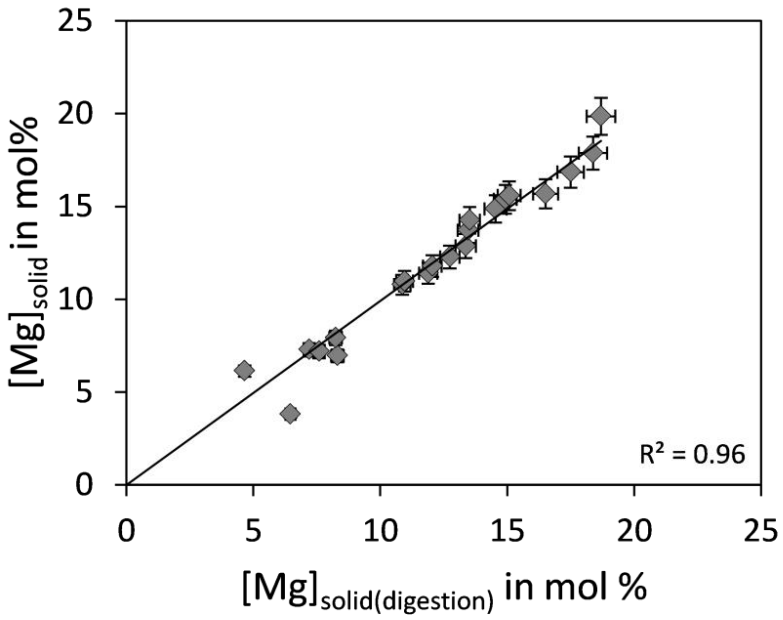

Fig. S1. Mg content of the precipitates calculated from digestion ($[Mg]_{solid(digestion)}$) versus Mg content of the solid calculated according to **Eq. 1** ($[Mg]_{solid}$). Solid line is the linear regression line: $[Mg]_{solid} = 0.995\ [Mg]_{solid(digestion)}$.

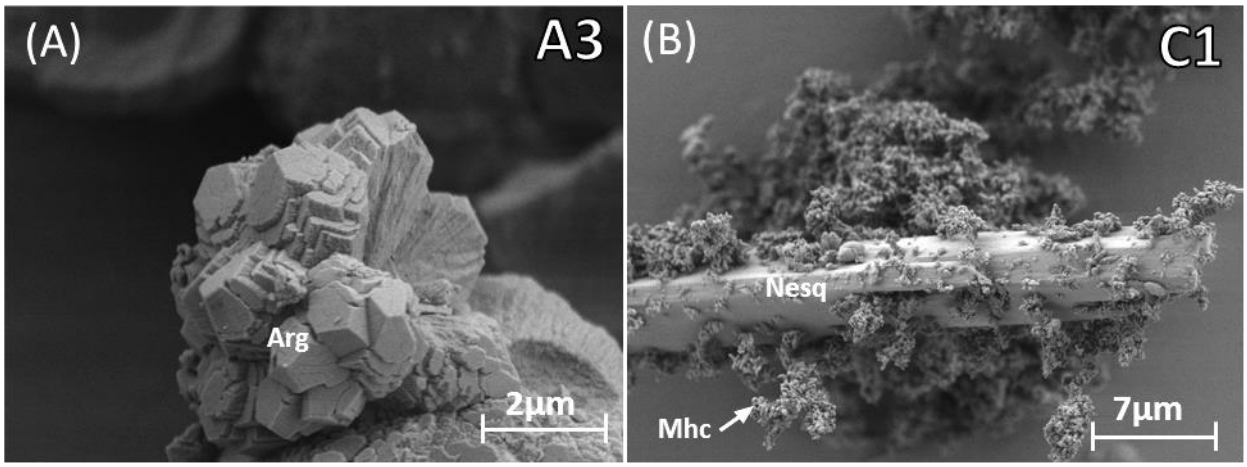

Fig. S2. SEM image of sampled precipitates obtained after 1 day of reaction time from experiment A3 **(A)** showing aragonite crystals and experiment C1 **(B)** showing monohydrocalcite (Mhc) and nesquehonite (Nesq) crystals.

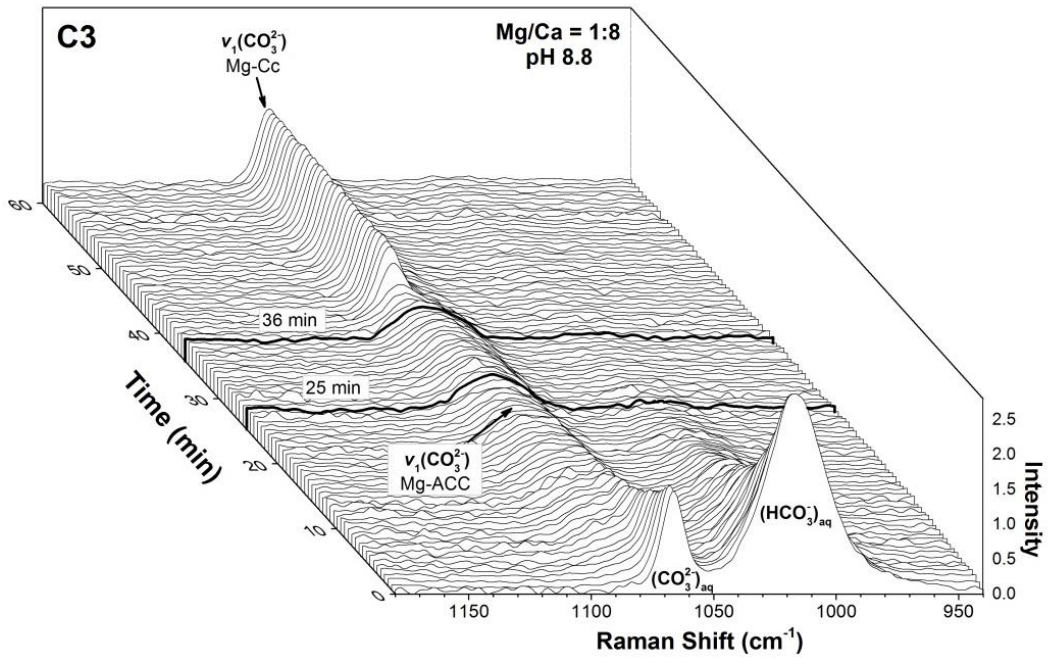

Fig. S3. Waterfall plot of *in situ* Raman spectra showing the vibration band of aqueous HCO_3^- and CO_3^{2-} as well as the v_1 band of Mg-ACC and Mg-calcite (Mg-Cc) of experiment C3.

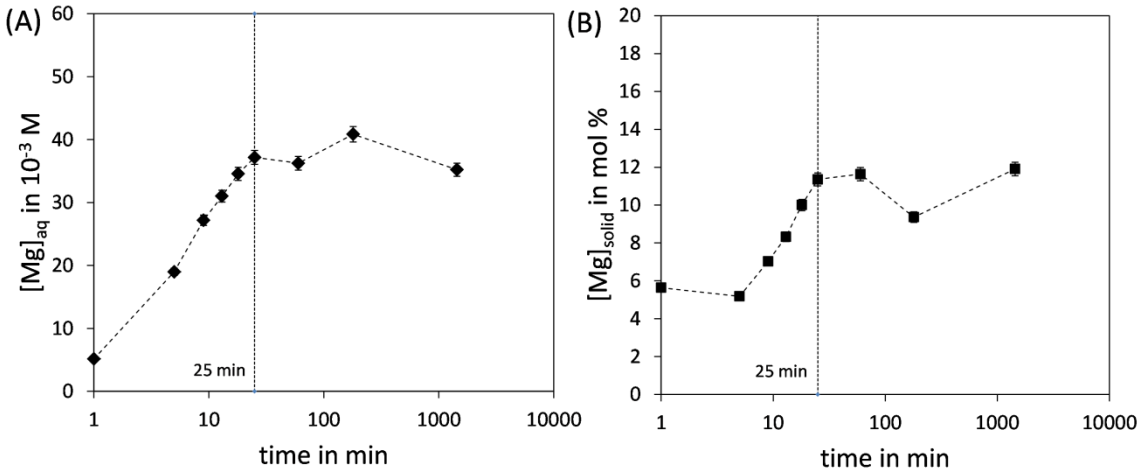

Fig. S4. (A) Concentration of dissolved Mg ions of the reactive solution, $[Mg]_{aq}$, and (B) Mg content of the precipitated solid, $[Mg]_{solid}$, calculated according to Eq. 1 versus experimental run time of experiment MgCa3 conducted at pH 8.3 with the Mg/Ca ratio 1/3. Titration of the $(Ca,Mg)Cl_2$ solutions into the $NaHCO_3$ solutions was stopped at 25 min of experimental time (dashed line). The error bars are smaller than the symbols.

6. Control of Temperature and aqueous Mg^{2+}/Ca^{2+} Ratio on the (Trans)Formation of Ikaite

Bettina Purgstaller[1], Martin Dietzel[1], Andre Baldermann[1], Vasileios Mavromatis[1,2]

[1]*Institute of Applied Geosciences, Graz University of Technology, Rechbauerstrasse 12, 8010 Graz, Austria*
[2] *Géosciences Environnement Toulouse (GET), CNRS, UMR 5563, Observatoire Midi-Pyrénées, 14 Av. E. Belin, 31400 Toulouse, France*

ABSTRACT

The calcium carbonate hexahydrate mineral ikaite ($CaCO_3 \cdot 6\ H_2O$) has been documented in aqueous environments at near-freezing temperatures. In the case of warming of the depositional environment, natural ikaite rapidly transforms into less soluble calcium carbonate phases occasionally leaving calcite pseudomorphs in the sediments, which are considered as an indicator for primary cold water temperatures. However, details on ikaite (trans)formation behavior, such as temperature limits and solution chemistry control, are still debated. In order to study the formation of ikaite, we conducted precipitation experiments under controlled physicochemical conditions (pH = 8.3 ±0.1; T = 6, 12, and 18 ±0.1 °C) at distinct aqueous molar Mg/Ca ratios. The transformation of ikaite into anhydrous calcium carbonate polymorphs was investigated in solution and at air exposure. Despite the fact that all experimental solutions are supersaturated with respect to ikaite, our data reveal the formation of ikaite at temperatures up to 12°C, whereas Mg-rich amorphous calcium carbonate precipitated at 18°C. The herein obtained temperature limit for ikaite formation is significantly higher than formerly expected and most probably caused by the slow dehydration kinetics of the aqueous Ca^{2+} ion at low versus high temperature. At aqueous molar Mg^{2+}/Ca^{2+} ratios of ≥ 14 the suspended ikaite transformed into aragonite. In contrast, ikaite separated from the solution and exposed to air transformed in all cases into calcite/vaterite. These findings show that the $CaCO_3$ polymorph formed from ikaite is strongly controlled by the physicochemical conditions, such as aqueous molar Mg^{2+}/Ca^{2+} ratio of the reactive fluid and H_2O availability throughout the transformation process.

6.1. INTRODUCTION

Ikaite is a hydrous crystalline calcium carbonate mineral ($CaCO_3 \cdot 6H_2O$) which is commonly found in environments characterized by near-freezing temperatures. The on-site formation of ikaite was first observed at the bottom of the Ikka Fjord in Greenland (Pauly et al., 1963), where ikaite precipitates by the mixing of submarine cold springs with seawater. Since then, the occurrence of ikaite was documented in recent sediments of the Antarctic shelf (Suess et al., 1982; Lu et al., 2012), Arctic and Antarctic Sea ice (Dieckmann et al., 2008; 2010; Rysgaard et al., 2012; Fischer et al., 2013), saline spring waters (Ito, 1996; Ito et al., 1999; Omelon et al., 2001), saline lakes (Council and Bennet, 1993; Bischoff et al., 1993; Oehlerich et al., 2013) and also in hyperalkaline (pH > 12), anthropogenic environmental settings at temperatures up to 8-9°C (e.g. Boch et al., 2015; Field et al., 2016).

Bischoff et al. (1993) showed that the solubility of ikaite increases with increasing temperature, a trend that is opposite to that of the anhydrous forms of $CaCO_3$ (calcite, aragonite and vaterite), which strongly supports the limitation of ikaite occurrence to low temperatures. Outside the aqueous depositional environment ikaite crystals typically disintegrates into a mush of water and calcite (Pauly et al., 1996; Bischoff et al., 1993; Omelon et al., 2001), sometimes with admixtures of vaterite (Ito, 1996; Ito et al., 1999, Shaikh 1990) and/or aragonite (Council and Bennet, 1993; Stein and Smith 1986). Along these lines, it has been suggested that anhydrous $CaCO_3$ minerals found in the sediments of saline lakes and springs during summer months originate from ikaite, which precipitated during winter months in these restricted environments (Council and Bennet, 1993; Ito, 1996; Ito et al., 1999; Omelon et al., 2001; Oehlrich et al., 2013). In some cases the shape of the original ikaite crystal is preserved as a pseudomorph (Selleck et al., 2007). These calcite pseudomorphs, also called glendonites, are frequently found in the sedimentary record and are considered to be an indicator of near-freezing temperatures (Shearman and Smith, 1985; Larsen, 1994; De Lurio and Frakes., 1999; Spielhagen and Tripati, 2009; Swainson and Hammond, 2001; Lu et al., 2012; Last et al., 2013).

Nonetheless, the parameters controlling ikaite formation in natural environments are still under debate. At a temperature above 0°C, seawater is undersaturated with respect to ikaite (Bischoff et al., 1993). Thus, its formation in seawater requires the addition of external Ca^{2+} and/or CO_3^{2-} ions (Bischoff et al. 1993; Hu et al., 2014). In marine sediments sufficient amounts of dissolved inorganic carbon can be provided by the decomposition of organic matter (Stein and Smith 1995;

Suess et al., 1982; Jansen et al., 1987). In alkaline lakes, where local fluids are close to equilibrium with respect to ikaite at 0°C, the inflow of Ca-rich groundwater can trigger the formation of ikaite (Bischoff et al., 1993). It has been suggested that elevated PO_4^{3-} and Mg^{2+} concentrations play a crucial role in the formation and stabilization of ikaite (Council and Bennet, 1993; Bischoff et al., 1993; Burchardt et al. 1997) due to their high chemical affinity to Ca^{2+} ions and the inhibition of $CaCO_3$ polymorph formation, respectively (Burton and Walter, 1990; Reddy 1977; Reddy et al., 1980). The present study aims at investigating the (i) parameters leading to ikaite formation and (ii) mechanisms controlling the transformation of ikaite into anhydrous $CaCO_3$ polymorphs in solution and at air exposure. Our findings provide new insights on the physicochemical limits of ikaite formation in natural and man-made environments and highlight the importance of the fluid composition on the formation of $CaCO_3$ minerals from intermediately occurring ikaite.

6.2. METHODS

6.2.1 Experimental setup and analytical methods

The experimental setup and the analytical methods used in the present study are described in detail in Purgstaller et al. (2016). Briefly, the precipitation of solid $Ca_{1-x}Mg_xCO_3 \cdot nH_2O$ was induced by the addition of 50 ml of a 0.6 M $(Ca,Mg)Cl_2$ solution at a rate of 2 ml/min (702 SM Titrino titrator; Methrom) into a 150 ml borosilicate reactor containing 50 ml of a 1 M $NaHCO_3$ solution (stirred at 200 rpm). The Mg/Ca ratio used in the $(Ca,Mg)Cl_2$ solution was either 1/8 or 1/4. The pH of the reactive solution was kept constant at pH 8.3 ±0.1 by the automatic titration (Schott; TitroLine alpha plus) of a 1 M NaOH solution into the reactor. The temperature of the reactive solution/suspension was controlled at 6.00 ±0.07°C, 12.00 ±0.05°C or 18.00 ± 0.03°C (Easy Max^{Tm} 102; Mettler Toledo) for 180 min of reaction time (**Table S1-S3**). Subsequently the suspension was transferred into a gas-tight 150 ml glass bottle and stored at 20 ±1°C in a temperature controlled room for 1 day to induce transformation of the transient hydrated $CaCO_3$ phases into their stable anhydrous counterparts. The experiments conducted in the context of the present study are labeled as T6_A, T6_B, T12_A, T12_B, T18_A and T18_B, where the number denotes the temperature of the reactive solution (°C) and the letter denotes the Mg/Ca ratio used in the $(Ca,Mg)Cl_2$ solution (A = 1/8; B = 1/4).

Raman spectra of the reactive solution/suspension were collected every 35 sec for 180 min of reaction time by *in situ* Raman spectroscopy (Raman RXN2^{TM} analyzer, Kaiser Optical Systems). Samples of the reactive solution/suspension (1-5 ml) were collected after certain reaction times for solid and/or solution analyses. The solids were separated from the solution by a 0.2 µm cellulose acetate filter using a suction filtration unit. Immediately after filtration the solids were analyzed using Attenuated Total Reflectance - Fourier Transform Infrared Spectroscopy (ATR-FTIR; Perkin Elmer Spectrum 100). An aliquot of the separated precipitates was subsequently exposed to air (T = 25 ±1 °C and relative humidity of 26 ±3 %) for 24 hours. X-ray diffraction (XRD) patterns of in this way dried solids were acquired using a PANalytical X´Pert PRO diffractometer. The mineral phase contents were quantified using Rietveld refinement (software HighScore Plus, PANalytical, PDF-2 database). Selected solids were gold-coated and imaged using a scanning electron microscope (SEM, ZEISS DSM 982 Gemini).

Immediately after sample filtration the total alkalinity of the solution was measured by a Schott TitroLine alpha plus titrator using a 0.02 M HCl solution, with an analytical precision of ±2%. The aqueous cation concentrations of the solutions and of digested solids were determined using inductively coupled plasma optical emission spectrometry (Perkin Elmer Optima 8300 DV). The analytical error is < ±3% for Ca and Mg.

6.2.2 Hydrochemical modeling

The aqueous speciation and the saturation index of the reactive solutions with respect to calcite and aragonite were calculated using the PHREEQC software together with its minteq.v4 database. The saturation index (SI) of the reactive solution with respect to ACC and ikaite is defined as

$$SI_{ACC/ikaite} = \log\left[\frac{a_{Ca^{2+}} \cdot a_{CO_3^{2-}} \cdot (a_{H_2O})^n}{K_{ACC/ikaite}}\right] \quad (1)$$

where a_i denotes the activity of the species i in aqueous solution and n the water content per formula unit. For simplification a_{H_2O} was assumed to be 1 in our experimental solutions. The values of the solubility product of ACC (K_{ACC}) and ikaite (K_{ikaite}) in the temperature range from 6 to 25°C were derived from $\log K_{ACC} = -6.1987 - 0.005336 \cdot T - 0.0001096 \cdot T^2$ (Brečević and

Nielsen, 1989) and log K_{ikaite}= 0.15981 - 2011.1/T (Bischoff et al., 1993), respectively, where T is given in °C.

6.3. RESULTS

6.3.1 Solid phase characterization

Experiments at 6°C and 12°C

In experiments conducted at 6°C and 12°C, the collected *in situ* Raman spectra documented the presence of ikaite during at least 180 min of reaction time. The Raman spectra of ikaite is characterized by a strong v_1 band at ~1071 cm^{-1} (e.g. exp. T6_A in **Fig. 1A**) and by weaker bands at ~282, ~223 and ~204 cm^{-1} which can be assigned to lattice vibrations (see values in **Table 1**). These Raman bands are in good agreement with published values of synthetic and natural ikaite (Mikkelsen et al., 1999; Coleyshaw et al., 2003; Hu et al., 2014; Sanchez-Pastor et al., 2016). The formation of ikaite was further confirmed by ATR-FTIR spectra of sampled precipitates, showing vibration bands at ~869 cm^{-1}, ~722 cm^{-1} and 667 cm^{-1} (exp. T6_A in **Fig. 1B, Table 1**). The former values can be assigned to the v_1 and v_4 bands of ikaite (Coleyshaw et al. 2003). The vibration band at 667 cm^{-1} has not yet been attributed to a vibration band, but is documented in FTIR spectra of natural ikaite (Coleyshaw et al. 2003, Boch et al., 2015). Despite the fact that ikaite was identified in suspensions until 180 min of reaction time, the separated and subsequently dried precipitates (exposed to air for 24 h) contain no ikaite (**Tab. 2**). Indeed, XRD patterns of the dried precipitates showed that the primary ikaite disintegrated into mixtures of calcite and vaterite (between 25 and 180 min in **Table 2**). The calcite consists of rhombohedral crystals (~8 μm) (**Fig. 3A-B**), whereas vaterite displays spherical aggregates (~6 μm) composed of nanoparticles (**Fig. 3A**).

The ATR-FTIR spectra of the precipitates collected from suspension at 5 min of reaction time in experiments conducted at 6°C and 12°C revealed the formation of ACC, beside ikaite (e.g. exp. T6_A in **Fig. 1B, Table 1**), by the presence of a broad v_1 band at 1072 cm^{-1} and of a v_2 band at 860 cm^{-1} (Loste et al., 2003; Purgstaller et al., 2016; Konrad et al., 2016). The characteristic vibration bands of ACC, however, were absent in the solids collected at a later reaction time in the experimental runs (e.g. exp. T6_A in **Fig. 1A, Table 1**). In contrast to the ATR-FTIR spectroscopic observations, the characteristic broad Raman band of ACC at 1080-1085 cm^{-1}

(Wang et al., 2012; Purgstaller et al., 2016) is not visible in the *in situ* Raman spectra after the onset of the experiments (e.g. exp. T6_A in **Fig. 1A**). The low resolution of *in situ* Raman spectra at the initial stage of the experiments is most probably caused by the low amount of solid in the reactive solution at the beginning of the experimental run. In experiment T12_A a weak Raman band at 1086 cm^{-1} appeared after about 18 min of reaction time (**Fig. S1**), corresponding to the v_1 band of either calcite or aragonite (Kontoyannis and Vagenas, 2000). The diagnostic lattice vibrations that could help to distinguish aragonite (205 cm^{-1}) and calcite (281 cm^{-1}) are less intense and are partly overlapping with the characteristic lattice vibrations of ikaite.

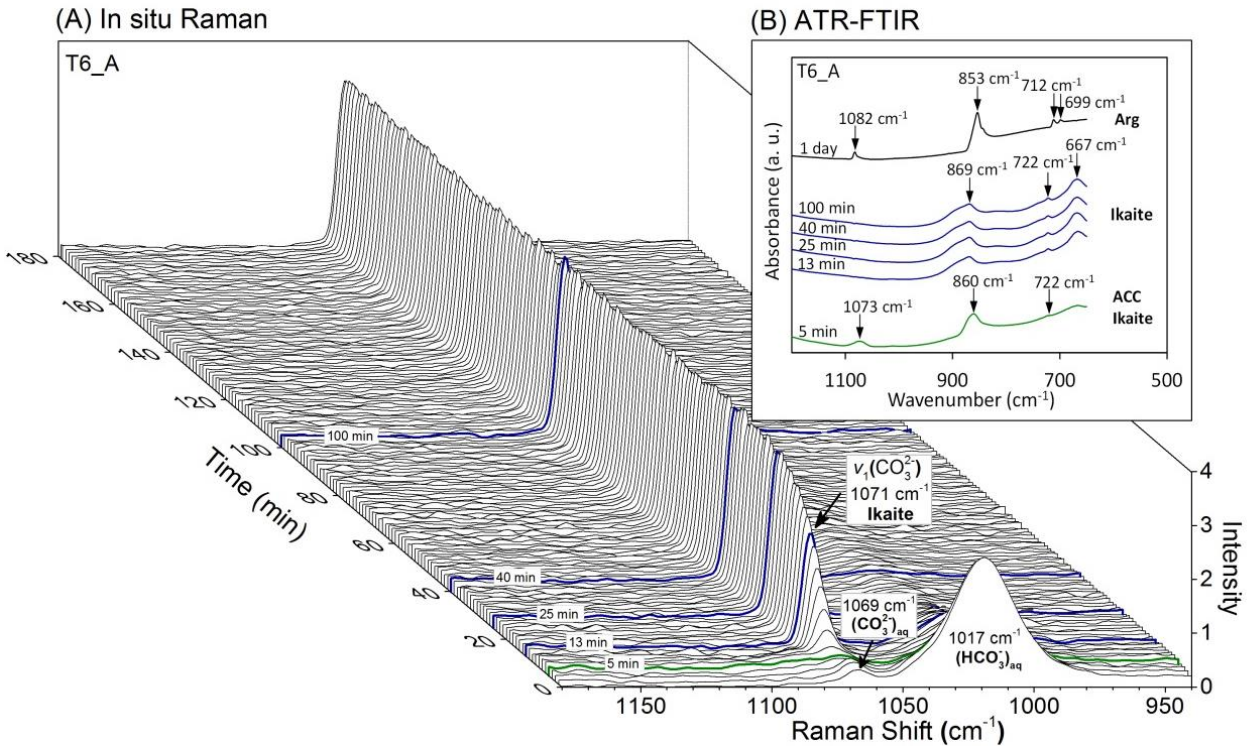

Fig. 1. (A) Waterfall plot of *in situ* Raman spectra showing the vibration band of aqueous HCO_3^- and CO_3^{2-} as well as of the v_1 band of CO_3^{2-} related to ikaite in experiment T6_A. **(B)** ATR-FTIR spectra of sampled precipitates at certain reaction times of the experiment T6_A. Arg: aragonite

In all experiments conducted at 6 and 12°C, ikaite disappeared in favor of aragonite after storage of the suspensions at 20 ±1°C for 1 day of reaction time, as it is indicated by the ATR-FTIR vibrations bands of aragonite at 1083 cm^{-1} (v_1), 852 cm^{-1} (v_2) and 712/699 cm^{-1} (v_4) (Kontoyannis and Vagenas, 1999) (e.g. exp. T6_A in **Fig. 1B, Table 1**). The XRD patterns of the air-exposed precipitates showed only aragonite in experiments initially conducted at 6°C, whereas in experiments initially conducted at 12°C the dried solids consist of aragonite (≥ 93 wt. %) with

minor amounts of calcite (≤ 7 wt.%) (**Table 2**). In experiment T12_A the presence of aragonite was first indicated in the dried sample at 60 min of reaction time (1 wt.%, **Table 2**). Between 60 min and 180 min of reaction time the fraction of aragonite in the dried samples increased (from 1 to 17 wt. %), while the fraction of calcite decreased (**Table 2**). The aragonite particles from experiments T6_A, T6_B and T12_B (after 1 day) and from experiment T12_A (after 180 min and 1 day of reaction time) consist of spherical nanoparticles (~15 nm), arranged in needles and spindle shaped aggregates (**Fig. 3C-F**), whereas the calcite crystals (~8 μm) of experiments T12_A and T12_B are rhombohedral (e.g. exp. T12_A in **Fig. 3F**).

Experiments at 18°C

In the experiments conducted at 18°C, ACC was detected by the presence of the broad Raman v_1 band at ~1082 cm^{-1} (exp. T18_B, **Fig. 2A**) and by the absence of lattice modes at lower frequencies in the Raman spectra (**Table 1**). After 29 and 35 min of reaction time in experiments T18_A and T18_B, respectively, the transformation of ACC to Mg-calcite was indicated by the rise of the v_1 band and libration mode of Mg-calcite at 1088 ±1 cm^{-1} and 283 cm^{-1}, respectively, and by the decrease of the broad v_1 band of ACC at ~1082 cm^{-1} (exp. T18_B in **Fig. 2A**, **Table 1;** Purgstaller et al., 2016). The results obtained by *in situ* Raman spectroscopy are in good agreement with those obtained by ATR-FTIR analysis, where characteristic vibration bands were observed only for ACC between 5 and 25 min in experiment T18_A 5 and between 5 and 30 min in experiment T18_B (e.g. exp. T18_B in **Fig. 2B**, **Table 1**). After 30 min and 40 min of reaction time, the vibration bands of Mg-calcite at ~1082 (v1), ~871 (v2) and ~711 were found in addition to the characteristic vibrations bands of ACC in the ATR-FTIR spectra. In both experiments the vibration bands of ACC were absent in the solids collected after 50 min of reaction time.

In experiments T18_A and T18_B, separated ACC that was exposed to air for 24 h transformed to Mg-calcite, as indicated by XRD analysis (25 min, **Table 2**). Accordingly, once the ACC was transformed to Mg-calcite in solution (after > 30 min in experiments T18_A and T18_B) subsequent air exposure of this material did not result in further mineralogical changes (**Table 2**). Thus, the mineralogical composition of the precipitate in suspension and of the dried precipitate is almost identical after 60 min (**Table 2**). The final precipitates from experiments T18_A and T18_B consist mainly of Mg-calcite; traces of aragonite (≤ 3 wt. %) were only found in one case (**Table 2**). The Mg content of the dried precipitates, calculated from the position of the d_{104} value of calcite (Goldsmith et al., 1961), is 8 mol% in experiment T18_A and 15 mol% in experiment

T18_B, which is indicative of high-Mg calcite. Note here that the difference in the Mg content of magnesian carbonates determined by XRD and wet chemical analysis ($[Mg]_{solid}$, **Table S3**) can be up to 2-3 mol%. The SEM images of the precipitates sampled after 1 day of reaction time display Mg-calcite aggregates (~1 μm), consisting of nanoparticles about 80 nm in diameter (**Fig. 3G-H**). These Mg-calcite aggregates show textures comparable to those in experiments conducted at 25°C, where ACC to Mg-calcite transformation was observed (Purgstaller et al., 2016).

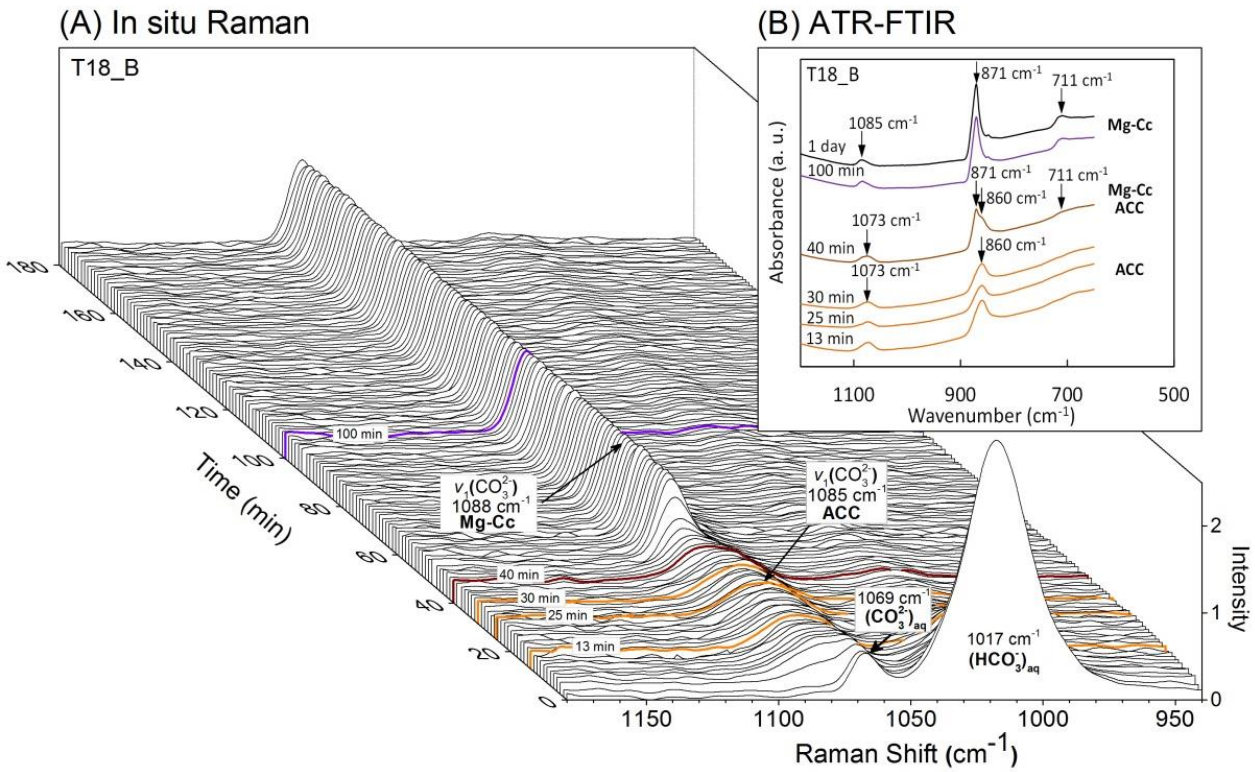

Fig. 2. (A) Waterfall plot of *in situ* Raman spectra showing the vibration band of aqueous HCO_3^- and CO_3^{2-} as well as of the ν_1 band of CO_3^{2-} related to ACC and Mg-calcite (Mg-Cc) in experiment T18_B. **(B)** ATR-FTIR spectra of sampled precipitates at certain reaction times of the experiment T18_B.

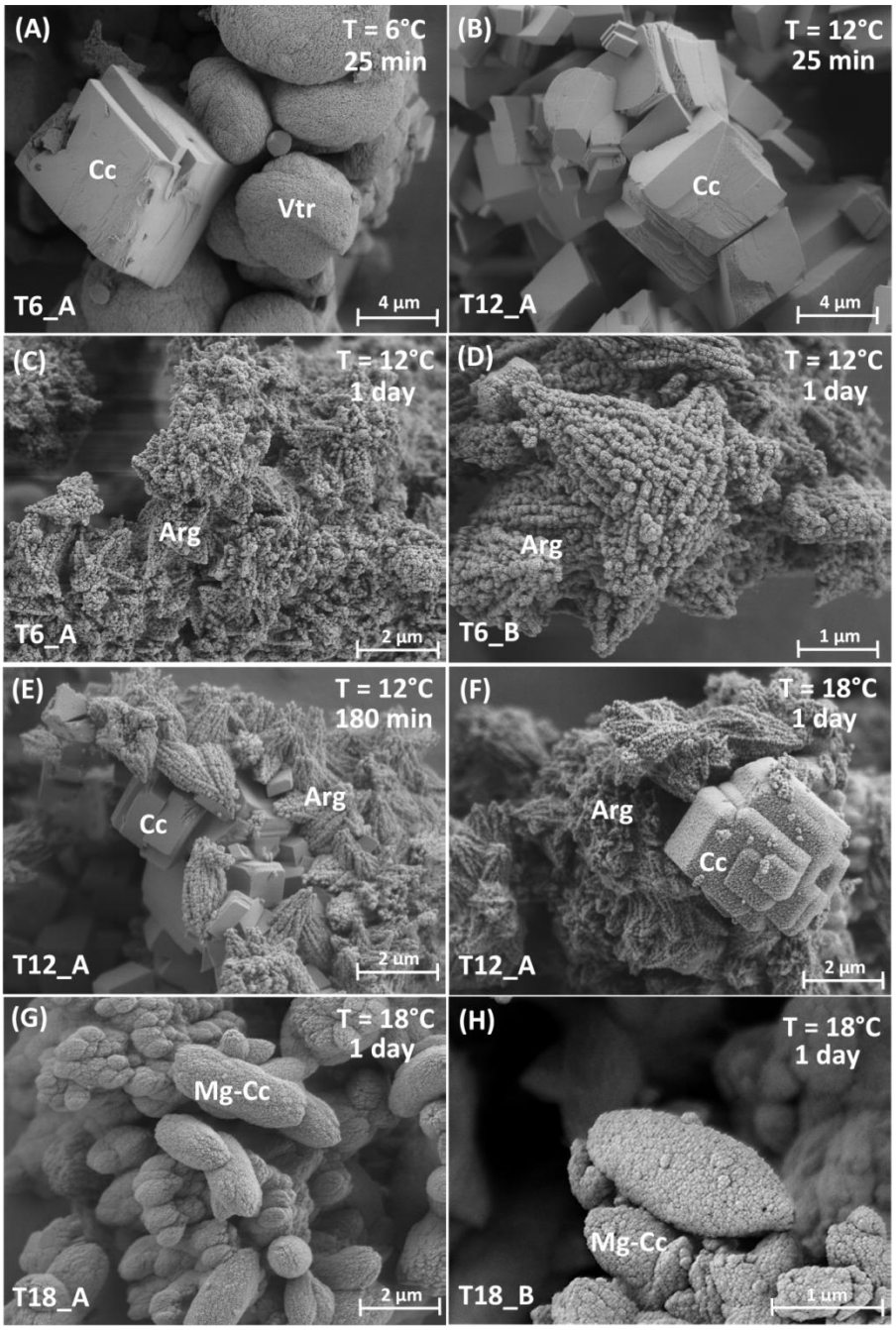

Fig. 3. SEM images of sampled precipitates from experiments T6_A **(A)** and T12_A **(B)** after 100 min of reaction time, from experiments T6_A **(C)** and T6_B **(D)** after 1 day of reaction time, from experiment T12_A after 180 min **(E)** and 1 day **(F)** of reaction time and from experiments T18_A **(G)** and T18_B **(H)** after 1 day of reaction time. Cc: calcite; Vtr: vaterite; Arg: aragonite; Mg-Cc: Mg-calcite.

Table 1

Frequencies (cm^{-1}) of observed characteristic carbonate vibration bands from *in situ* Raman and ATR-FTIR spectra, corresponding to ikaite, ACC, Mg-calcite (Mg-Cc) and aragonite (Arg) at certain reaction times. (w): vibration band of weak intensity.

Experiment	**time**	**Raman**		**Mineralogy**	**ATR-FTIR**				**Mineralogy**
	min/d	ν_1	Libration mode		ν_3	ν_1	ν_2	ν_4	
T6_A	5 min	1071	-	Ikaite	1379	1074	860	722(w)/667(w)	ACC, Ikaite
6 °C	13 min	1071	283/223/205	Ikaite	1388	-	869	722/666	Ikaite
Mg/Ca = 1/8	25 min	1071	283/223/205	Ikaite	1388	-	868	722/667	Ikaite
	30 min	1071	283/224/205	Ikaite	1387	-	869	722/667	Ikaite
	40 min	1071	282/224/205	Ikaite	1388	-	869	722/667	Ikaite
	50 min	1071	283/223/205	Ikaite	1387	-	868	722/667	Ikaite
	60 min	1071	282/224/205	Ikaite	1387	-	869	722/667	Ikaite
	100 min	1071	282/223/205	Ikaite	1388	-	868	722/667	Ikaite
	180 min	1072	283/224/205	Ikaite	1387	-	868	721/667	Ikaite
	1d	n.a.	n.a	n.a	1441	1082	853	712/699	Arg
T6_B	5 min	1071	205/223	Ikaite	1384	1073(w)	869	722/667	ACC, Ikaite
6°C	13 min	1071	281/222/203	Ikaite	1384	-	869	722/667	Ikaite
Mg/Ca=1/4	25 min	1072	282/223/204	Ikaite	1387	-	868	721/667	Ikaite
	30 min	1072	282/223/205	Ikaite	1383	-	869	722/667	Ikaite
	40 min	1072	282/224/205	Ikaite	1383	-	869	722/667	Ikaite
	50 min	1072	282/223/205	Ikaite	1383	-	869	722/667	Ikaite
	60 min	1072	282/223 205	Ikaite	1387	-	868	721/666	Ikaite
	100 min	1072	280/224/206	Ikaite	1387	-	868	721/666	Ikaite
	180 min	1072	282/223/206	Ikaite	1384	-	869	722/667	Ikaite
	1d	n.a.	n.a	n.a		1083	853	712/699	Aragonite
T12_A	5 min	1071	205	Ikaite	1387	1073(w)	870	722/667	ACC, Ikaite
12 °C	13 min	1071	282/223/205	Ikaite	1384	-	869	722/667	Ikaite
Mg/Ca = 1/8	25 min	1072/1086(w)	284/223/205	Ikaite,*	1385	-	869	722/668	Ikaite
	30 min	1071/1086(w)	283/223/204	Ikaite,*	1387	-	868	721/668	Ikaite
	40 min	1071/1086(w)	283/224/205	Ikaite,*	1384	-	869	722/669	Ikaite
	50 min	1071/1086(w)	284/224/204	Ikaite,*	1384	-	869	722/669	Ikaite
	60 min	1071/1086(w)	283/224/204	Ikaite,*	1384	-	869	722/669	Ikaite
	100 min	1071/1086(w)	282/224/204	Ikaite,*	1384	-	869	721/669	Ikaite
	180 min	1071/1086(w)	283/223/204	Ikaite,*	1388	-	869	722/670	Ikaite
	1d	n.a.	n.a	n.a	1436	1083	853	712/699	Arg
T12_B	5 min	1071	283/220/203	Ikaite	1367	1074(w)	863	721	ACC, Ikaite
12°C	13 min	1071	281/222/204	Ikaite	1384	-	869	722/668	Ikaite
Mg/Ca = 1/4	25 min	1071	282/223/204	Ikaite	1383	-	869	721/669	Ikaite
	30 min	1071	282/224/204	Ikaite	1384	-	869	722/670	Ikaite
	40 min	1071	283/223/204	Ikaite	1383	-	869	722/670	Ikaite
	50 min	1071	283/223/205	Ikaite	1384	-	869	722/670	Ikaite
	60 min	1071	282/223/204	Ikaite	1385	-	869	721/670	Ikaite

	100 min	1071	282/224/204	Ikaite	1384	-	869	722/670	Ikaite
	180 min	1071	283/224/205	Ikaite	1384	-	869	721/670	Ikaite
	1d	n.a.	n.a	n.a	1432	1083	852	712/699	Arg
T18_A	5 min	1080	-	ACC	1387	1073	860	-	ACC
18 °C	13 min	1080	-	ACC	1386	1073	860	-	ACC
Mg/Ca = 1/8	25 min	1080	-	ACC	1385	1074	860	-	ACC
	30 min	1080/1087	281	ACC, Cc	1388	1081/1074	871/860	-	ACC, Mg-Cc
	40 min	1080(w)/1087	281	ACC, Cc	1389	1081	871/860(w)	711	ACC, Mg-Cc
	50 min	1087	282	Mg-Cc	1376	1084	871	710	Mg-Cc
	60 min	1087	282	Mg-Cc	1398	1084	871	711	Mg-Cc
	100 min	1087	282	Mg-Cc	1387	1084	871	711	Mg-Cc
	180 min	1087	282	Mg-Cc	1379	1084	871	711	Mg-Cc
	1d	1087	282	Mg-Cc	1380	1084	871	711	Mg-Cc
T18_B	5 min	1081	-	ACC	1396	1073	860	-	ACC
18 °C	13 min	1081	-	ACC	1375	1073	860	-	ACC
Mg/Ca = 1/4	25 min	1082	-	ACC	1387	1074	860	-	ACC
	30 min	1082	-	ACC	1383	1074	860	-	ACC
	40 min	1082/1086(w)	283(w)	ACC, Mg-Cc	1380	1082/1076	871/860	711	ACC, Mg-Cc
	50 min	1088	283	Mg-Cc	1397	1083	871	711	Mg-Cc
	60 min	1088	283	Mg-Cc	1403	1084	871	711	Mg-Cc
	100 min	1089	283	Mg-Cc	1388	1084	871	710	Mg-Cc
	180 min	1089	283	Mg-Cc	1387	1084	871	710	Mg-Cc
	1d	n.a.	n.a	n.a	1388	1084	871	710	Mg-Cc

*weak Raman band at 1086 cm^{-1} indicates the presence of calcite and/or aragonite in the suspension

Table 2

Mineralogical composition of the precipitates in suspension obtained by *in situ* Raman and FTIR analysis (see Table 1). The mineralogical composition of dried samples, which were exposed to air (for 24 h), was quantified by Rietveld refinement using XRD patterns. Note that the precipitates in suspension from experiments conducted at 6 and 12°C consist primary of ikaite, whereas those from experiments conducted at 18°C consist of ACC. The intermediate ikaite and ACC decomposed to calcite/vaterite and Mg-calcite, respectively, during their exposure to air. Cc: calcite, Vtr: vaterite, Arg: aragonite and MgCc: Mg-calcite.

experiment	**time**	**suspension (Raman/FTIR)**	**air exposure/dried samples (XRD)**			
			Mg-Cc	Cc	Vtr	Arg
	min/d	mineralogy	wt.%	wt.%	wt.%	wt.%
T6_A	25 min	Ikaite	-	82	18	-
6°C	60 min	Ikaite	-	69	31	-
Mg/Ca = 1/8	180 min	Ikaite	-	87	13	-
	1d	Arg	-	-	-	100
T6_B	25 min	Ikaite	-	48	52	-
6°C	60 min	Ikaite	-	56	44	-
Mg/Ca=1/4	180 min	Ikaite	-	66	34	-
	1d	Arg	-	-	-	100
T12_A	25 min	Ikaite	-	100	-	-
12 °C	60 min	Ikaite,*	-	99	-	1
Mg/Ca = 1/8	180 min	Ikaite,*	-	83	-	17
	1d	Arg	-	8	-	92
T12_B	25 min	Ikaite	-	100	-	-
12°C	60 min	Ikaite	-	100	-	-
Mg/Ca = 1/4	180 min	Ikaite	-	100	-	-
	1d	Arg	-	4	-	96
T18_A	25 min	ACC	100	-	-	-
18 °C	60 min	Mg-Cc	100	-	-	-
Mg/Ca = 1/8	180 min	Mg-Cc	100	-	-	-
	1d	Mg-Cc	97	-	-	3
T18_B	25 min	ACC	100	-	-	-
18 °C	60 min	Mg-Cc	100	-	-	-
Mg/Ca = 1/4	180 min	Mg-Cc	100	-	-	-
	1d	Mg-Cc	100	-	-	-

*weak Raman band at 1086 cm^{-1} indicates the presence of calcite and/or aragonite in the suspension

6.3.2. Temporal evolution of the solution chemistry and solid chemistry

The titration of the $(Ca,Mg)Cl_2$ solution into the $NaHCO_3$ solution caused an instant precipitation of $Ca_xMg_{1-x}CO_3 \cdot nH_2O$. Thus, between 0 and 25 min elapsed time the carbonate alkalinity of the reactive solution decreased from 1044 ±28 to 135 ±11 mM in all experiments (**Table S1**). In experiments conducted at 6 and 12°C the molar concentration of Ca in the reactive solution, $[Ca]_{aq}$, decreased from 6 ±2 mM to 2 ±1 mM between the reaction time of 1 and 25 min, respectively (**Fig. 4A, B**). After the titration of the $(Ca,Mg)Cl_2$ solution was stopped, the $[Ca]_{aq}$ remained quasi-constant at 2 ±1 mM till the end of the experimental runs (**Fig. 4A, B**). Conversely, in experiments conducted at 18°C the $[Ca]_{aq}$ increased during the titration of the $(Ca,Mg)Cl_2$ solution (**Fig. 4A, B**). After 25 min of reaction time, the reactive solutions contained 9 ±1 mM of $[Ca]_{aq}$ in both experiments, followed by a decrease in the $[Ca]_{aq}$ concentration from 9.0 ±0.6 to <1 mM between 30 min and 1 day of reaction time (**Fig. 4A, B**).

The molar concentration of aqueous Mg in the reactive solutions, $[Mg]_{aq}$, increased during the titration of the $(Ca,Mg)Cl_2$ solution in all experimental runs (**Fig. 4C, D**). However, the $[Mg]_{aq}$ concentration is significantly lower in experiments conducted at 18°C, compared to the experiments conducted at 6 and 12°C. After the titration of the $(Ca,Mg)Cl_2$ solution was stopped, the $[Mg]_{aq}$ remained nearly constant in experiments conducted at 6 and 12°C, whereas in experiments conducted at 18°C the $[Mg]_{aq}$ decreased between ~30 min and 1 day of reaction time (**Fig. 4C, D**).

In experiments conducted at 6 and 12°C, the Mg content of the solid, $[Mg]_{solid}$, remained quasi constant at 1.6 ±0.6 mol% between 5 min and 1 day of reaction time (**Fig. 4E, F**). In contrast, in experiments conducted at 18°C the $[Mg]_{solid}$ became progressively higher during the experimental runs (**Fig. 4E, F**).

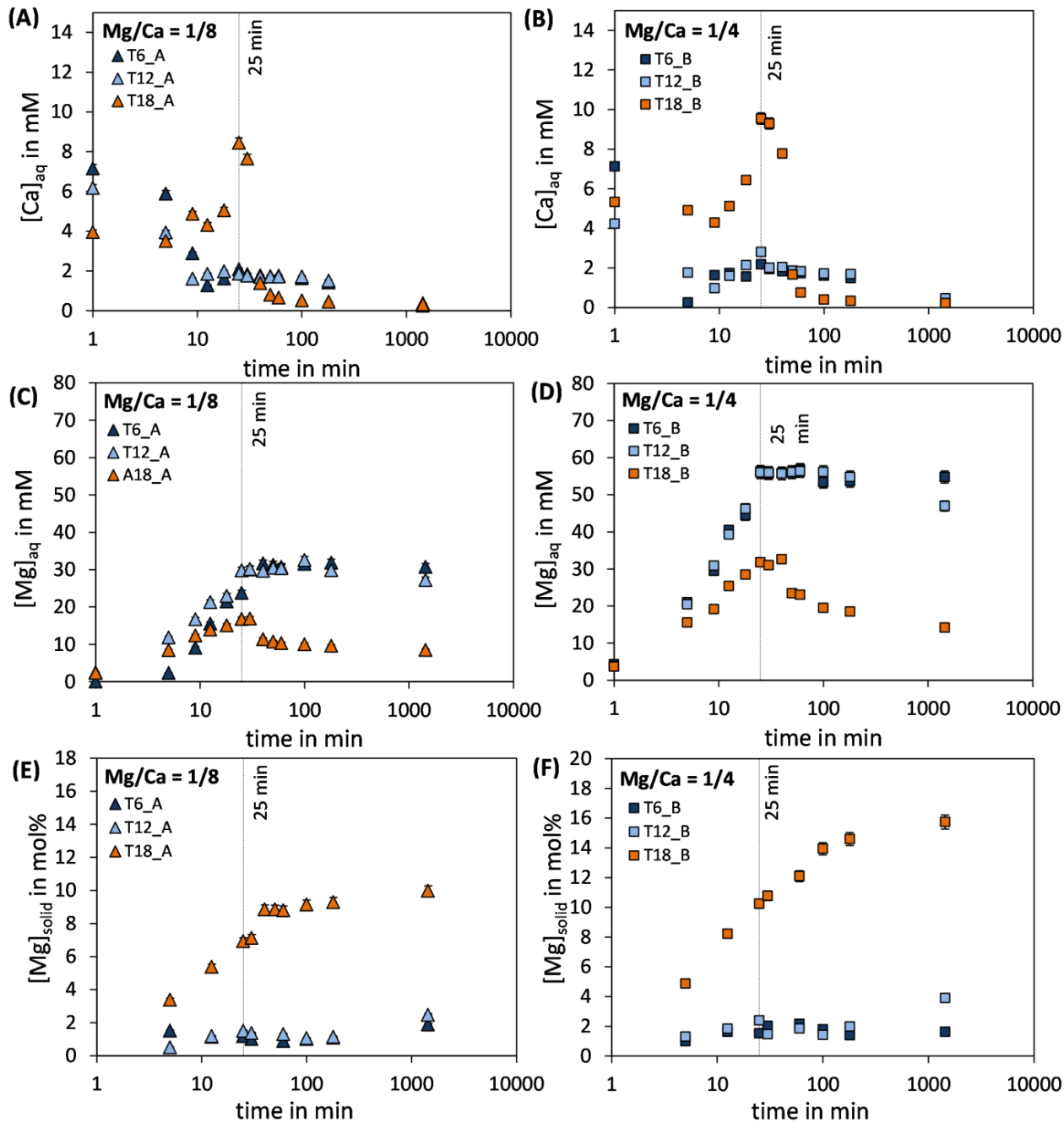

Fig. 4. (A-D) Concentration of aqueous Ca and Mg ions in the reactive solution and **(E, F)** Mg content of the precipitated solid, $[Mg]_{solid}$, versus the experimental run time of experiments conducted at initial Mg/Ca ratios of 1/8 and 1/4.

6.4. DISCUSSION

6.4.1. Formation and stability of amorphous calcium carbonate and ikaite

In experiments conducted at 6 and 12°C, ACC was found beside ikaite within a limited reaction time of ~5 min (**Fig. 1B**, **Table 1**). In contrast, in experiments conducted at 18°C, where ikaite formation was not observed, the presence of ACC was prolonged up to at least 40 min after the onset of the experimental run (**Fig. 2B**, **Table 1**). The observed difference in the stability of ACC is in particular related to the competing formation of ikaite at lower temperatures. Indeed, as it is illustrated in **Fig. 5A**, the saturation index of the reactive solutions with respect to ACC (SI_{ACC}) is > 0 at 1 min of reaction time in all experiments. In experiments conducted at 6 and 12°C, however, the rapid formation of ikaite (e.g. exp. T6_A in **Fig. 1A**) resulted in the significant removal of Ca^{2+} and CO_3^{2-} ions from the reactive solution, leading to its undersaturation with respect to ACC (after ~5 min in **Fig. 5A**). This suggests that initially formed ACC dissolved at the expense of ikaite formation.

Conversely, in experiments conducted at 18°C the SI_{ACC} remained constant at 0.2 ±0.1 for about 30 min of reaction time (**Fig. 5B**). After 29 and 35 min elapsed time Mg-calcite formation occurred in experiments T18_A and T18_B, respectively, as it is indicated by the *in situ* Raman spectroscopy data (e.g. experiment T18_B in **Fig. 1B**). The formation of Mg-calcite resulted in the decrease of the SI_{ACC} (**Fig. 5A**, **Table 1**), which initiated the transformation of ACC, similar to the results at 25°C shown by Purgstaller et al. (2016).

The experimental results revealed the formation of ikaite only in experiments conducted at temperatures ≤ 12°C, although the reactive solutions are supersaturated with respect to ikaite in all experiments (**Fig. 5B**). This observation leads us to suggest that the temperature limit for ikaite formation is linked to the kinetics of Ca^{2+} ion interaction with the aqueous media. The rate of H_2O exchange in the first hydration shell of aqueous Ca^{2+} is controlling its reactivity in aqueous environments (Di Tomaso et al. 2014). In this context, molecular dynamic simulations suggested that the rate of water exchange of the Ca^{2+} ion decreases with decreasing temperature (Hofmann et al., 2012). For the formation of anhydrous crystalline forms of $CaCO_3$ from aqueous solution the dehydration of aqueous Ca^{2+} prior to its incorporation at the lattice growth site is one of the most important rate controlling processes (Nancollas and Purdie, 1964; Nielsen, 1984). Ikaite has a monoclinic structure with Ca bonded closely to six H_2O molecules (Dickens and Brown, 1970). Thus, the complete dehydration of Ca^{2+} can be reasonably suggested not to be

required for its incorporation into the ikaite crystal lattice (Bischoff et al., 1993). Compared to ikaite, ACC is less hydrated (0.4 to 1 mole H_2O per formula unit, e.g. Konrad et al., 2016 and Lin et al., 2015), which suggests that the formation of ikaite is favored over ACC in the reactive solutions at low temperatures (**Table 1**), due to the slower exchange of H_2O within the Ca^{2+} hydration sphere.

The calculated activities of Ca^{2+} and CO_3^{2-} ions in the reactive solutions, after the titration of the $(Ca,Mg)Cl_2$ solution was stopped, were used to calculate individual "solubility" values for ikaite (IAP_{Ikaite}), according to the equation:

$$IAP_{ikaite} = (a_{Ca^{2+}}) \cdot (a_{CO_3^{2-}}) \quad (2)$$

In experiments conducted at 6°C and in experiment T12_B log IAP_{Ikaite} values equal to -6.80 ±0.02 and -6.67, respectively, were obtained for ikaite (**Fig. 5C**), which are slightly higher than the solubility products for ikaite given by Bischoff et al. (1993). Note that the IAP_{ikaite} values obtained from experiment T12_A were not considered in our solubility product calculations, because the *in situ* Raman spectroscopy data of the particles-in-suspension revealed formation of calcite/aragonite at about 20 min of reaction time (**Fig. S1**, **Table 1**).

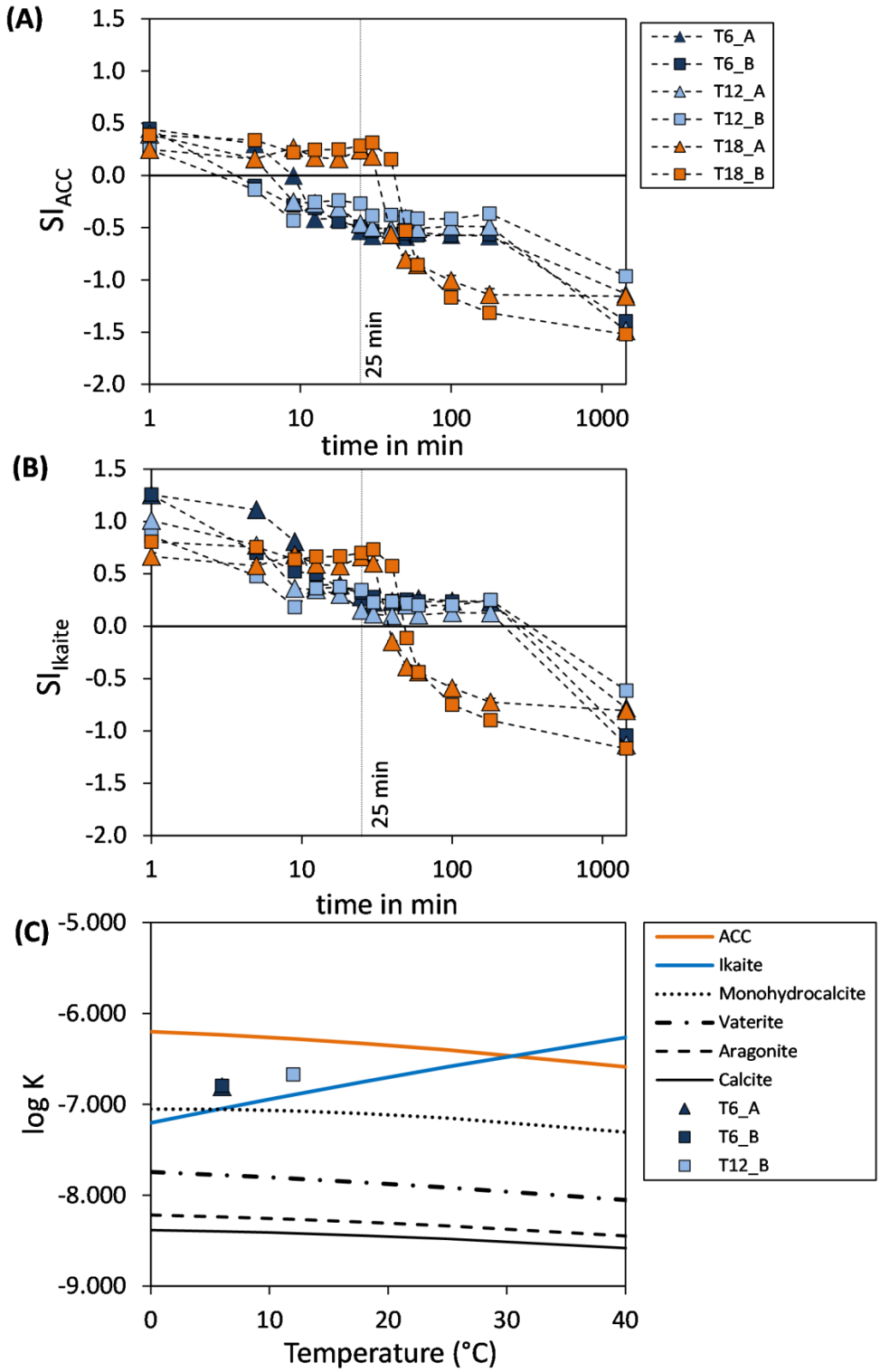

Fig. 5. Evolution of the saturation index (SI) with respect to **(A)** ACC and **(B)** ikaite over the experimental time for all experiments. **(C)** Solubility product (K) as a function of temperature for ikaite (Bischoff et al., 1993), ACC (Brecevic and Nielsen, 1989), aragonite (Plummer and Busenberg, 1982), calcite (Plummer and Busenberg, 1982) and monohydrocalcite (Kralj and Brecevic, 1995). Obtained "solubility products" for ikaite (exp. T6_A, T6_B, and T12_A) calculated according to **Eq. 2** are plotted.

6.4.2. Transformation of ikaite into aragonite in solution

In all experiments conducted at 6 and 12°C, the collected *in situ* Raman and ATR-FTIR spectra documented the presence of ikaite in the reactive solutions for at least 180 min of reaction time (e.g. exp. T6_A in **Fig. 1**, **Table 1**). Although the experimental data presented here do not allow forecasting the "long-term" stability of ikaite in aqueous solution at temperatures < 12°C, our results clearly show that after 1 day of reaction time at 20°C, the final product consisted mainly of aragonite, with minor amounts of calcite (**Table 2**). The formation of aragonite via intermediate ikaite can be explained by the high aqueous molar Mg^{2+}/Ca^{2+} ratios in the reactive solutions.

Due to the fact that the substitution of the Mg^{2+} ion for the Ca^{2+} ion in the ikaite crystal lattice is highly limited, compared e.g. to ACC and calcite (Chaka and Felmy, 2014; **Fig. 4E, F**), the remaining reactive solutions are characterized by high aqueous molar Mg^{2+}/Ca^{2+} ratios in the range $14 \leq [Mg^{2+}]/[Ca^{2+}] \leq 38$ (**Fig 6**). Under these high $[Mg^{2+}]/[Ca^{2+}]$ ratios, inhibition of calcite precipitation resulted in the formation of aragonite (e.g. Falini et al., 1994; Fernández-Díaz et al., 1996). Indeed, the aragonite aggregates obtained after 1 day of reaction time (**Fig. 3C, D, F**) show some textural and morphological similarities to natural occurring ikaite crystals (Omelon et al., 2001; Dieckmann et al., 2008; Boch et al., 2015) and glendonites (Dana, 1884; Shearman and Smith, 1985), indicating a pseudomorphic replacement of ikaite by a coupled dissolution-precipitation reaction (Ruiz-Agudo et al., 2014; Sanchez-Pastor et al., 2016) in the supersaturated aqueous solution with respect to aragonite ($SI_{aragonite} \geq 1.4$). The final aragonite pseudomorphs are highly porous (**Fig. 2D**), due to the volumetrically important loss in structural water (~52 wt.%) when ikaite transformed into aragonite (Sanchez-Pastor et al., 2016).

In contrast to ikaite, ACC is well-known to incorporate Mg ions at significantly higher levels (e.g. Long et al., 2011; Lin et al., 2015). In experiments T18_A and T18_B the Mg content of ACC was determined to be ~7 and ~10 mol%, respectively, after 25 min of reaction time (**Fig. 4E, F**). Thus, the sufficient removal of the aqueous Mg ions due to rapid precipitation of volumetrically significant amounts of magnesian ACC (Mg-ACC) resulted in a lower aqueous $[Mg^{2+}]/[Ca^{2+}]$ ratio (≤ 4), compared to the experiments where ikaite was the predominant phase over ACC (**Fig. 6**). Lower $[Mg^{2+}]/[Ca^{2+}]$ ratios facilitated the observed formation of Mg-calcite rather than of aragonite. These findings highlight the importance of the prevailing physicochemical conditions of the reactive solutions, e.g. $[Mg^{2+}]/[Ca^{2+}]$ ratio, on controlling

ikaite or (Mg-)ACC to transform into distinct anhydrous $CaCO_3$ polymorphs, i.e. calcite or aragonite (**Fig. 6**).

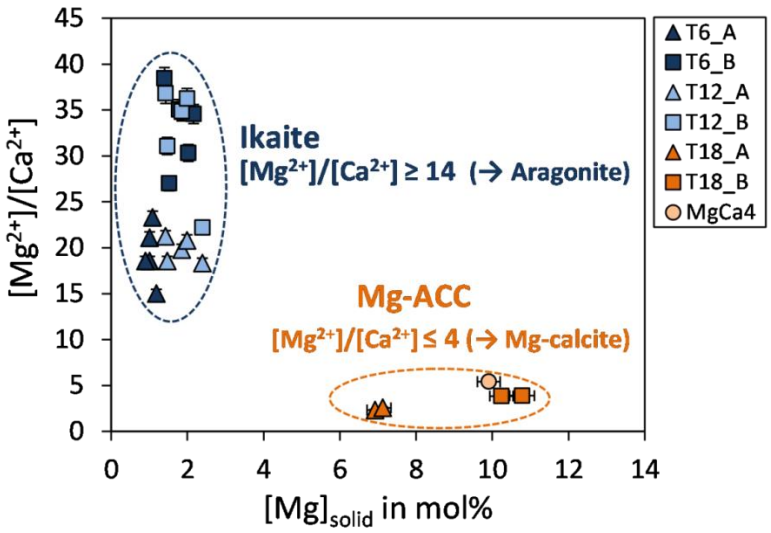

Fig. 6. Molar Mg^{2+} to Ca^{2+} ratio, $[Mg^{2+}]/[Ca^{2+}]$, of the reactive solution versus Mg content, $[Mg]_{solid}$, of ikaite in experiments conducted at 6 and 12°C and Mg bearing ACC (Mg-ACC) in experiments conducted at 18 and 25°C (MgCa4, Purgstaller et al., 2016).

6.4.3. Transformation of ikaite into calcite and vaterite under air exposure

Our experimental results documented different transformation products when ikaite was separated from the suspension and was exposed to air for 1 day at ~25°C (relative humidity of ~26%). Ikaite initially precipitated at 12°C transformed into calcite, whereas ikaite initially formed at 6°C transformed into mixtures of calcite and vaterite under the same air expose conditions (**Table 2**). These experimental results suggest that the temperature difference (ΔT) between the experimental conditions and the air exposure conditions is responsible for the formation of calcite versus calcite and vaterite through decomposition of transient ikaite. Sanchez-Pastor et al. (2016) reported that ikaite synthesized at 3°C transformed into pure calcite at 10°C (ΔT = 7°C), whereas ikaite synthesized at the same temperature transformed into calcite and vaterite at 20°C (ΔT = 17°C). These findings appear to be consistent with the results obtained in the present study, showing that ikaite transformed to pure calcite at a lower ΔT (13°C) and to admixtures of calcite and vaterite at a higher ΔT (19°C) (**Table 2**). Higher ΔT values could foster adsorption of atmospheric H_2O on the ikaite crystal surface (see also Sanchez-Pastor et al., 2016), which triggers the dissolution of ikaite at water-crystal interfaces and therefore accelerates the release of Ca^{2+} and CO_3^{2-} ions and structural water (6 moles of H_2O for each mole of $CaCO_3$). Consequently, the decomposition rate of ikaite is higher at higher ΔT values, resulting in fluids

supersaturated with respect to both calcite and vaterite. Accordingly, SEM images obtained from the reacted precipitates originally present as ikaite indicated the formation of euhedral calcite (and vaterite) crystals (**Fig. 3A-B**). In contrast, Sanchez-Pastor et al. (2016) showed that the texture and the particle shape of the large (~800 μm) ikaite crystal were preserved during its pseudomorphic transformation into anhydrous $CaCO_3$ minerals. These differences may be best explained by distinct surface properties of the reacting ikaite, i.e. high versus low surface area related to the nanocrystalline (this study) versus well-crystalline (Sanchez-Pastor et al., 2016) character of the individual ikaite crystals. Using the ACC transformation dynamics recently reported in Konrad et al. (2016) as an analogue for the decomposition mechanism of ikaite we argue that the availability of H_2O during the air exposure state and the related adsorption of H_2O onto the ikaite crystal surface play a decisive role in the formation of anhydrous $CaCO_3$ polymorphs. At the given relative humidity of ~26% it is suggested that a fast interface-coupled surface dissolution process of ikaite created particle surface solutions that were highly supersaturated with respect to crystalline $CaCO_3$ polymorphs (**Fig.3A, B, E**). In this respect, the formation of either calcite ± vaterite or aragonite strongly depends on the $[Mg^{2+}]/[Ca^{2+}]$ ratio created at reactive mineral-fluid interfaces. Thus, during air exposure the $[Mg^{2+}]/[Ca^{2+}]$ ratio at the reactive surface layer is most likely controlled by the Mg/Ca_{solid} ratio of the preexisting ikaite ($Mg/Ca \approx 0.02$, **Fig. 4E, F**). This low $[Mg^{2+}]/[Ca^{2+}]$ ratio promotes the formation of calcite/vaterite over aragonite in air at 25°C, whereas aragonite is the predominant phase at high $[Mg^{2+}]/[Ca^{2+}]$ ratios, as is seen by ikaite transformation in solution at 20°C (**Fig. 6**).

6.4.4. Implications to natural environments

Our experimental results revealed the formation of ikaite at temperatures up to 12°C (**Table 1**); a temperature that exceeds the actual limit of up to 9°C documented in former studies (e.g. Pauly 1963; Bischoff et al., 1993; Burchardt et al., 2001; Field et al., 2016). At 18°C, ikaite precipitation was not observed despite the fact that all reactive solutions were supersaturated with respect to this mineral (**Fig. 5B**). In the present study, fast precipitation of hydrous carbonate minerals, such as ACC and ikaite, was induced by titration technique using highly concentrated stock solutions. We argue that the formation of ikaite over ACC at temperatures below 12°C may be related to the limited time provided for Ca^{2+} ion dehydration at initial high supersaturation states (**Fig. 5B**). Accordingly, the upper temperature limit for ikaite formation is controlled by the

interplay of the (i) oversaturation of the solution with respect to ikaite and the (ii) temperature-dependent dehydration kinetics of the aqueous Ca^{2+} ions.

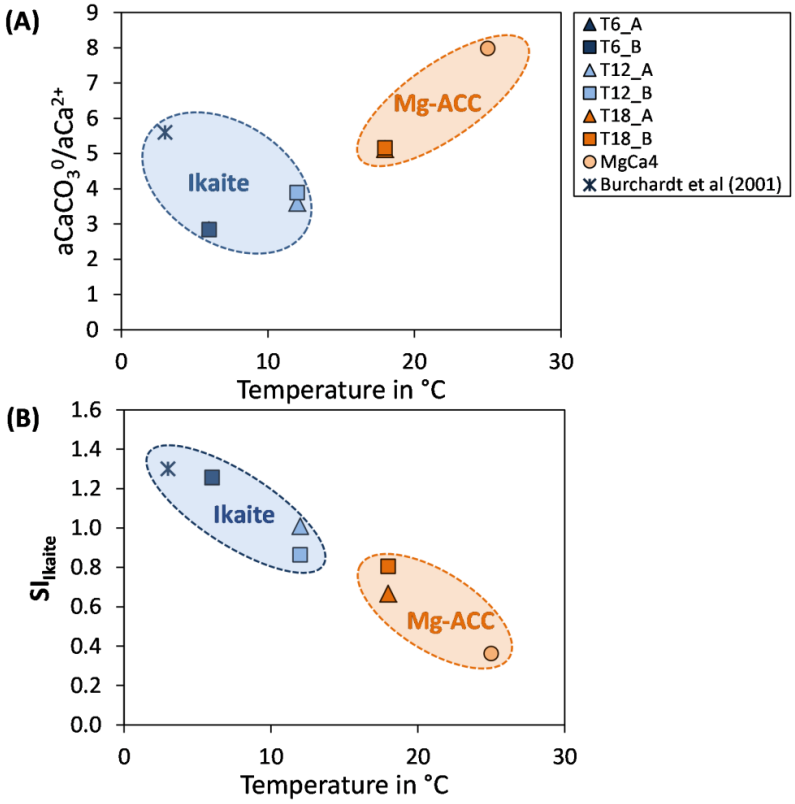

Fig. 7. Temperature of the solution versus **(A)** the ratio of $CaCO_3^0$ to Ca^{2+} activities ($aCaCO_3^0/aCa^{2+}$) in the reactive solution and **(B)** the saturation index of the reactive solution with respect to ikaite (SI_{Ikaite}) from experiments conducted at 6, 12 and 18°C (after 1 min of reaction time) and from experiment MgCa4 (25°C; Purgstaller et al., 2016) calculated by PhreeqC as well as from the mixed spring and column water (1:1 mixture) reported by Burchardt et al. (2001).

At the environmental conditions of the Ikka Fjord (< 6°C) ikaite precipitates by mixing of seawater with a molar Mg/Ca ratio of 5 and spring water with high alkalinity (Burchardt et al., 1997). Burchardt et al. (2001) argued that the inorganic formation of ikaite is facilitated by the direct incorporation of aqueous $CaCO_3^0$ complexes, which is the dominating aqueous Ca species in the highly alkaline (pH > 10) mixing water solutions (**Fig. 7A**). In contrast, our results showed that ikaite is preferentially formed in inorganic precipitation experiments at low activity ratios of aqueous $CaCO_3^0$ relative to the free Ca^{2+} ion complexes (**Fig. 7A**). As reported by Burchardt et al. (2001) the precipitation rate of ikaite in the column water-seawater mixture is high due its high supersaturation with respect to ikaite ($SI_{Ikaite} \approx 1.3$, **Fig. 7B**). At a first glance, this suggests that the abiotic formation of ikaite at the Ikka Fjord may be strongly controlled by high SI_{Ikaite}

values rather than by the high fraction of aqueous $CaCO_3^0$ complexes (**Fig. 7A-B**). More recently, however, Trampe et al. (2016) proofed the presence of endolithic biofilms and extrapolymeric substances secreted by microbial phototrophs in the Ikka Fjord sediments and argued that both the precipitation and the early cementing of the highly porous ikaite crystals may be attributed to microbial activity. For these reasons, it remains questionable if there is a direct microbial control on the formation and stability of ikaite in natural surroundings. Notwithstanding the above, our findings clearly indicate that the inorganic formation of ikaite is also possible at elevated temperatures up to at least 12°C, if adequately high SI_{Ikaite} values are achieved (**Fig. 7B**). This raises serious questions about the use of glendonites in the sedimentary environments as an indicator for near-freezing temperatures.

Over the years, numerous studies suggested that ikaite is a transient phase in the formation of calcite (Pauly et al., 1996; Bischoff et al., 1993; Omelon et al., 2001) and/or vaterite (Ito et al., 1996; 1999; Shaikh 1990), while less attention was given to its transformation into aragonite. To the best of our knowledge, only Stein and Smith (1986) and Council and Bennet (1993) indicated that ikaite found in authigenic carbonate nodules in the Nakai Through sediments (Japan) and during the winter months in the Mono Lake sediments (California, US), respectively, decomposed to mixtures of calcite and aragonite. However, in these studies the sampling and the storage conditions (e.g. temperature and presence of a fluid phase) are not well documented. Our findings revealed different anhydrous transformation products depending on the physicochemical conditions under which the ikaite is transformed: (i) ikaite separated from the reactive solution transformed into calcite/vaterite under air exposure (**Fig.3A, B, E**), whereas (ii) ikaite remained in reactive solutions characterized by a high aqueous molar Mg^{2+}/Ca^{2+} ratio (> 14 **Fig. 7A**) transformed into aragonite pseudomorphs (**Fig. 3C-F**). Thus, the physicochemical conditions under which natural ikaite transforms (e.g H_2O availability, $[Mg^{2+}]/[Ca^{2+}]$ ratio of the fluid) seem to be of high relevance in predefining the nature of the transformation products. For instance, aragonite is believed to be formed only at high aqueous molar Mg^{2+}/Ca^{2+} ratios, in contrast to calcite, vaterite and monohydrocalcite that precipitate at low aqueous molar $Mg^{2+/}Ca^{2+}$ ratios (< 4; Ito et al., 1996; 1999). Due to the fact that most natural occurrences of ikaite are ultimately linked to (peri-)marine environmental settings where the aqueous molar $Mg^{2+/}Ca^{2+}$ ratio is relatively low (~5), glendonites are frequently found in the marine sedimentary record (e.g. Shearman and Smith, 1985; Last et al., 2013), whereas aragonite pseudomorphs have not yet been documented. Anyhow, our results revealed the formation of porous aragonite pseudomorphs

in consequence of the decomposition of intermediate ikaite. Considering, that aragonite is a thermodynamically unstable phase under the various Earth`s surface conditions (Morse and Mackenzie, 1990; Bischoff et al., 1993), the temporary formation of aragonite in low temperature regimes at high aqueous molar Mg^{2+}/Ca^{2+} ratio could serve as an intermediate step during the transformation of ikaite into calcite.

6.5. SUMMARY AND CONCLUSIONS

The (trans-)formation of ikaite was investigated in the temperature range from 6 to 18°C under constant pH (8.3 ±0.1) and distinct aqueous molar Mg/Ca ratios (1/4 and 1/8). Summing up our experimental results led us to the following conclusions:

(1) Ikaite formation was only observed at $T \leq 12$°C due to the temperature-dependent kinetics of aqueous Ca^{2+} ion dehydration despite the fact that all reactive solutions were supersaturated with respect to this mineral phase at the onset of the experiments.

(2) Ikaite in contact with a reactive solution for 1 day at 20°C is transformed into aragonite pseudomorphs at aqueous molar Mg^{2+}/Ca^{2+} ratios ≥ 14 through a coupled dissolution-re-precipitation mechanism, which is driven by the high supersaturation of the fluid with respect to aragonite and excess Mg^{2+} ions inhibiting calcite and vaterite formation.

(3) Ikaite separated from the reactive solution ($T \leq 12$°C) and exposed to air (T = 25°C) is transformed either into pure calcite or into calcite-vaterite admixtures, mainly depending on the temperature difference (ΔT = 13 versus 19°C) between the synthesis conditions and the storage conditions. Physisorption of a critical level of H_2O onto the primary ikaite crystal surface induces a fast interface-coupled surface dissolution process and is thus controlling the nature of the anhydrous $CaCO_3$ products.

(4) The precipitation of ikaite in natural environments can be reasonably suggested to occur at temperatures up to 12°C or higher, if the mineralizing fluids are characterized by high supersaturation degrees with respect to ikaite and, accordingly, high precipitation rates are reached. Thus, the use of glendonite as a valuable indicator for near-freezing temperatures seems to be an equivocal proxy.

(5) The formation of anhydrous $CaCO_3$ polymorphs through transformation of intermediate ikaite is controlled mainly by the prevailing physicochemical conditions, such as aqueous molar Mg^{2+}/Ca^{2+} ratio and H_2O availability. Accordingly, the storage conditions of

samples originally containing ikaite have to be considered when studying the $CaCO_3$ polymorph content after ikaite decomposition.

6.6. SUPPLEMENTARY DATA

Table S1

Chemical composition of experimental solutions and solids from experiments T6_A and T6_B, time: reaction time during the experimental run; pH: pH of the reactive solution, $[Ca]_{aq}$, $[Mg]_{aq}$: Ca and Mg concentration of the reactive solution; Alkalinity: carbonate alkalinity concentration of the reactive solution; $[Mg]_{solid}$: Mg content of the solid.

Exp.	time min/d	T °C	pH	$[Ca]_{aq}$ x 10^{-3} M	$[Mg]_{aq}$ x 10^{-3} M	Alkalinity x 10^{-3} M	$[Mg]_{solid}$ mol%
	0 min	6.00	8.30	-	-	1055	-
	1 min	5.99	8.33	7.15	2.34	986	-
	5 min	5.96	8.30	5.87	9.10	719	1.5
	9 min	6.04	8.36	2.87	15.55	536	-
	13 min	5.95	8.34	1.26	21.45	404	1.1
	18 min	5.99	8.36	1.61	23.76	252	-
T6_A	25 min	5.97	8.31	2.08	30.04	126	1.2
	30 min	6.00	8.34	1.83	31.66	125	1.0
	40 min	6.00	8.35	1.76	31.28	125	-
	50 min	5.99	8.36	1.73	30.75	126	-
	60 min	6.00	8.37	1.75	31.57	129	0.9
	100 min	6.00	8.40	1.62	31.85	129	1.0
	180 min	5.99	8.47	1.41	30.72	125	1.1
	1 d	20.50	8.33	0.36	28.59	110	1.9
	0 min	6.00	8.31	-	-	1002	-
	1 min	5.95	8.34	7.12	4.33	966	-
	5 min	5.93	8.34	0.26	21.05	709	1.0
	9 min	5.99	8.31	1.62	29.47	554	-
	13 min	5.96	8.32	1.74	40.46	384	1.6
	18 min	5.95	8.33	1.56	44.43	263	-
T6_B	25 min	6.06	8.31	2.19	56.17	141	1.5
	30 min	5.99	8.31	1.94	55.75	144	2.0
	40 min	6.01	8.32	1.82	55.79	137	-
	50 min	5.99	8.33	1.82	56.04	139	-
	60 min	6.00	8.34	1.73	56.71	139	2.2
	100 min	6.01	8.37	1.61	53.38	140	1.8
	180 min	5.99	8.42	1.48	53.64	142	1.4
	1 d	20.30	8.38	0.25	54.79	115	1.6

Table S2
Chemical composition of experimental solutions and solids from experiments T12_A and T12_B, time: reaction time during the experimental run; pH: pH of the reactive solution, $[Ca]_{aq}$, $[Mg]_{aq}$: Ca and Mg concentration of the reactive solution; Alkalinity: carbonate alkalinity concentration of the reactive solution; $[Mg]_{solid}$: Mg content of the solid.

Exp.	time min/d	T °C	pH	$[Ca]_{aq}$ x 10^{-3} M	$[Mg]_{aq}$ x 10^{-3} M	Alkalinity x 10^{-3} M	$[Mg]_{solid}$ mol%
	0 min	12.00	8.30	-	-	1053	-
	1 min	11.98	8.30	6.17	2.51	974	-
	5 min	11.99	8.30	3.92	11.81	686	0.5
	9 min	11.95	8.33	1.60	16.69	494	-
	13 min	12.01	8.30	1.84	21.27	376	1.2
	18 min	12.00	8.30	1.97	22.95	244	-
T12_A	25 min	11.99	8.36	1.85	29.78	134	1.5
	30 min	12.00	8.37	1.75	30.15	118	1.4
	40 min	12.00	8.37	1.69	29.68	120	-
	50 min	11.99	8.38	1.70	30.51	119	-
	60 min	12.00	8.38	1.70	30.39	120	1.3
	100 min	12.00	8.40	1.71	32.54	123	1.1
	180 min	11.99	8.44	1.50	29.88	120	1.1
	1 d	20.10	8.30	0.24	27.21	100	2.5
	0 min	12.00	8.30	-	-	1020	-
	1 min	11.98	8.33	4.23	3.86	985	-
	5 min	11.95	8.36	1.77	20.43	711	1.3
	9 min	12.01	8.35	0.97	30.89	524	-
	13 min	11.98	8.37	1.60	39.30	415	1.8
	18 min	11.99	8.34	2.14	46.20	271	-
T12_B	25 min	12.02	8.33	2.80	56.01	155	2.4
	30 min	12.00	8.38	2.00	55.94	151	1.5
	40 min	12.00	8.39	2.04	55.71	151	-
	50 min	12.00	8.40	1.86	56.16	149	-
	60 min	11.99	8.40	1.83	56.40	149	1.9
	100 min	12.00	8.44	1.72	56.11	149	1.4
	180 min	12.00	8.49	1.68	54.77	154	2.0
	1 d	20.05	8.40	0.47	46.99	120	4.2

Table S3
Chemical composition of experimental solutions and solids from experiments T18_A and T18_B, time: reaction time during the experimental run; pH: pH of the reactive solution, $[Ca]_{aq}$, $[Mg]_{aq}$: Ca and Mg concentration of the reactive solution; Alkalinity: carbonate alkalinity concentration of the reactive solution; $[Mg]_{solid}$: Mg content of the solid.

Exp.	time	T	pH	$[Ca]_{aq}$	$[Mg]_{aq}$	Alkalinity	$[Mg]_{solid}$
	min/d	°C		x 10^{-3} M	x 10^{-3} M	x 10^{-3} M	mol%
	0 min	18.00	8.30	-	-	1092	-
	1 min	17.97	8.33	3.94	2.33	998	-
	5 min	18.02	8.31	3.49	8.41	738	3.4
	9 min	17.97	8.29	4.86	12.34	542	-
	13 min	17.99	8.30	4.30	13.95	409	5.4
	18 min	17.99	8.30	5.04	15.06	256	-
T18_A	25 min	18.01	8.30	8.44	16.78	140	6.9
	30 min	18.00	8.31	7.64	16.92	129	7.1
	40 min	18.00	8.30	1.37	11.40	121	8.9
	50 min	17.99	8.30	0.79	10.71	122	8.8
	60 min	17.99	8.32	0.65	10.30	119	8.8
	100 min	18.00	8.32	0.50	10.03	117	9.1
	180 min	18.00	8.35	0.44	9.60	121	9.3
	1 d	20.70	8.38	0.31	8.52	114	10.0
	0 min	18.00	8.30	-	-	1080	-
	1 min	17.98	8.34	5.33	3.64	984	-
	5 min	18.01	8.36	4.91	15.52	696	4.9
	9 min	17.99	8.32	4.29	19.17	513	-
	13 min	17.97	8.31	5.12	25.39	387	6.9
	18 min	18.00	8.30	6.44	28.50	240	-
T18_B	25 min	17.98	8.33	9.54	31.80	127	10.2
	30 min	18.00	8.32	9.30	31.00	115	10.8
	40 min	18.01	8.32	7.78	32.61	112	-
	50 min	18.01	8.32	1.66	23.48	99	-
	60 min	18.00	8.34	0.76	23.07	94	12.1
	100 min	18.01	8.34	0.40	19.54	90	13.9
	180 min	17.99	8.31	0.33	18.51	90	14.6
	1 d	20.30	8.21	0.22	14.18	82	17.5

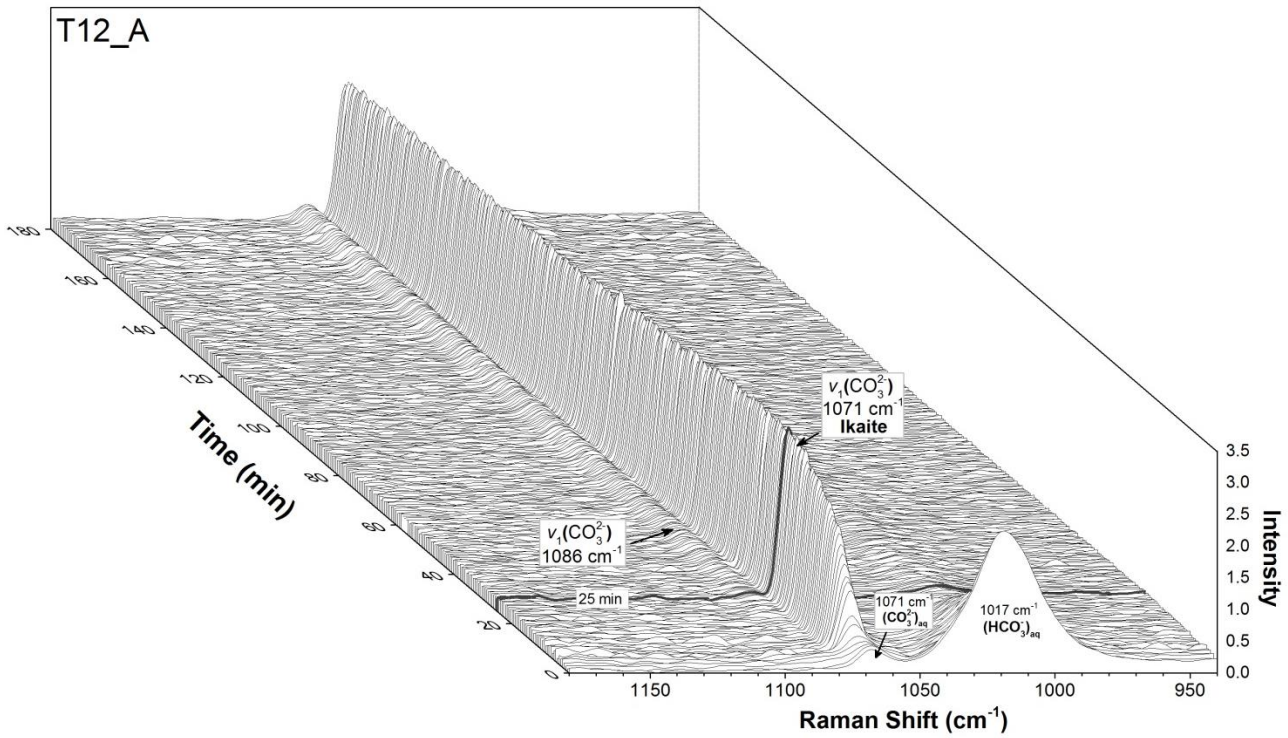

Fig. S1. Waterfall plot of *in situ* Raman spectra showing the vibration band of aqueous HCO_3^- and CO_3^{2-} as well as of the ν_1 band of CO_3^{2-} related to ikaite and calcite and/or aragonite in experiment T12_A.

7. CONCLUDING REMARKS

The experimental results obtained during this work documented that the presence of an amorphous precursor phase plays a significant role in the formation of high Mg-calcite. Considering an ACC transformation step, the Mg content of ACC is as low as about 10 mol%, but the uptake of Mg ions into the precipitate throughout and subsequent to Mg-ACC transformation, resulted in calcite with up to about 20 mol% Mg. The incorporation of Mg into the calcite lattice seems to be favored by the intensive supply of carbonate ions and high Mg/Ca ratios present in the aqueous solution. Moreover, the obtained results revealed that the Mg isotopic composition of Mg-calcite formed via an amorphous precursor does not reflect the fluid isotopic composition at the time of Mg-ACC precipitation. The fractionation of Mg isotopes between Mg-ACC and the reactive solution is significantly smaller compared to that of Mg-calcite that crystallizes directly from the solution. However, the Mg isotopic signature of Mg-ACC is not preserved during its transformation into the crystalline phase. Based on the evolution of the chemical and isotopic composition of the solid and fluid, it is suggested that the transformation of Mg-ACC to Mg-calcite takes place via a dissolution and re-precipitation mechanism. In this context, the experiments indicate that once a solution is close to saturation with respect to ACC, the formation of the less soluble crystalline phase (Mg-calcite, monohydrocalcite, ikaite, etc.) induces the dissolution/transformation of the amorphous precursor. The time period of Mg-ACC metastability in aqueous solution is significantly extended at higher aqueous Mg/Ca ratios due to the inhibition of Mg-calcite formation and the slow precipitation kinetics of monohydrocalcite. In contrast, at lower temperatures ($\leq$ 12°C) the presence of Mg-ACC in aqueous solution is significantly reduced (few minutes) due to slow water exchange of the aqueous Ca^{2+} ion at lower temperatures and the instant formation of ikaite. Overall, the experimental results highlight that the formation of certain carbonate minerals such as (Mg-)calcite and aragonite via intermediate phases (e.g. Mg-ACC and ikaite) is significantly affected by the physicochemical conditions of the transformation environment (e.g. prevailing aqueous Mg/Ca ratio, etc.). The outcome of this thesis contributes to better understanding of the mechanisms involved during the formation of (magnesium) calcium carbonate minerals via carbonate precursor phases in natural environments and have important implications for the interpretation of elemental and isotopic proxy data from carbonate archives.

REFERENCES

Addadi L., Raz S. And Weiner S. (2003) Taking advantage of disorder: Amorphous calcium carbonate and its roles in biomineralization. Adv. Mater. 15, 959-970.

Aizenberg J., Lambert G., Addadi L. and Weiner S. (1996) Stabilization of Amorphous Calcium Carbonate by Specialized Macromolecules in Biological and Synthetic Precipitates. Adv. Mater. 8, 222-226.

Aizenberg J., Lambert G., Weiner S. and Addadi L. (2002) Factors Involved in the Formation of Amorphous and Crystalline Calcium Carbonate: A Study of an Ascidian Skeleton. J. Am. Chem. Soc. 124, 32-39.

Aizenberg J., Weiner S. and Addadi L. (2003) Coexistence of amorphous and crystalline calcium carbonate in skeletal tissues. Connect. Tissue Res. 44, 20-25.

Astilleros J. M., Fernández-Díaz L. and Putnis A. (2010) The role of magnesium in the growth of calcite: An AFM study. Chemical Geology 271, 52-58

Beck J. W., Edwards R. L., Ito E., Taylor F. W., Recy J., Rougerie F., Joannot P. and Henin C. (1992) Sea-surface temperature from coral skeletal strontium/calcium ratios. Science 257, 644-647

Beinlich A., Mavromatis V., Austrheim H. and Oelkers E.H. (2014) Inter-mineral Mg isotope fractionation during hydrothermal ultramafic rock alteration – Implications for the global Mg-cycle. Earth Planet. Sci. Lett. 392, 166-176.

Beniash E., Aizenberg J., Addadi L. and Weiner S. (1997) Amorphous calcium carbonate transforms into calcite during sea urchin larval spicule growth. Proc. R. Soc. Lond. B 264, 461-465.

Bentov S., and Erez J. (2005) Impact of biomineralisation processes on the Mg content of foraminiferal shells: A biological perspective. Geochem. Geophys. Geosyst. 7, 1-11.

Benzerara K., Menguy N., Lopez-Garcıa P., Yoon T.-H., Kazmierczak J., Tyliszczak T., Guyot F., Brown Jr. G.E. (2006) Nanoscale detection of organic signatures in carbonate microbialites. PNAS 103, 9440–9445.

Berner R. A. (1975) The role of magnesium in the crystal growth of calcite and aragonite from sea water. Geochim. Cosmochm. Acta 39, 489-504

Bischoff W. D., Sharma S. K., MacKenzie F. T. (1985) Carbonate ion disorder in synthetic and biogenic magnesian calcites: a Raman spectral study. American Mineralogist, 70, 581-589.

Bischoff W. D., Mackenzie F. T. and Bishop F. C. (1987) Stabilities of synthetic magnesian calcites in aqueous solution; comparison with biogenic materials. Geochim. Cosmochim. Acta 51, 1413-1423.

Bischoff J. L., Fitzpatrick J.A. and Rosenbauer R. J. (1993) The solubility and stabilization of ikaite ($CaCO_3 \cdot 6H_2O$) from 0° to 25°C: Environmental and Paleoclimatic Implications for Thinolite Tufa. J. Geol. 101:21–33

Bischoff W. D. (1998) Dissolution enthalpies of magnesian calcites. Aquat. Geochem. 4, 321-336.

Boch R., Dietzel M., Reichl P., Leis A., Baldermann A., Mittermayr F., Pölt Peter (2015) Rapid ikaite ($CaCO_3$ $6H_2O$) crystallization in a man-made river bed: Hydrogeochemical monitoring of a rarely documented mineral formation. Applied Geochemistry 63, 366-379

Böttcher M. E., Gehlken P.-L. and Steele D. F. (1997) Characterization of inorganic and biogenic magnesian calcites by Fourier Transform infrared spectroscopy. Solid State Ionics 101-103, 1379-1385.

Böttcher M. and Dietzel M. (2010) Metal-ion partitioning during low-temperature precipitation and dissolution of anhydrous carbonates and sulfates. In Ion Partitioning in Low Temperature Aqueous Systems (Eds.: M. Prieto and H. Stoll). EMU Notes in Mineralogy 10, 139-187

Bontognali T. R. R., Vasconcelos C., Warthmann R. J., Bernasconi S. M., Dupraz C., Strohmenger C. J., McKenzie J. A. (2010). Dolomite formation within microbial mats in the coastal sabkha of Abu Dhabi (United Arab Emirates). Sedimentology 57, 824-844.

Bots P., Benning L. G., Rodriguze-Blanco J. D., Roncal-Herrero T. and Shaw, S. (2012) Mechanistic insights into the crystallization of amorphous calcium carbonate. Crys. Growth Des. 12, 3806-3814

Brečević L. and Nielsen A. E. (1989) Solubility of amorphous calcium carbonate. Journal of Crystal Growth 98, 504-510.

Brown, B.E. (1982). The form and function of metal-containing granules in invertebrate tissues. Biol. Rev. Cambridge Philosophic. Soc. 57, 621-667.

Buchardt B., Seaman P., Stockmann G., Vous M., Wilken U., Duwel L., Kristiansen A., Jenner C., Whiticar M. J., Kristensen R. M., Petersen G. H. and Thorbjørn L. (1997) Submarine Columns of Ikaite Tufa. Nature 390, 129–130

Buchardt B., Israelson C., Seaman P. and Stockmann G. (2001) Ikaite Tufa Towers in Ikka Fjord, Southwest Greenland: Their formation by mixing of seawater and alkaline spring water. Journal of Sedimentary Research 71, 176-189.

Burton W. K., Cabrera N. and Frank F. C. (1951) The growth of crystals and the equilibrium structure of their surfaces. Philos. Trans. R. Soc. A 243, 299–358.

Burton E. A. and Walter L.M. (1990) The role of pH in phosphate inhibition of calcite and aragonite precipitation rates in seawater. Geochim. Cosmochim. Acta 54 (3), 797–808.

Busenberg E. and Plummer L. N. (1989) Thermodynamics of magnesian calcite solid-solutions at 25°C and 1 atm total pressure. Geochim. Cosmochim. Acta 53, 1189-1208.

Cartwright J.H.E., Checa A.G., Gale D., Gebauer D. and Sainz-Diaz C.I. (2012) Calcium Carbonate Polyamorphism and its role in biomineralization: How many amorphous calcium carbonates are there? Angewandte Chemie - International Edition 51, 11960-11970.

Chaka A. M. and Felmy A. R. (2014) Ab Initio Thermodynamic Model for Magnesium Carbonates and Hydrates. J. Phys. Chem. A 118, 7469−7488

Chave K. E. (1954) Aspects of the biogeochemistry of magnesium 1. Calcareous marine organisms. J. Geol. 62, 266-283.

Chernov A. A. (1984) Modern Crystallography III: Crystal growth. Springer-Verlag, Berlin.

Coleyshaw E. E., Crump G. and Griffith, W. P. (2003) Vibrational spectra of the hydrated carbonate minerals ikaite, monohydrocalcite, landsfordite and nesquehonite. Spectrochimica Acta Part A 59, 2231-2239

Council TC, Bennett PC (1993) Geochemistry of ikaite formation at Mono Lake, California: implications for the origin of tufa mounds. Geology 21:971–974

Couradeau E.; Benzerara K.; Gérard E.; Moreira D.; Bernard S.; Brown G.E. Jr.; López-García P. (2012) Science 336, 459-462

Criss R. E. (1999) Principles of Stable Isotope Distribution. Oxford University Press, Oxford.

Dahl K. and Buchardt B. (2006) Monohydrocalcite in the arctic Ikka Fjord, SW Greenland: first reported marine occurrence. J. Sediment. Res. 76, 460–471.

Dana E. S. (1884) A crystallographic study of the thinolite of Lake Lahontan. U.S. Geological Survey Bulletin. Washington, D.C.: U.S. Government Printing Office (12), 429–450

De Choudens-Sanchez V. and Gonzalez L. A. (2009) Calcite and aragonite precipitation under controlled instantaneous supersaturation: elucidating the role of CaCO3 saturation state and Mg/Ca ratio on calcium carbonate polymorphism. J. Sediment. Res. 79, 363-376

De Lurio J. L. and Frakes L. A. (1999) Glendonites as a paleoenvironmental tool: implications for early Cretaceous high latitude climates in Australia. Geochim. Cosmochim. Acta 63, 1034–1048.

Demény A.; Czuppon G.; Kern Z.; Leél-Ossy S.; Németh A.; Szabó M.; Tóth M.; Wu C-.C.; Shen C.-C.; Molnár M.; Németh T.; Németh P.; Óvári M. (2016) Quaternary International, 415, 25-32

Dickens B. and Brown W. (1970) The crystal structure of calcium carbonate hexahydrate at ~-120°. Inorganic Chemistry 9, 480-486

Dieckmann G. S., Nehrke G., Papadimitriou S., Göttlicher J., Steininger R., Kennedy H., Wolf-Gladrow D. and Thomas D. N. (2008) Calcium carbonate as ikaite crystals in Antarctic sea ice, Geophys. Res. Lett., 35, L08501, doi:10.1029/2008GL033540,

Dieckmann G. S., Nehrke G., Uhlig C., Göttlicher J., Gerland S., Granskog M. A. and Thomas D. N. (2010) Brief communication: Ikaite ($CaCO_3$ $6H_2O$) discovered in Artic sea ice. Cryosphere 4, 227–230.

Di Tommaso D., Ruiz-Agudo E.,de Leeuw N. H., Putnis A. and Putnis C. V. (2014) Modelling the effects of salt solutions on the hydration of calcium ions. Phys. Chem. Chem. Phys. 16, 7772-7785

Dietzel M. and Usdowski E. (1996) Coprecipitation of Ni^{2+}, Co^{2+}, and Mn^{2+} with galena and covellite, and of Sr^{2+} with calcite during crystallization via diffusion of H_2S and CO_2 through polyethylene at 20°C: Power law and Nernst law control of trace element partitioning. Chemical Geology 131, 55-65.

Dietzel M., Gussone N. and Eisenhauer A. (2004) Co-precipitation of Sr^{2+} and Ba^{2+} with aragonite by membrane diffusion of CO_2 between 10 and 50°C. Chem. Geol. 203, 139-151.

Dietzel M., Tang J.W., Leis A. and Kohler S.J. (2009) Oxygen isotopic fractionation during inorganic calcite precipitation - Effects of temperature, precipitation rate and pH. Chem. Geol. 268, 107-115.

Dietzel M. (2011) Carbonates. In Encyclopedia of Geobiology (eds. J. Reitner and V. Thiel). Springer, Berlin, 261-266

Dupont L., Portemer F. and Figlarz M. (1997) Synthesis and study of a well crystallized $CaCO_3$ vaterite showing a new habitus. J. Mater. Chem 7, 797-800.

Dupraz C., Reid R.P., Braissant O., Decho A.W., Norman R.S., Visscher P.T. (2009) Processes of carbonate precipitation in modern microbial mats. Earth Sci. Rev., 96, 141-162

Elderfield H. and Ganssen G. (2000) Past temperature and $\delta^{18}O$ of surface ocean waters inferred from foraminiferal Mg/Ca ratios. Nature 405, 442-445.

Edwards H. G. M., Villar S. E. J., Jehlicka J. and Munshi T. (2005). FT–Raman spectroscopic study of calcium-rich and magnesium-rich carbonate minerals. Spectrochimica Acta Part A 6, 2273-2280.

Falini G., Gazzano M. and Ripamonti A. (1994) Crystallization of calcium carbonate in presence of magnesium and polyelectrolytes. Journal of Crystal Growth 137, 577-584

Falini G., Fermani G., Gazzano M. and Ripamonti A. (1998) Structure and morphology of synthetic magnesium calcite. J. Mater. Chem. 8, 1061-1065

Fantle and DePaolo (2006) Sr isotopes and pore fluid chemistry in carbonate sediment of the Ontong Java Plateau: Calcite recrystallization rates and evidence for a rapid rise in seawater Mg over the last 10 million years. Geochimica et Cosmochimica Acta 70, Issue 15, p. 3883-3904.

Farkasˇ J., Buhl D., Blenkinsop J. and Veizer J. (2007) Evolution of the oceanic calcium cycle during the late Mesozoic: evidence from $d^{44}/^{40}Ca$ of marine skeletal carbonates. Earth Planet. Sci. Lett. 253, 96–111.

Fernández-Díaz L., Putnis A., Prieto M. and Putnis C. V. (1996) The role of magnesium in the crystallization of calcite and aragonite in a porous medium. Journal of Sedimentary Research 66, 482–491.

Field L. P., Milodowski A. E., Shaw R. P., Stevens, L. A., Hall M. R., Kilpatrick A., Gunn J., Kemp S. J., Ellis M.A. (2016) Unusual morphologies and the occurrence of pseudomorphs after ikaite ($CaCO_3$•$6H_2O$) in fast growing, hyperalkaline speleothem. Mineralogical Magazine. doi.org/10.1180/minmag.2016.080.111

Fischer M., Thomas D. N., Krell A., Nehrke G., Göttlicher J., Norman L., Meiners K. M., Riaux-Gobin C. and Dieckmann G. S. (2013) Quantification of ikaite in Antarctic sea ice. Antarct. Sci. 25, 421–432.

Flügel E. (2010) Microfacies of Carbonate Rock — Analysis, Interpretation and Application, 2nd ed. Springer-Verlag, Heidelberg.

Foster G. L., Lear C. H. and Rae J. W. B. (2012) The evolution of pCO_2, ice volume and climate during the middle Miocene. Earth Planet. Sci. Lett. 341, 243–254.

Fyfe W. S and Bischoff J. L. (1965) The calcite-aragonite problem. In Dolomitization and Limestone Diagenesis: A Symposium SEPM Spec. Pub. 13 (Pray LC, Murray RC (eds.) 13: 3-13.

Gabrielli C., Jaouhari R., Joiret S. and Maurin G. (2000). In situ Raman spectroscopy applied to electrochemical scaling. Determination of the structure of vaterite. J. Raman Spectrosc. 31, 497-501

Gal A., Habraken W., Dvir, G., Fratzl P., Weiner S., Addadi L. (2012) Calcite Crystal Growth by a Solid-State Transformation of Stabilized Amorphous Calcium Carbonate Nanospheres in a Hydrogel. Angewandte Chemie International Edition 52, 4867-4870

Gauldie R. W., Sharma S. K. and Volk, E. (1997) Micro-Raman Spectral Study of Vaterite and Aragonite Otoliths of the Coho Salmon, Oncorhynchus kisutch. Camp, Biochem. Physiol. 118A, 753-757.

Gayathri S., Lakshminarayanan R., Morse D. E., Kini R. M., Valiyaveettil S. (2007) In vitro study of magnesium-calcite biomineralization in the skeletal materials of the seastar Pisaster giganteus. Chem. Eur. J. 13, 3262-3268

Gebauer D., Völkel A. and Cölfen H. (2008) Stable Prenucleation Calcium Carbonate Clusters. Science 322, 1819-1822

Gebauer D., Gunawidjaja P. N., Ko J. Y. P., Bacsik Z., Aziz B., Liu L. J., Hu Y. F., Bergström L., Tai C. W., Sham T. K., Edén M. and Hedin N. (2010) Proto-Calcite and Proto-Vaterite in Amorphous Calcium Carbonates. Angewandte Chemie 122, 9073-9075

Geisler T., Perdikouri C., Kasioptas A. and Dietzel M. (2012) Real-time monitoring of the overall exchange of oxygen isotopes between aqueous CO_3^{2-} and H_2O by Raman spectroscopy. Geochim. Cosmochim. Acta 90, 1-11.

Geske A., Goldstein R. H., Mavromatis V., Richter D. K., Buhl D., Kluge T., John C. M. Immenhauser, A. (2015) The magnesium isotope ($\delta^{26}Mg$) signature of dolomites. Geochim. Cosmochim. Acta 149, 131-151.

Giuffre A. J., Gagnon A. C., De Yoreo J. J. and Dove P. M. (2015) Isotopic tracer evidence for the amorphous calcium carbonate to calcite transformation by dissolution–reprecipitation. Geochim. Cosmochim. Acta 165, 407-417

Goldsmith J., R., Graf D., L., Heard H., C. (1961) Lattice constants of the calcium magnesium carbonates. The American Mineralogist 46, 453-459.

Gong Y. U. T., Killian C. E., Olson I. C., Appathurai N. P., Amasino A. L., Martin M. C., Holt L. J., Wilt F. H. and Gilbert P. U. P. A. (2012) Phase transitions in biogenic amorphous calcium carbonate. Proc. Natl. Acad. Sci. USA 109, 6088–6093.

Goodwin A.L., Michel F.M., Phillips B.L., Keen D.A., Dove M.T. and Reeder R.J. (2010) Nanoporous structure and medium-range order in synthetic amorphous calcium carbonate. Chem. Mater 22, 3197-3205

Gussone N.; Eisenhauer A., Tiedemann R., Haug G. H., Heuser A., Bock B., Nägler T. F. and Müller A. (2004) Reconstruction of Caribbean Sea surface temperature and salinity fluctuations in response to the Pliocene closure of the Central American Gateway and radiative forcing, using $\delta^{44/40}$Ca, δ^{18}O and Mg/Ca ratios. Earth and Planetary Science Letters 227, 201-214

Griesshaber E., Kelm K., Sehrbrock A., Mader W., Mutterlose J., Brand U. and Schmahl W. W. (2009) Amorphous calcium carbonate in the shell material of the brachiopod Megerlia truncata. European Journal of Mineralogy, 21, 715-723.

Han S. Y., Hadiko G., Fuji M. and Takahashi M. (2006) Crystallization and transformation of vaterite at controlled pH. Journal of Crystal Growth 289, 269-274

Han N., Blue, C. R., De Yoreo, J. J. and Dove, P. M. (2013) The effect of carboxylates on the Mg content of calcites that transform from ACC. Procedia Earth and Planetary Science 7, 223-227

Helgeson H.C. (1969) Thermodynamics of hydrothermal systems at elevated temperatures and pressures. Amer. J. Sci. 267, 729–804.

Hensen C., Wallmann K., Schmidt M., Ranero C. R. and Suess E. (2004) Fluid expulsion related to mud extrusion off Costa Rica; a window to the subducting slab. Geology 32, 201-204.

Higgins J.A. and Schrag D.P. (2010) Constraining magnesium cycling in marine sediments using magnesium isotopes. Geochim. Cosmochim. Acta 74, 5039-5053.

Hippler D.; Eisenhauer A. and Nägler T. F. (2006) Tropical Atlantic SST history inferred from Ca isotope thermometry over the last 140ka. Geochimica et Cosmochimica Acta 70, 90-100

Hippler D., Buhl D., Witbaard R., Richter D. K. and Immenhauser A. (2009) Towards a better understanding of magnesium-isotope ratios from marine skeletal carbonates. Geochim. Cosmochim. Acta 73, 6134-6146.

Hofmann A. E., Bourg I. C. and DePaolo D. J. (2012) Ion desolvation as a mechanism for kinetic isotope fractionation in aqueous systems. PNAS 109, 18689–18694

Hu Y.-B., Wolf-Gladrow D. A., Dieckmann G. S., Völker C. and Nehrke G. (2014) A laboratory study of ikaite ($CaCO_3 \cdot 6H_2O$) precipitation as a function of pH, salinity, temperature and phosphate concentration. Marine Chemistry 162, 10-18

Ihli J., Wong W. C., Noel E. H., Kim Y.-Y., Kulak A. N., Christenson H. K., Duer M. J., Meldrum F. C. (2014) Dehydration and crystallization of amorphous calcium carbonate in solution and in air. Nat. Comm. 5, 3169

Immenhauser A., Buhl D., Richter D., Niedermayr A., Riechelmann D., Dietzel M. and Schulte U., (2010) Magnesium-isotope fractionation during low-Mg calcite precipitation in a limestone cave - Field study and experiments. Geochim. Cosmochim. Acta 74, 4346-4364.

Immenhauser A., Schoene B., Hoffmann R. and Niedermayr A. (2016) Mollusc and brachiopod skeletal hard parts: intricate archives of their marine environment. Sedimentology, 63, 1-59.

Ito T. (1993) The occurrence of monohydrocalcite from calcareous sinter of cold spring of Shiowakka, Asyoro. J. Mineral. Petrol. Econ. Geol. 88, 485–491.

Ito T. Matsubara S. and Miyawaki R. (1999) Vaterite after ikaite in carbonate sediment. J. Min. Petr. Econ. Geol. 94, 176-182

Jacob D.E., Soldati A.L., Wirth R., Huth J., Wehrmeister U. and Hofmeister W. (2008) Nanostructure, composition and mechanisms of bivalve shell growth. Geochimica et Cosmochimica Acta, 72.

Jacob D. E., Wirth R., Soldati A. L., Wehrmeister U. and Schreiber A. (2011) Amorphous calcium carbonate in the shells of adult Unionoida. J. Struct. Biol. 173, 241–249.

Jansen J.H.F., Woensdregt C.F., Kooistra M.J. and van der Gaast S.J. (1987) Ikaite pseudomorphs in the Zaire deep-sea fan: an intermediate between calcite and porous calcite. Geology 15, 245-248.

Jones, B. and Peng, X. (2012) Amorphous calcium carbonate associated with biofilms in hot spring deposits. Sedimentary Geology 269-270, 58-68

Kapschulte A. and Strauss H. (2004) The sulfur isotopic evolution of Phanerozoic seawater based on the analysis of structurally substituted sulfate in carbonates. Chemical Geology 204, 255-286

Khairoun I., Magne D., Gauthier O., Bouler J. M., Aguado E., Daculsi G., Weiss P. J. (2002) In vitro characterization and in vivo properties of a carbonated apatite bone cement. Biomed. Mat. Res. 2002, 60, 633-642

Kitano Y. and Hood D. W. (1965) The influence of organic material on the polymorphic crystallization of calcium carbonate. Geochim. Cosmochim. Acta 29:29-41.

Konrad F., Gallien F., Gerard D. E. and Dietzel M. (2016) Transformation of Amorphous Calcium Carbonate in Air. Crystal Growth & Design, 16, 6310-6317

Kontoyannis C. G. and Vagenas V. (2000) Calcium carbonate phase analysis using XRD and FT-Raman spectroscopy. Analyst 125, 251-255

Kralj D. and Brecevic L. (1995) Dissolution kinetics and solubility of calcium carbonate monohydrate. Colloids and Surfaces A: Physicochemical and Engineering Aspects 96, 287-293

Krukenberg C. F. W. (1982) "Die Pigmente: ihre Eigenschaften, ihre Genese und ihre Metamorphosen bei wirbellosen Tieren." Vergleichende physiologische Studien. Heidelberg Reihe 2, 92-93.

Lakshtanov L. Z. and Stipp S. L. S. (2007) Experimental study of Nickel (II) Interaction with Calcite: Adsorption and Coprecipitation. Geochim. Cosmochim. Acta 71, 3686-3697

Lam R. S. K., Charnock J. M., Lennie A. and Meldrum F. C. (2007) Synthesis-dependant structural variations in amorphous calcium carbonate. CrystEngComm, 9, 1226-1236

Larsen D. (1994) Origin and paleoenvironmental significance of calcite pseudomorphs after ikaite in the Oligocene Creede

Last F. M., Last W. M., Fayek M. and Halden N. M. (2013) Occurrence and significance of a cold-water carbonate pseudomorph in microbialites from a saline lake. J. Paleolimnol. 50, 505–517.

Lea D. W. and Boyle E. A. (1989). Barium content of benthic foraminifera controlled by bottom water composition. Nature 338,751-753.

Lee Y. J., Reeder R. J., 2006. The role of citrate and phthalate during Co(II) coprecipitation with calcite. Geochim. Cosmochim. Acta 70, 2253-2263.

Li W., Beard B.L., Li C. and Johnson C. M. (2014) Magnesium isotope fractionation between brucite $Mg(OH)_2$ and Mg aqueous species: Implications for silicate weathering and biogeochemical processes. Earth Planet. Sci. Lett. 394, 82-93.

Li W., Beard B. L., Li C., Xu H. and Johnson C. M. (2015) Experimental calibration of Mg isotope fractionation between dolomite and aqueous solution and its geological implications. Geochim. Cosmochim. Acta 157, 164-181.

Li W., Chakraborty S., Beard B. L., Romanek C. S., Johnson, C. M. (2012). Magnesium isotope fractionation during precipitation of inorganic calcite under laboratory conditions. Earth Planet. Sci. Lett. 333-334, 304-316.

Lin Y. P. and Singer P. C. (2005) Effects of seed material and solution composition on calcite precipitation. Geochim. Cosmochim. Acta 69, 4495-4504.

Lin C. J., Yang S. Y., Huang S. J. and Chan, J. C. C. (2015) Structural Characterization of Mg-Stabilized Amorphous Calcium Carbonate by Mg^{25} Solid-State NMR Spectroscopy. J. Phys. Chem. C 119, 7225-7233.

Lippmann F. (1973) Sedimentary carbonate minerals. Springer, Berlin.

Long X., Ma Y. and Qi L. (2011) In Vitro Synthesis of High Mg Calcite under Ambient Conditions and Its Implication for Biomineralization Process. Cryst. Growth Des. 11, 2866-2873.

Lorens R.B. (1981) Sr, Cd, Mn and Co distribution coefficients in calcite as a function of calcite precipitation rate. Geochim. Cosmochim. Acta 45, 553-561.

Loste E., Wilson R. M., Seshadri R. and Meldrum F. C. (2003) The role of magnesium in stabilising amorphous calcium carbonate and controlling calcite morphologies. Journal of Crystal Growth 254, 206-218.

Lowenstam H. A. (1981) Minerals formed by organisms. Science 211, 1126-1131.

Lu Z., Rickaby R. E. M., Kennedy H., Kennedy P., Pancost R. D., Shaw S., Lennie A., Wellner J. and Anderson J. B. (2012) An ikaite record of late Holocene climate at the Antarctic Peninsula. Earth and Planetary Science Letters 325-326, 108-115.

Ma Y., Aichmayer B., Paris O., Fratzl P., Meibom A., Metzler R. A., Politi Y., Addadi L., Gilbert P. U. P. A., Weiner S. (2009) The grinding tip of the sea urchin tooth exhibits exquisite control over calcite crystal orientation and Mg distribution. PNAS 106, 6048-6053.

Mackenzie F. T., Bischoff W. B., Bishop F. C., Loijens M., Schoonmaker J. and Wollast R. (1983) Magnesian calcites: low-temperature occurrence, solubility and solid-solution behavior. In Carbonates, Mineralogy and Chemistry (eds. R. J. Reeder). BookCrafters, Chelsea, Mich., 97-144.

Matsunuma S., Kagi H., Komatsu K., Maruyama K. and Yoshino T. (2014) Doping incompatible elements into calcite through amorphous calcium carbonate. Crystal Growth and Design 14, 5344-5348.

Mavromatis V., Pearce C. R., Shirokova L. S., Bundeleva I. A., Pokrovsky O. S., Benezeth P. and Oelkers E. H. (2012a) Magnesium isotope fractionation during hydrous magnesium carbonate precipitation with and without cyanobacteria. Geochim. Cosmochim. Acta 76, 161-174.

Mavromatis V., Schmidt M., Botz R., Comas-Bru L. and Oelkers E.H. (2012b) Experimental quantification of the effect of Mg on calcite-aqueous fluid oxygen isotope fractionation. Chem. Geol. 310-311, 97-105.

Mavromatis V., Gautier Q., Bosc O. and Schott J. (2013) Kinetics of Mg partition and Mg stable isotope fractionation during its incorporation in calcite. Geochim. Cosmochim. Acta 114, 188-203.

Mavromatis V., Prokushkin A. S., Pokrovsky O. S., Viers J. and Korets M. A. (2014a). Magnesium isotopes in permafrost-dominated Central Siberian larch forest watersheds. Geochim. Cosmochim. Acta 147, 76-89.

Mavromatis V., Botz R., Schmidt M., Liebetrau V. and Hensen C. (2014b) Formation of carbonate concretions in surface sediments of two mud mounds, offshore Costa Rica: a stable isotope study. International Journal of Earth Sciences 103, 1831-1844

Mavromatis V., Montouillout V., Noireaux J., Gaillardet J. and Schott J. (2015). Characterization of boron incorporation and speciation in calcite and aragonite from co-precipitation experiments under controlled pH, temperature and precipitation rate. Geochim. Cosmochim. Acta 150, 299-313.

Mavromatis V., Rinder T., Prokushkin A. S., Pokrovsky O. S., Korets M. A., Chmeleff J. and Oelkers E. H. (2016a). The effect of permafrost, vegetation, and lithology on Mg and Si

isotope composition of the Yenisey River and its tributaries at the end of the spring flood. Geochim. Cosmochim. Acta 191, 32-46.

Mavromatis V., van Zuilen K., Purgstaller B., Baldermann A., Nägler T.F. and Dietzel M. (2016b) Barium isotope fractionation during witherite ($BaCO_3$) dissolution, precipitation and at equilibrium. Geochim. Cosmochim. Acta 190, 72-84.

Marriott C. S., Henderson G. M., Belshaw N. S., and Tudhope A. W. (2004) Temperature dependence of ^{7}Li, ^{44}Ca and Li/Ca during growth of calcium carbonate. Earth Planet. Sci. Lett. 222, 615–624.

McDermott F. (2004) Palaeo-climate reconstruction from stable isotope variations in speleothems: a review. Quaternary Sci. Rev. 23, 901–908.

Meiron O. E, Bar-David E., Aflalo E. D, Shechter A., Stepensky D., Berman A. and Sagi A. (2011) Solubility and Bioavailability of Stabilized Amorphous Calcium Carbonate. Journal of Bone and Mineral Research 26, 364–372.

Michel F. M., MacDonald J., Feng J., Phillips B. L. Ehm L., Tarabrella C., Parise J. B. and Reeder R. J. (2008) Structural Characteristics of Synthetic Amorphous Calcium Carbonate. Chem. Mater. 20, 4720-4728.

Mikkelsen A., Andersen A.B., Engelsen S. B., Hansen H. C. B., Larsen O. and Skibsted L. H. (1999) Presence and Dehydration of Ikaite, Calcium Carbonate Hexahydrate, in Frozen Shrimp Shell. J. Agric. Food. Chem. 47, 911-917

Millero F., Huang F., Graham T. and Pierrot D. (2007) The dissociation of carbonic acid in NaCl solutions as a function of concentration and temperature. Geochim. Cosmochim. Acta 71, 46-55.

Minchin E. A. (1898) Materials for a monograph of the ascons. I. On the origin and growth of the triradiate and quadriradiate spicules in the family Clathrinidae. Quart. J. micr. Sci. 40, 469–588.

Morse J.W. and Mackenzie F.T. (1990) Geochemistry of Sedimentary Carbonates. Developments in Sedimentology 48, 707 pp, Elsevier.

Morse J. W., Arvidson R. S. and Lüttge A. (2007) Calcium carbonate formation and dissolution. Chem. Rev. 107, 342-381.

Moseley G. E., Lawrence Edwards R., Wendt K. A., Cheng, H., Dublyansky, Y., Lu,Y., Boch R., Spötl C. (2016) Reconciliation of the Devils Hole climate record with orbital forcing. Science 351, 165-168

Mucci A. and Morse J. W. (1984) The solubility of calcite in seawater solutions of various magnesium concentration, It = 0.697 m at 25°C and one atmosphere total pressure. Geochim. Cosmochim. Acta 48, 815–822.

Nancollas G. H. and Purdie N. (1964) The kinetics of Crystal Growth. Q. Rev. Chem. Soc. 18, 1-20

Nassif N., Pinna N., Gehrke N., Antonietti M., Jäger C. and Cölfen H. (2005) Amorphous layer around aragonite platelets in nacre. PNAS, 102, 12653-12655.

Nielsen A. E. (1984) Electrolyte crystal growth mechanisms. Journal of Crystal Growth 67, 289-310

Nielsen M. H., Aloni S. and De Yoreo J. J. (2014) In situ TEM imaging of $CaCO_3$ nucleation reveals coexistence of direct and indirect pathways. Science 345, 1158–1162.

Niedermayr A., Köhler S. J. and Dietzel M. (2013) Impacts of aqueous carbonate accumulation rate, magnesium and polyaspartic acid on calcium carbonate formation (6-40°C). Chemical Geology 340, 105-120.

Oehlerich M., Mayr C. C., Griesshaber E., Lücke A., Oeckler O. M., Ohlendorf C., Schmahl W. W. and Zolitschka B. (2013) Ikaite precipitation in a lacustrine environment – implications for palaeoclimatic studies using carbonates from Laguna Potrok Aike (Patagonia, Argentina). Quat. Sci. Rev. 71, 46–53.

Ogino T., Suzuki T. and Sawada K. (1987) The formation and transformation mechanism of calcium carbonate in water. Geochim. Cosmochim. Acta 51, 2757-2767.

Oliver B. G. and Davis A. R. (1972) Vibrational spectroscopic studies of aqueous alkali metal bicarbonate and carbonate solutions. Canadian Journal of Chemistry 51, 698-702.

Omelon C. R., Pollard W. H. and Marion G. M. (2001) Seasonal formation of ikaite (CaCO3·6H2O) in saline spring discharge at Expedition Fiord, Canadian High Artic: assessing conditional constrains for natural crystal growth. Geochim. Cosmochim. Acta 65, 1429–1437.

Palmer D. A., Wesolowski D. J. (1997) Potentiometric measurements of the first hydrolysis quotient of magnesium(II) to 250 degrees C and 5 molal ionic strength (NaCl). J. Solut. Chem. 26, 217-232.

Park S. Y. and Choi W. S. (2004). Effects of operating factors on the particle size distribution and particle shape of synthesized precipitated $CaCO_3$: effect of reaction temperature, blowing

rate of CO_2 gas and initial slurry concentration of $Ca(OH)_2$ on reaction completion time. Advanced Powder Technology 15, 1-12.

Pauly H. (1963) ‘‘Ikaite”, a new mineral from Greenland. Arctic 16, 263–264.

Pavlov M., Siegbahn P.E.M. and Sandstrom M. (1998) Hydration of beryllium, magnesium, calcium, and zinc ions using density functional theory. J. Phys. Chem. A 102, 219-228.

Peckmann J., Reimer A., Luth U., Luth C., Hansen B. T., Heinicke C., Hoefs J., Reitner J. (2001) Methane-derived carbonates and authigenic pyrite from the northwestern Black Sea. Mar. Geol. 177, 129-150.

Pearce C. R., Saldi G. D., Schott J. and Oelkers E.H. (2012) Isotopic fractionation during congruent dissolution, precipitation and at equilibrium: Evidence from Mg isotopes. Geochim. Cosmochim. Acta 92, 170-183.

Pinilla C., Blanchard M., Balan E., Natarajan S. K., Vuilleumier R. and Mauri F. (2015) Equilibrium magnesium isotope fractionation between aqueous Mg^{2+} and carbonate minerals: Insights from path integral molecular dynamics. Geochim. Cosmochim. Acta 163, 126-139.

Plummer L. N. and Busenberg E. (1982) The solubilities of calcite, aragonite and vaterite in CO_2-H_2O solutions between 0 and 90°C, and an evaluation of the aqueous model for the system $CaCO_3$-CO_2-H_2O. Geochim. Cosmochim. Acta 46, 1011-1040.

Pogge von Strandmann P. A. E., Forshaw J. and Schmidt D. N. (2014) Modern and Cenozoic records of seawater magnesium from foraminiferal Mg isotopes. Biogeosciences 11, 5155-5168.

Politi Y., Arad T., Klein E., Weiner S., Addadi L. (2004) Sea urchin spine calcite forms via a transient amorphous calcium carbonate phase. Science 306, 1161-1164.

Politi Y., Metzler R. A., Abrecht M., Gilbert B., Wilt F. H., Sagi I., Addadi L., Weiner S., Gilbert P. (2008). Transformation mechanism of amorphous calcium carbonate into calcite in the sea urchin larval spicule. Proceedings of the National Academy of Sciences of the United States of America 105, 17362-17366.

Politi Y., Batchelor D. R., Zaslansky P., Chmelka B. F., Weaver J. C., Sagi I., Weiner S. and Addadi L. (2010) Role of magnesium ion in the stabilization of biogenic amorphous calcium carbonate: A Structure-function investigation. Chem. Mat. 22, 161-166.

Prokrovsky B. G., Mavromatis V. and Prokrosvsky O. (2011) Co-variation of Mg and C isotopes in late Precambrian carbonates of the Siberian Platform: A new tool for tracing the change in weathering regime? Chemical Geology 290, 67-74

Purgstaller B., Mavromatis V., Immenhauser A. and Dietzel M. (2016) Transformation of Mg bearing amorphous calcium carbonate to Mg-calcite - In situ monitoring Geochim. Cosmochim. Acta 174, 180-195.

Putnis A. (2014) Why Mineral Interfaces Matter, Science 343, 1441-1442

Radha A. V., Forbes T.. Z.; Killian C. E., Gilbert P. U. P. A. and Navrotsky A. (2010) Transformation and crystallization energetics of synthetic and biogenic amorphous calcium carbonate. PNAS 107, 16438-16443

Radha A. V., Fernandez-Martinez A., Hu Y., Jun Y., Waychunas G. A., Navrotsky A. (2012) Energetic and structural studies of amorphous Ca1-xMgxCO3nH2O ($0 \leq x \leq 1$) Geochim. Cosmochim. Acta 90, 83-95.

Radha A. V. and Navrotsky A. (2015) Direct Experimental Measurement of Water Interaction Energetics in Amorphous Carbonates MCO_3 (M = Ca, Mn, and Mg) and Implications for Carbonate Crystal Growth. Cryst.Growth Des. 15, 70-78.

Raz S, Weiner S. and Addadi L. (2000) Formation of high-magnesian calcites via an amorphous precursor phase: Possible biological implications. Adv. Mater. 12, 38-42.

Raz S., Hamilton P. C., Weiner S. and Addadi L. (2003). The Transient Phase of Amorphous Calcium Carbonate in Sea Urchin Larval Spicules: The Involvement of Proteins and Magnesium Ions in Its Formation and Stabilization. Adv. Funct. Mater. 13, 480-486.

Reeder R. J. (1990) Carbonates: Mineralogy and Chemistry. Reviews in Mineralogy 11. Mineralogical Society of America, Virginia, pp. 399

Reddy M. M. (1977) Crystallization of calcium carbonate in the presence of trace concentrations of phosphorus-containing anions: I. Inhibition by phosphate and glycerophosphate ions at pH 8.8 and 25 °C. J. Cryst. Growth 41 (2), 287–295.

Reddy M. M and Wang K.K. (1980) Crystallization of calcium carbonate in the presence of metal ions: I. Inhibition by magnesium ion at pH 8.8 and 25 °C. J. Cryst. Growth 50 (2), 470–480.

Riechelmann D. F. C.; Schröder-Ritzrau A.; Scholz D., Fohlmeister J., Spötl C.; Richter D. K. and Mangini A. (2011) Monitoring Bunker Cave (NW Germany): A prerequisite to

interpret geochemical proxy data of speleothems from this site. Journal of Hydrology 409, 682-695

Riechelmann, S., Buhl, D., Schröder-Ritzrau, A., Spötl, C., Riechelmann, D.F.C., Richter, D., Kluge, T., Marx, T. and Immenhauser, A. (2012) Hydrogeochemistry and fractionation pathways of Mg isotopes in a continental weathering system: Lessons from field experiments. Chem. Geol., 300-301, 109-122

Riechelmann S., Schröder - Ritzrau A., Wassenburg J. A., Schreuer J., Richter D. K., Riechelmann D. F. C., Terente M., Constantin S., Mangini A. and Immenhauser A. (2014) Physicochemical characteristics of drip waters: Influence on mineralogy and crystal morphology of recent cave carbonate precipitates. Geochimica et Cosmochimica Acta, 145, 13-29

Riechelmann, S., Mavromatis, V., Buhl, D., Dietzel, M., Eisenhauer, A., Immenhauser, A. (2016). Impact of diagenetic alteration on brachiopod shell magnesium isotope (δ^{26}Mg) signatures: Experimental versus field data. Chem. Geol. 440, 191-206.

Rinder T., Dietzel M. and Leis A. (2013) Calcium Carbonate Scaling under Alkaline Conditions – Case Studies and Hydrochemical Modelling. Applied Geochemistry

Ripperdan R.L. (2001) Stratigraphic variation in marine carbonate carbon isotope ratios. Rev. Mineral. Geochem. 43, 637–662.

Rodriguez-Blanco J. D., Shaw S. and Benning L. G. (2008) How to make `stable´ ACC: protocol and preliminary structural characterization. Mineralogical Magazine 72, 283-286.

Rodriguez-Blanco J. D., Shaw S. and Benning L. G. (2011). The kinetics and mechanisms of amorphous calcium carbonate (ACC) crystallization to calcite, via vaterite. Nanoscale 3, 265-271

Rodriguez-Blanco J. D., Shaw S., Bots P., Roncal-Herrero T. and Benning L. G. (2012) The role of pH and Mg on the stability and crystallization of amorphous calcium carbonate. Journal of Alloys and Compounds 536S, 477-479.

Rodriguez-Navarro C, Kudlacz K., Cizer Ö. and Ruiz-Agudo E. (2015) Formation of amorphous calcium carbonate and its transformation into mesostructured calcite. CrystEngComm 17, 58-72

Rysgaard S., Glud R. N., Lennert K., Cooper M., Halden N., Leakey R. J. G., Hawthorne F. C. and Barber D. (2012) Ikaite crystals in melting sea ice – implications for pH and pCO_2 levels in Arctic surface waters. The Cryosphere 6, 901–908.

Saenger C. and Wang Z. (2014) Magnesium isotope fractionation in biogenic and abiogenic carbonates: Implications for paleoenvironmental proxies. Quaternary Science Reviews 90, 1-21.

Sawada K. (1997) The mechanisms of crystallization and transformation of calcium carbonates, Pure Appl. Chem 69: 921-928

Schauble E. A. (2004) Applying stable isotope fractionation theory to new systems. Rev. Mineral. Geochem. 55, 65–111.

Schmidt M., Hensen C., Moerz T., Mueller C., Grevemeyer I., Wallmann K., Mau S., Kaul N. (2005) Methane hydrate accumulation in "Mound 11" mud volcano, Costa Rica forearc. Mar. Geol. 216, 83-100.

Schott J., Mavromatis V., Fujii T., Pearce C., Oelkers E.H. (2016) The control of magnesium aqueous speciation on Mg isotope composition in carbonate minerals: theoretical and experimental modeling. Chem. Geol., http://dx.doi.org/10.1016/j.chemgeo.2016.03.011.

Señorale-Pose M., Chalar C., Dauphin Y., Massard P., Pradel P. and Marı´n M. (2008) Monohydrocalcite in calcareous corpuscles of Mesocestoides corti. Exp. Parasitol. 118, 54–58.

Sethmann I., Hinrichs R., Woerheide G. and Putnis A. 2006. Nano-cluster composite structure of calcitic sponge spicules—a case study of basic characteristics of biominerals. J. Inorg. Biochem. 100, 88–96.

Shaikh A. M. (1990) A New Crystal Growth Form of Vaterite, $CaCO_3$. J. Appl. Cryst. 23, 263-265

Sánchez-Pastor N., Oehlerich M., Astilleros J.´ M., Kaliwoda M., Mayr C. C., Fernández-Díaz L., Schmahl W. W. (2016) Crystallization of ikaite and its pseudomorphic transformaiton into calcite: Raman spectroscopy evidence. Geochimica et Cosmochimica Acta 175, 271-281

Selleck B. E., Carr P. F., Jones B. G. (2007) A Review and Synthesis of Glendonites (Pseudomorphs after Ikaite) with New Data: Assessing Applicability as Recorders of Ancient Coldwater Conditions. Journal of Sedimentary Research 77, 980-991

Shearman D. J., Smith A. J. (1985). Ikaite, the parent mineral of jarrowite-type pseudomorphs. Proceedings of the Geological Association 96, 305e314

Shirokova L.S., Mavromatis V., Bundeleva I.A., Pokrovsky O.S., Benezeth P., Gerard E., Pearce C. R., Oelkers E. H. (2013) Using Mg Isotopes to Trace Cyanobacterially Mediated Magnesium Carbonate Precipitation in Alkaline Lakes. Aquat. Geochem. 19, 1-24.

Solotchina E. P., Prokopenko A. A., Kuzmin M. I., Solotchin P. A. and Zhdanova A. N. (2009) Climate signals in sediment mineralogy of Lake Baikal and Lake Hovsgol during the LGM-Holocene transition and the 1-Ma carbonate record from the HDP-04 drill core. Quatern. Int. 205, 38–52.

Souchon V., Aleixo M., Delpoux O., Sagnard C., Mougin P., Wender A. and Raynal L. (2011) In situ determination of species distribution in alkanolamine H_2O-CO_2 systems by Raman spectroscopy. Energy Procedia 4, 554-561.

Spielhagen R. and Tripati A. (2009) Evidence for near-freezing temperatures and climate oscillations in the Arctic during the early Cenozoic. Palaeogeography, Palaeoecology, Palaeoclimatology 278, 48-56.

Stefánsson A., Bénézeth P. and Schott J. (2013) Carbonic acid ionization and the stability of sodium bicarbonate and carbonate ion pairs to 200°C – A potentiometric and spectrophotometric study. Geochim. Cosmochim. Acta 120, 600-611.

Stefánsson A., Bénézeth P. and Schott J. (2014) Potentiometric and spectrophotometric study of the stability of magnesium carbonate and bicarbonate ion pairs to 150°C and aqueous inorganic carbon speciation and magnesite solubility. Geochim. Cosmochim. Acta 138, 21-31.

Suess E., Balzer W., Hesse K. F., Müller P. J., Ungerer C. A. and Wefer G. (1982) Calcium carbonate hexahydrate from organicrich sediments of the Antarctic Shelf: precursors of Glendonites. Science 216, 1128–1131.

Stein C. I. and Smith A. J. (1986) Authigenic carbonate nodules in the Nankai Trough, site 583. Initial Reports of the Deep Sea Drilling Project 77, 659-668

Swainson I. P. and Hammond R. P. (2001) Ikaite, $CaCO_3 6H_2O$: cold comfort for glendonites as paleothermometers. Am. Mineral. 86, 1530–1533.

Swart P. K. (2015) The geochemistry of carbonate diagenesis: The past, present and future. Sedimentology, 62, 1233-1304

Tao J. H., Zhou D. M., Zhang Z. S., Xu X. R. and Tang R. K. (2009) Magnesium-aspartate-based crystallization switch inspired from shell molt of crustacean. PNAS 106, 22096-22101.

Tang J., Dietzel M., Boehm F., Koehler S. J. and Eisenhauer A. (2008a) Sr^{2+}/Ca^{2+} and $^{44}Ca/^{40}Ca$ fractionation during inorganic calcite formation: II. Ca isotopes. Geochim. Cosmochim. Acta 72, 3733-3745.

Tang J., Koehler S. J. and Dietzel M. (2008b) Sr^{2+}/Ca^{2+} and $^{44}Ca/^{40}Ca$ fractionation during inorganic calcite formation: I. Sr incorporation. Geochim. Cosmochim. Acta 72, 3718-3732.

Tang J., Dietzel M., Fernandez A., Tripati A. K., Rosenheim B. E. (2014) Evaluation of kinetic effects on clumped isotope fractionation (Δ_{47}) during inorganic calcite precipitation. Geochimica et Cosmochimica Acta 134, 120-136.

Tesoriero A. J. and Pankow J. F. (1996) Solid solution partitioning of Sr^{2+}, Ba^{2+} and Cd^{2+} to calcite. Geochimica et Cosmochimica Acta 60, 1053-63.

Trampe E. C., Larsen J. E., Glaring M. A., Stougaard P. and Kühl M. (2016) In situ Dynamics of O_2, pH, Light, and Photosynthesis in Ikaite Tufa Columns (Ikka Fjord, Greenland)—A Unique Microbial Habitat. Frontiers in Microbiology 7, doi: 10.3389/fmicb.2016.00722

Tripati A., Thiagarajan, Eagle R, Gagnon A., Bauch H. and Eiler J. (2010). Equilibrium $^{13}C^{18}O$ isotope signatures and 'clumped isotope' thermometry in foraminifera and coccoliths. Geochimica et Cosmochimica Acta 74, 5697-5717.

Tripati A. K., Hill P. S., Eagle R. A., Mosenfelder J. L., Tang J., Schauble E. A., Eiler J. M., Zeebe R. E., Uchikawa J., Coplen T. B., Ries J. B. and Henry D. (2015) Beyond temperature: Clumped isotope signatures in dissolved inorganic carbon species and the influence of solution chemistry on carbonate mineral composition. Geochim. Cosmochim. Acta 166, 344–371.

Vonhof H.B., van Breukelen M.R., Postma O., Rowe P. J., Atkinson T. C., Kroon D. (2006) A continuous-flow crushing device for on-line d^2H analysis of fluid inclusion water in speleothems. Rapid Communications in Mass Spectrometry 20, 2553-2558.

von Allmen, K., Böttcher, M.E., Samankassou, E. and Nägler, T. (2010) Barium isotope fractionation in the global barium cycle: first evidence from barium minerals and precipitation experiments. Chem. Geol., 277, 70–77.

Wang D., Hamm L. M., Giuffre A. J., Echigo T., Rimstidt J. D., De Yoreo J. J., Grotzinger J., Dove P. M. (2012) Revisiting geochemical controls on patterns of carbonate deposition through the lens of multiple pathways to mineralization. Faraday Discussions 159, 371-386.

Wang D., Hamm L. M., Bodnar R. J., Dove P. M. (2012b) Raman spectroscopic characterization of the magnesium content in amorphous calcium carbonates. Journal of Raman Spectroscopy 43, 543-548.

Wassenburg J., Immenhauser A., Richter D.K., Jochum K.P., Fietzke J., Deininger M., Goos M., Scholz D. and Sabaoui A. (2012) Climate and cave control on Pleistocene/Holocene calcite-to-aragonite transitions in speleothems from Morocco: Elemental and isotopic evidence. Geochimica et Cosmochimica Acta 92, 23-47.

Wehrmeister U., Jacob D.E., Soldati A.L., Loges N., Hager T. and Hofmeister W. (2011) Amorphous, nanocrystalline and crystalline calcium carbonates in biological materials. Journal of Raman Spectroscopy 42, 926-935.

Weiner S. and Dove P. M. (2003) An overview of biomineralization processes and the problem of the vital effect. In Biomineralization (eds. P. M. Dove, J. J. De Yoreo and S. Weiner). Reviews in Mineralogy and Geochemistry 54, pp. 1-29. 249-283.

Weiner S., Sagi I. and Addadi L. (2005) Choosing the Crystallization Path Less Traveled. Science 309, 1027.

Weiner, S., Mahamid, J., Politi, Y., Ma, Y. and Addadi, L. (2009) Overview of the amorphous precursor phase strategy in biomineralization. Frontiers in Material Sciences China, 3, 104-108.

Weiner S. and Addadi L. (2011) Crystallization Pathways in Biomineralization. Ann. Rev. Mat. Res. 41, 21-2961 40.

Weiss I.M., Tuross N., Addadi L. and Weiner S. (2002) Mollusc Larval Shell Formation: Amorphous Calcium Carbonate Is a Precursor Phase for Aragonite. Journal of Experimental Zoology, 293, 478-491.

White W. B. (1974) The carbonate minerals. In The Infrared Spectra of Minerals (eds. V. C. Farmer). Mineralogical Society, London, pp. 227-284.

Xu N., Yanan L., Zheng L., Gao Y., Yin H., Zhao J., Chen Z., Chen J. and Chen M. (2014) Synthesis and application of magnesium amorphous calcium carbonate for removal of high concentration of phosphate. Chemical Engineering Journal 251,102-110.

Yan H., Shao D., Wang Y. H. and Sun L. G. (2013) Sr/Ca profile of long-lived Tridacna gigas bivalves from South China Sea: A new high-resolution SST proxy. Geochim. Cosmochim. Acta, 112, 52-65.

Zhang Y., Shaw H., Farquhar R., and Dawe R. (2001) The kinetics of carbonate scaling – application for the prediction of downhole carbonate scaling. Journal of Petroleum Science and Engineering 29, 85-95.

Zolotoyabko E., Caspi E. N., Fieramosca J. S., Von Dreele R. B., Marin F. , Mor G., Addadi L., Weiner S., and Politi Y. (2010) Differences between Bond Lengths in Biogenic and Geological Calcite. Crystal Growth & Design 10, 1207-1214.